UNIVERSITÀ DEGLI STUDI DI PADOVA

DIPARTIMENTO DI INGEGNERIA INDUSTRIALE

CORSO DI LAUREA MAGISTRALE IN INGEGNERIA CHIMICA E DEI PROCESSI INDUSTRIALI

Tesi di Laurea Magistrale in
Ingegneria Chimica e dei Processi Industriali
(Laurea triennale DM 270/04 – indirizzo Chimica)

SCR CATALYST APPLICATION UNDER PRESSURE ON TWO-STROKE MARINE ENGINE

Relatore: Prof. Paolo Canu
Correlatore: Dott. Tommaso Melchiori
Dott. Stein Loevskar & Dott. Ola Sonesson

Laureando: ALESSANDRO PACE

ANNO ACCADEMICO 2012 – 2013

Abstract

In this work, developed jointly with a Norwegian marine SCR system supplier called Yarwil, a joint venture company of Yara, chemical producer, and Whilelmsen, a ship service company, it is investigated the influence of flue gas pressure on the operating conditions of a DeNOx SCR system. This condition appears when, in case of SCR system installed on a two-stroke engine, it is necessary to keep the DeNOx in appropriate condition of operating temperature. The best condition for the SCR catalyst (300-400 °C) in this application can be reached only in between of the engine and the relevant turbo-charger, after which the flue gas temperature decrease below 200 °C. In this condition, if the process is governed by the kinetic phenomena, the only effect that will happen is a better performance of the SCR, due to the increase of the concentration of the reactant.

But the experimental campaign, conducted by Yarwil in cooperation with MARINTEK, the technological department in maritime sciences of the University of Trondheim, has shown less conversion of NOx compared with the conversion calculated with a standard approach, thought for atmospheric pressure SCR systems.

Due to this fact, the purpose of this work is to understand the phenomena governing the SCR process, trying to found an appropriate model capable to describe both physical and chemical parameters of the SCR process under pressure, and to explain the right criteria to approach the SCR problem at pressure higher than atmospheric.

.

Index

INTRODUCTION 1

CHAPTER 1 – NOx air pollution 3

1.1 NOx AS DANGEROUS POLLUTANT 3

1.1.1 Nitrogen oxides as cause of Acid Rain 3

1.1.2 Nitrogen oxides as greenhouse gases 5

1.2 ENVIRONMETAL IMPACTS OF SHIPPING AND NOX EMISSION 6

1.3 THE MARPOL AND THE EMISSION CONTROLLED AREA 9

1.4 NOX REDUCTION TECHNOLOGY 14

1.5 THE IMPORTANCE TO INVESTIGATE THE HIGH PRESSURE SCR PROCESS 16

CHAPTER 2 – The SCR process: Chemicals Kinetics: A Partial Review 19

2.1 SCR PROCESS: BACKGROUND OF CHEMISTRY 19

2.1.1 Kinetic reaction: some aspects 20

2.1.2 Micro-Kinetic of SCR process 23

CHAPTER 3 – The MARINTEK pilot engine: experiment and data collection 27

3.1 THE ENGINE : WICHMANN WX28 HEAVY FUEL DIESEL 2-STROKE ENGINE 27

3.2 THE MARINTEK TEST PLAN AND YARWIL SCR SYSTEM 31

3.2.1 The experiment : composition measured Vs engine load 32

CHAPTER 4 – Reactor Models 41

4.1 1D MODEL 42

4.2 1D AND 3D MODELS 45

4.3 1D+1D MODEL: THE MODEL SELECTED 52

CHAPTER 5– Results and Discussion 57

5.1 NUMERICAL IMPLEMENTATION OF THE SELECTED REACTOR MODEL 57
5.2 MODEL PREDICTIONS AND SENSITIVITY ANALYSIS 61
5.3 COMPARISON WITH MARINTEK EXPERIMENTAL DATA AND YARWIL DESIGN 74
5.4 COMPARATIVE ANALYSIS BETWEEN YARWIL SIZING CRITERIA AND PRESENT MODEL 77

CONCLUSION 83

REFERENCES 89

APPENDIX 95

Introduction

The worldwide attention regarding the air pollution and environmental protection is enormously increasing in this years. A principal role in maritime pollution control is by Norway and the Scandinavian countries in general. Thanks to their interest in the past years, it has been planned a road map that will conduct most of the ship owners and engine producers to make possible ships even less polluting.

The last step in the environmental control legislation in marine sector will be the MARPOL Tier III, that will be applied starting from 2016 in the ECA, Emission Controlled Area (see Chapter 1 section 1.3); the Tier III includes the new emissions limits for NOx, SOx and other pollutant.

In particular, for the NOx emission, the limit imposed by the new rule can be reached only applying the BAT in the field of NOx control. Nowadays the BAT in this sector is the SCR process that use Urea solution, instead of Ammonia solution (because of safety rules on board of the ship), as selective reducer of NOx and a catalyst to make the reaction fast even at low temperature (less than 400 °C).

The SCR process for standard applications, both stationary sources such as power plant, diesel/oil 4-stroke engines, gas turbine, and mobile sources such as automotive and marine engines, has been widely studied, since 1980 and in literature is possible to find a lot of informations about the kinetic of the process, with different mechanism of reactions proposed, in particular different adsorption of the reactants, as Eley-Rideal mechanism or Langmuir-Hinshelwood (see Chapter 2).

The purpose of this work is to find and develop a model accurate enough to describe the SCR process, with parameters that are accurate enough to be used in operating conditions completely different respect on what were used to fit them, but even enough simple to be used in industrial application that often don’t give to the users accurate informations.

In fact, what it is needed in this work is to apply this selected model to the experimental data collected by Yarwil in cooperation with MARINTEK (see Chapter 3), and to try to understand what is not taken into account in the simplified model normally used by Yarwil to size the reactor, that make the empirical data different respect the concentration calculated in that way.

After the understanding of the phenomena affected by the pressure and if this phenomena are important for the SCR process, it will be interesting to compare the results and possibly to modify the way to size the SCR system in all under-pressure applications.

Chapter 1

NOx air pollution

1.1 NOx as dangerous pollutant

A large amount of technical and academic articles can be found in literature about the air pollution and about the role of nitrogen oxides in human health and in the environmental pollution. It is not among the aims of this Thesis to describe in detail all the effects of the NOx emission, but just to report the main effects of the NOx air pollution

1.1.1 Nitrogen oxides as cause of Acid Rain

Acid rain is caused by a chemical reaction that begins when compounds like sulfur dioxide and nitrogen oxides are released into the air. These substances can rise very high into the atmosphere, where they mix and react with water, oxygen, and other chemicals to form more acidic pollutants, known as acid rain.

In some areas of the United States, the pH of rainwater can be 3.0 or lower, approximately 1000 times more acidic than normal rainwater. In 1982, the pH of a fog on the West Coast of the United States was measured at 1.8! When rainwater is too acidic, it can cause problems ranging from killing freshwater fish and damaging crops, to eroding buildings and monuments.[1]

Acid rain does not kill trees immediately or directly. Instead, it is more likely to weaken the tree by destroying its leaves, thus limiting the nutrients available to it. Or, acid rain can seep into the ground, poisoning the trees with toxic substances that are slowly being absorbed through the roots. When acid rain falls, the acidic rainwater dissolves the nutrients and helpful minerals from the soil. These minerals are then washed away before trees and other plants can use them to grow. Not only does acid rain strip away the nutrients from the plants, they help release toxic substance such as aluminum into the soil. This occurs because these metals are bound to the soil under normal conditions, but the additional dissolving action of hydrogen ions causes rocks and small bound soil particles to break down. When acid rain is frequent, leaves tend to lose their protective waxy coating, When leaves lose their coating, the plant itself is open to any possible

disease. By damaging the leaves, the plant cannot produce enough food energy for it to remain healthy. Once the plant is weak, it can become more vulnerable to disease, insects, and cold weather which may ultimately kill it.

Acid rain does not only effect organisms on land, but also effect organisms in aquatic biomes. Most lakes and streams have a pH level between six and eight. Some lakes are naturally acidic even without the effects of acid rain. For example, Little Echo Pond in New York has a pH level of 4.2.

Most importantly, acid rain can affect health of a human being. It can harm us through the atmosphere or through the soil from which our food is grown and eaten from. Acid rain causes toxic metals to break loose from their natural chemical compounds. Toxic metals themselves are dangerous, but if they are combined with other elements, they are harmless. They release toxic metals that might be absorbed by the drinking water, crops, or animals that human consume. These foods that are consumed could cause nerve damage to children or severe brain damage or death. Scientists believe that one metal, aluminum, is suspected to relate to Alzheimer's disease.

One of the serious side effects of acid rain on human is respiratory problems. The nitrogen oxide emission gives risk to respiratory problems such as dry coughs, asthma, headaches, eye, nose, and throat irritation. Polluted rainfall is especially harmful to those who suffer from asthma or those who have a hard time breathing. But even healthy people can have their lungs damaged by acid air pollutants. Acid rain can aggravate a person's ability to breathe and may increase disease which could lead to death.

1.1.2 Nitrogen oxides as greenhouse gases

Nitrogen oxides (NOx) act as indirect greenhouse gases by producing the tropospheric greenhouse gas 'ozone' via photochemical reactions in the atmosphere.

No	REACTION	RATE CONSTANT $(cm^{\alpha} molec^{\beta} sec^{-1})$
1	$NO_2 + h\nu \rightarrow NO + O$	$0.533\ min^{-1}$
2	$O + O_2 + M \rightarrow O_3 + M$	$6 * 10^{-34} * \left(\frac{T}{300}\right)^{2.3}$
3	$NO + O_3 \rightarrow NO_2 + O_2$	$2.2 * 10^{-12} * exp\left(\frac{-1430}{T}\right)$
4	$RH + OH\cdot \rightarrow RO_2\cdot + H_2O$	$1.68 * 10^{-11} * exp\left(\frac{-559}{T}\right)$
5	$RCHO + OH\cdot \rightarrow RC(O)O_2\cdot + H2O$	$6.9 * 10^{-12} * exp\left(\frac{250}{T}\right)$
6	$RCHO + h\nu \rightarrow RO_2\cdot + HO_2\cdot + CO$	$1.91E-4\ min^{-1}$
7	$HO_2\cdot + NO \rightarrow NO_2 + OH\cdot$	$3.7 * 10^{-12} * exp\left(\frac{240}{T}\right)$
8	$RO_2\cdot + NO \rightarrow NO_2 + RCHO + HO_2\cdot$	$4.2 * 10^{-12} * exp\left(\frac{180}{T}\right)$
9	$RC(O)O_2\cdot + NO \rightarrow NO_2 + RO_2\cdot + CO_2$	$4.2 * 10^{-12} * exp\left(\frac{180}{T}\right)$
10	$OH\cdot + NO_2 \rightarrow HNO_3$	$1.11 * 10^{-11}$
11	$RC(O)O_2\cdot + NO_2 \rightarrow RC(O)O_2NO_2$	$4.7 * 10^{-12}$
12	$RC(O)O_2NO_2 \rightarrow RC(O)O_2\cdot + NO_2$	$1.95 * 10^{16} * exp\left(\frac{-13,543}{T}\right)$

Figure 1.1 *Semplified scheme of NO_2 reactions on atmosphere*

The impact of NOx gases on global warming is not all bad though. Like tropospheric ozone, NOx gases also affect the global greenhouse gas budget through their effect on the atmospheric abundance of hydroxyl (OH) radicals.

The breakdown of NOx gases gives rise to increased OH abundance and so helps to reduce the lifetimes of greenhouse gases like methane. Sources of NOx include fossil fuel burning, biomass burning and emission from soils. NOx is also emitted directly into the troposphere by lightning, ammonia oxidation and aircraft. The main sink for NOx gases is oxidation in the atmosphere, however significant amounts of NOx arising from soils can be used up in the tree canopy before it escapes to the troposphere. Another pathway for NOx in the atmosphere is that of dry deposition back on land, such deposition can then lead to increased emissions of the direct greenhouse gas nitrous oxide (N2O).[2,3]

1.2 Environmental impacts of shipping and NOx emission

April 23, 2009 *The Guardian*[27] has reported on new research showing that in one year, a single large container ship can emit cancer and asthma-causing pollutants equivalent to that of 50 million cars.

Shipping is by far the biggest transport polluter in the world. There are 760 million cars in the world today emitting approx 15-30% of NOx emission annually.

Statisticians estimate that 90% of world trade is transported by the shipping industry [4], and, with increasing globalization and the expansion of the global economy, the actual tonnage of goods being shipped over the past 60 years has increased dramatically [5]. This means that even though low-speed diesel propelled vessels may have low emissions relative to the amount of goods they transport, they are becoming responsible for an increasingly significant portion of the total global emissions inventory.

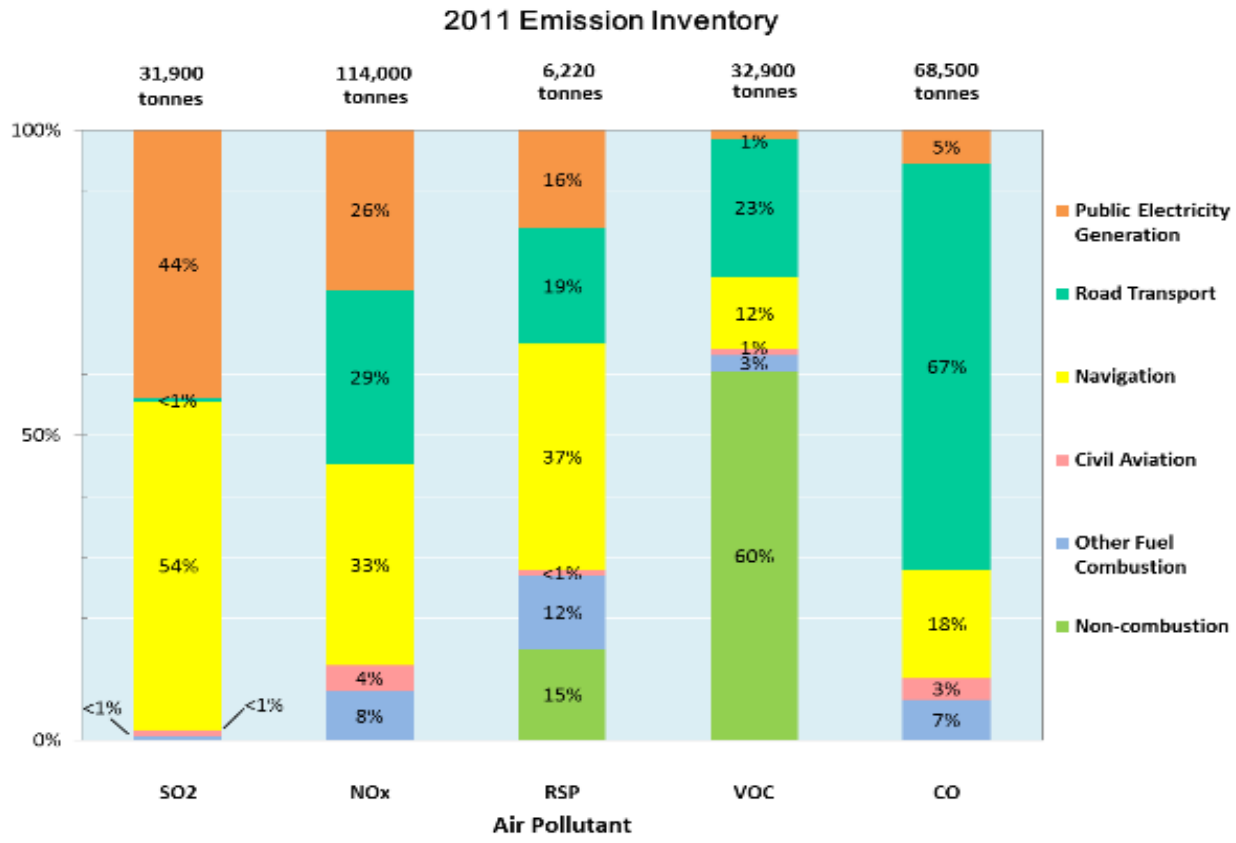

Figure1. 2 *2011 Emission Inventory in Honk Kong area by Environmental Protection Department of Honk Kong*

According to *Corbett et al*. [6], oceangoing ships are responsible for the release of between 5-6.9 million metric tons of NOx a year which is equivalent to approximately 18% of annual worldwide NOx emissions. The effect of NOx emissions is particularly significant in coastal areas near major shipping routes which also tend to have the highest population densities [7]. The significance of the impact of NOx emissions upon these communities is illustrated by the statistic that marine diesel engines may contribute up to 17% of the local NOx inventory on a typical sunny summer day in San Diego, CA [8]. NOx emissions are known to have negative impacts on the environment. These include the contribution to the formation of acid rain, over fertilization of lakes and soils, ozone depletion, smog formation, and reduction in air quality by facilitating the formation of small particulates [7]. Additionally, prolonged exposure to NOx is also known to cause adverse health effects including respiratory irritation, lung tissue damage, and possibly premature death. Persons with preexisting heart disease and respiratory diseases, such as emphysema, are considered to be particularly susceptible to the adverse health effects of NOx emissions.

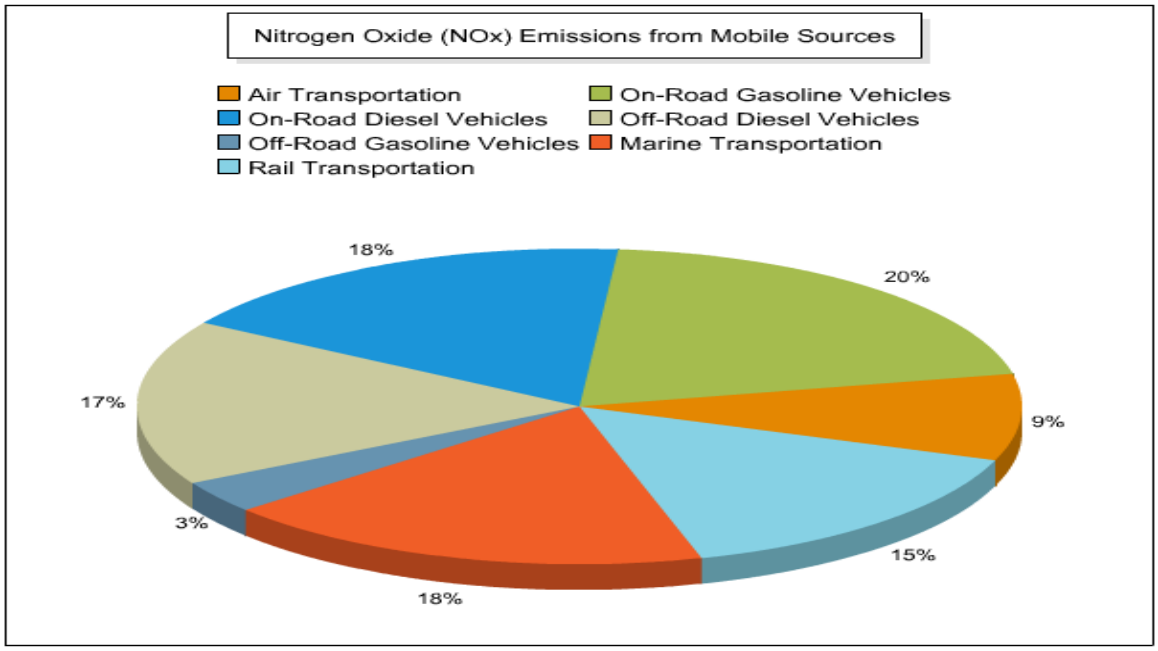

Figure 1.3 *Global Vehicles NOx Emission by BCairquality*

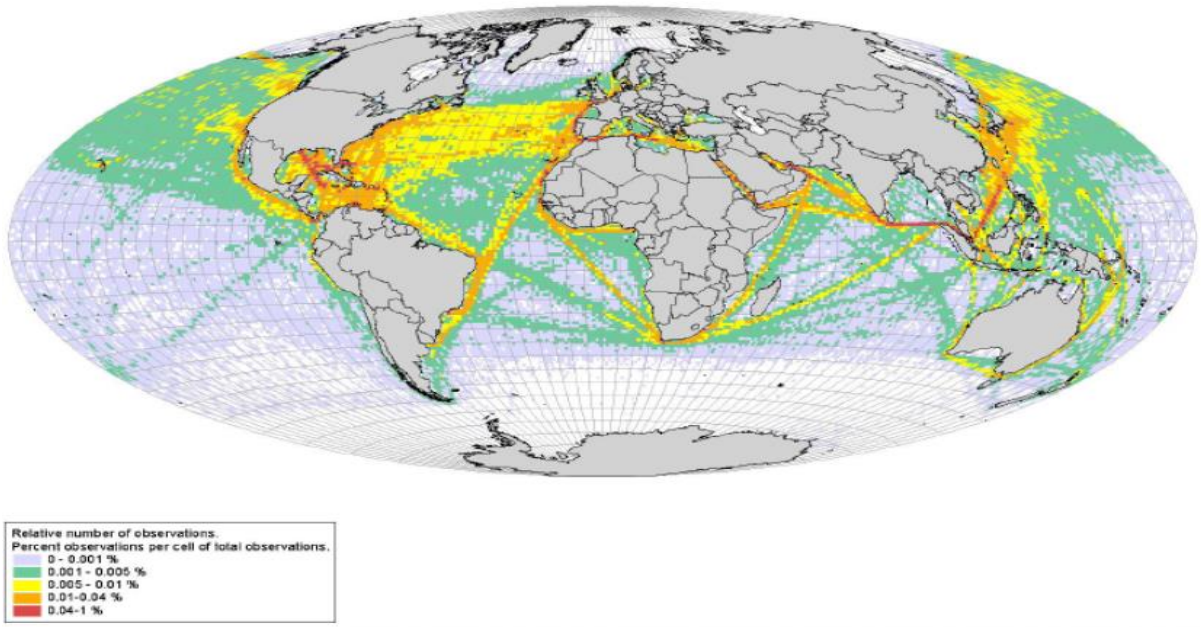

Figure 1.4 *Global Marine Route by www.ec.europa.eu*

One of the area most affected by NOx pollution is the North Sea. Mainly for this reasons the North countries were the first that start to apply rules on the NOx emissions both for stationary and mobile sources.

As show in figure 1.5 the marine transportation is the principal , together with the urban traffic in the major cities like London, Paris, Milan, source of NOx emission

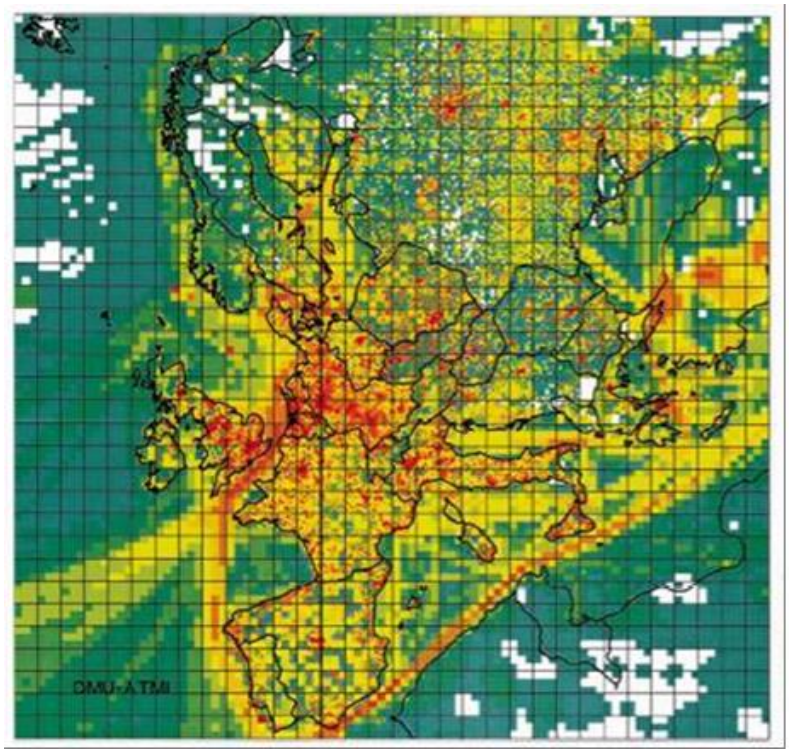

Figure 1.5 *NOx emissions in Europe. In red the main sources*

1.3 The MARPOL and the Emission Controlled Area

The control of diesel engine NOx emissions is achieved through the survey and certification requirements leading to the issue of an Engine International Air Pollution Prevention (EIAPP) Certificate and the subsequent demonstration of in service compliance in accordance with the requirements of the mandatory, regulations 13.8 and 5.3.2 respectively, NOx Technical Code 2008 (resolution MEPC.177(58)). The NOx control requirements of Annex VI apply to installed marine diesel engine of over 130 kW output power other than those used solely for emergency purposes irrespective of the tonnage of the ship onto which such engines are installed. Definitions of 'installed' and 'marine diesel engine' are given in regulations 2.12 and 2.14 respectively. Different levels (Tiers) of control apply based on the ship construction date, a term defined in regulations 2.19 and hence 2.2, and within any particular Tier the actual limit value is determined from the engine's rated speed:

Tier	Ship construction date on or after	Total weighted cycle emission limit (g/kWh) n = engine's rated speed (rpm)		
		n < 130	n = 130 - 1999	n ≥ 2000
I	1 January 2000	17.0	$45.n^{-0.2}$ e.g., 720 rpm – 12.1	9.8
II	1 January 2011	14.4	$44.n^{-0.23}$ e.g., 720 rpm – 9.7	7.7
III	1 January 2016*	3.4	$9.n^{-0.2}$ e.g., 720 rpm – 2.4	2.0

* subject to a technical review to be concluded 2013 this date could be delayed, regulation 13.10.

Figure 1.6 *NOx limits [g/kWh] per engine's speed rate*

The Tier III controls apply only to the specified ships while operating in Emission Control Areas (ECA) established to limit NOx emissions, outside such areas the Tier II controls apply. In accordance with regulation 13.5.2, certain small ships would not be required to install Tier III

engines. The North American ECA came into force on 1 August 2011 and will take effect from the 1 August 2012. In July 2011, the 62nd session of the Marine Environment Protection Committee adopted the United States Caribbean Sea ECA, which is expected to enter into force on 1 January 2013, taking effect 12 months after (1 January 2014). The emission value for a diesel engine is to be determined in accordance with the NOx Technical Code 2008 in the case of Tier II and Tier III limits.

Tier	Date	NOx Limit, g/kWh		
		n < 130	130 ≤ n < 2000	n ≥ 2000
Tier I	2000	17.0	$45 \cdot n^{-0.2}$	9.8
Tier II	2011	14.4	$44 \cdot n^{-0.23}$	7.7
Tier III	2016†	3.4	$9 \cdot n^{-0.2}$	1.96
† In NOx Emission Control Areas (Tier II standards apply outside ECAs).				

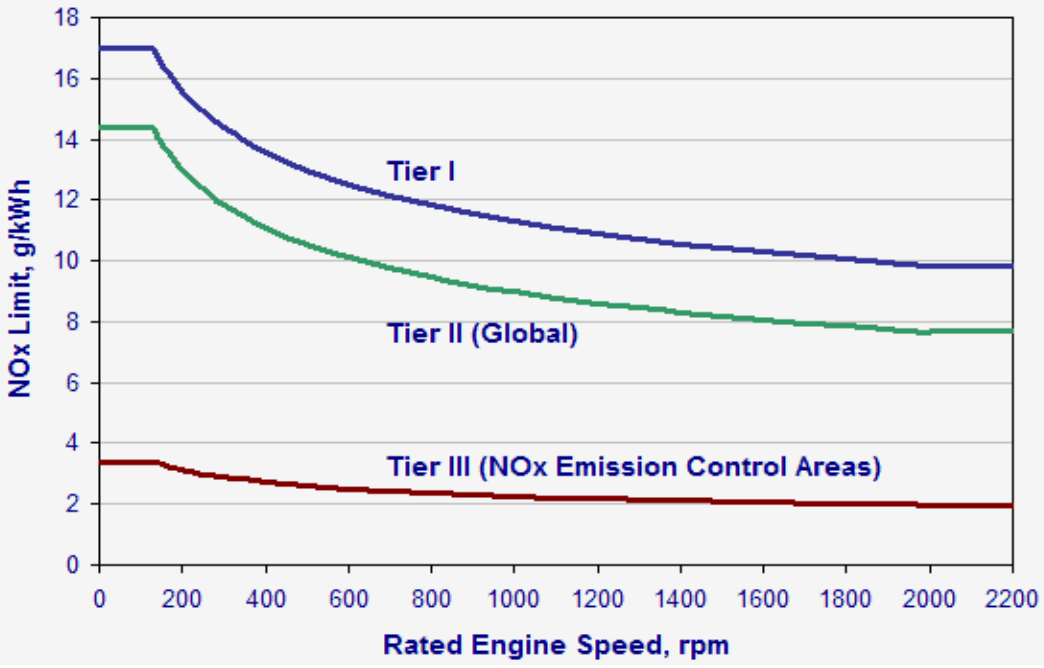

Figure 1.7 *NOx emission limit starting from 2016*

Most Tier I engines have been certified to the earlier, 1997, version of the NOx Technical Code which, in accordance with MEPC.1/Circ.679, may continue to be used in certain cases until 1 January 2011. Certification issued in accordance with the 1997 NOx Technical Code would still remain valid over the service life of such engines. An engine may be certified on an individual, Engine Family or Engine Group basis in accordance with one or more of the four duty test cycles as

given in appendix II of the Annex. In the case of Engine Family or Engine Group engines it is the Parent Engine which is actually emissions tested, this is the engine which has the combination of rating (power and speed) and NOx critical components, settings and operating values which results in the highest NOx emission value or, where more than one test cycle is to be certified, values which, to be acceptable, each of which must be no higher than the applicable Tier limit value. Subsequent series engines, Member Engines, are thereafter constructed with a rating, components, settings and operating values within the bounds established for the respective Engine Family or Engine Group. Generally all new engine certification leading to the issue of an EIAPP Certificate is undertaken at the engine builder's works where the necessary pre-certification survey takes place.

Consequently a diesel engine having an EIAPP Certificate is approved, by, or on behalf of (since almost all engine certification work is delegated to Recognized Organizations), the flag State of the ship onto which it is to be installed, to a stated Tier for one or more duty test cycles, for a particular rating or rating range, and with defined NOx critical components, settings and operating values including options if applicable. Any amendments to these aspects are to be duly approved and documented.

Figure 1.8 *The Emission Controlled Area, where Tier III will be applied starting from 2016*

For each NOx certified diesel engine there must be onboard an approved Technical File, NOx Technical Code 2008 2.3.4, which both defines the engine as approved and provides the applicable survey regime together with any relevant approved amendment documentation. As of October 2010 virtually all engines are surveyed using the Parameter Check method, NOx Technical Code 2008 2.4.3.1, whereby the actual duty, rating and NOx critical components, settings and operating values are checked against the given data in the Technical File. A key document in the Parameter Check procedure is the Record Book of Engine Parameters, NOx Technical Code 2008 6.2.2.8, which is maintained to record all replacements and changes to NOx critical components, settings and operating values. Engine surveys are undertaken on completion of manufacture and subsequently as part of the overall ship survey process; flowcharts illustrating the aspects checked at the various survey stages are given in NOx Technical Code 2008 appendix II.

In addition, there is the case where a diesel engine is subject to "major conversion", regulation 13.2. Of the three routes given, "substantial modification" and uprating, both as defined, involve changes to an existing installed engine and under these circumstances the relevant Tier is that applicable to the construction date of the ship onto which the engine is installed except, in the case of ships constructed before 1 January 2000, where Tier I is applied. In the third route, that of the installation of a replacement, non-identical, or additional engine then the Tier appropriate to the date of installation applies although, subject to acceptance by the Administration taking into account guidelines to be developed, in some circumstances it would permitted to install a Tier II replacement engine as opposed to one certified to Tier III, regulation 13.2.2. In the case of an identical replacement engine the Tier appropriate to the ship construction date applies.

The revised Annex VI has also introduced the prospect of retrospective NOx certification, regulation 13.7, in the case of diesel engines of more than 5000 kW power output and a per cylinder displacement of 90 litres and above installed on ships constructed between 1 January 1990 and 31 December 1999. This will generally therefore affect only the main engines on such ships, the 90 litre/cylinder criteria represents, for example in current medium speed engine designs, engines with a bore of 460 mm and above. For these engines if a Party, not necessarily the ship's flag State, has certified an "Approved Method" which results in an emission value no higher than the relevant Tier I level and has advised of that certification to IMO then that Approved Method must be applied no later than the first renewal survey which occurs more than 12 months after deposition of the advice to IMO. However, if the ship owner can demonstrate that the Approved Method is not commercially available at that time then it is to be installed no later than the next annual survey

after which it has become available. Given within regulation 13.7 are constraints on the Approved Method that limit its cost and detrimental effects on engine power and fuel consumption.

Further requirements are given in chapter 7 of the NOx Technical Code 2008 which includes an outline of the Approved Method File which must be retained with the engine. To date several notifications of Approved Methods have been advised to the Organization. It is not clear the extent to which others will become available however it is expected that, if so developed, these will be limited to involving aspects such as changing the engine's fuel injection nozzles. Consequently, in the case of engines potentially subject to the requirement to install an Approved Method it will be necessary for ship owners (and also surveyors and port State inspectors) to remain vigilant over the service life of those engines as to the availability of such arrangements and to ensure that they are duly fitted and thereafter retained as required. For those engines where an Approved Method exists there is the alternative option, regulation 13.7.1.2, whereby the engine is instead certified in accordance with the conventional NOx Technical Code requirements.[9]

1.4 NOx REDUCTION TECHNOLOGY

Several technologies have been developed to limit the emission of NOx from various power sources including marine diesel engines. Although the majority of these technologies have been developed for applications other than low-speed diesel engines, many of these methods can also be used with low-speed diesel engines, provided that adequate consideration is given to the unique aspects of the application. NOx reduction technologies are generally grouped into one of two categories: primary and secondary methods. Primary methods are those methods which reduce NOx by altering the conditions within the combustion chamber so that the actual production of NOx is reduced. Examples of primary methods include such approaches as the modulating of fuel injection timing, control and optimization of fuel injection profiles, and the introduction of water into the combustion chamber. Secondary technologies normally require greater modification to shipboard systems and include after treatment methods such as selective catalytic reduction (SCR) and exhaust gas scrubbers, which remove NOx after it has been generated, and exhaust gas recirculation (EGR), which lowers NOx by re-circulating a portion of the exhaust gas back through the combustion chamber. The overall rates of reduction can also be increased by combining more than one of the methods described above. Given the exponential dependence of the *Zeldovich* mechanism on temperature, primary methods are designed to reduce NOx formation by limiting peak temperatures in the combustion chamber. This can either be achieved by optimizing the combustion chamber and controlling the rate of heat release so as to avoid local (spot) regions with high temperatures, or by changing the timing of fuel injection so that fuel ignition does not coincide with peak cylinder temperatures. Significant reductions in NOx production can theoretically be achieved with relatively modest reductions in temperature and many of these technologies can be combined to achieve further reductions. The main drawback of this approach, however, is that the overall potential for NOx reduction is limited which means that the application of these methods alone is not sufficient to satisfy the IMO Tier III requirements. Additionally, the majority of these methods create less than optimal combustion and therefore incur non-negligible penalties in fuel consumption. Estimates put these penalties at approximately 0-3% for 15-20% reduction and up to 10% for 40% NOx reduction [45]. Another means of reducing combustion temperatures is by introducing fluids with higher heat capacities into the stream of reactants in order to reduce the overall temperature of the reaction. Many of these methods rely on introduction of water into the combustion chamber, either by humidification of the intake air

(also known as Humid Air Motor), emulsification of water into the fuel, or through the direct injection of water into the cylinder. Some care must be taken with the design of this equipment as uncontrolled moisture (such as from condensation from the intake after the charge air cooler) can have the undesired effect of disrupting the cylinder lubricating oil layer, thereby resulting in rapidly accelerated (and thereby very expensive) wear. Another possibility which has been adopted from mobile truck applications has been the use of exhaust gas recirculation (EGR). NO_X reduction by EGR is a result of lower combustion temperature due to the high specific heat of CO2 and H2O, and of decreased NO_X generation due to the decreased oxygen content of the recirculated gas [45]. In contrast to this, exhaust gas treatment methods tend to have much higher installation cost and space requirements, but are also capable of the highest NOx reduction levels. Although scrubber technologies have been shown to have some effects on the reduction of NO_X , their main application and significance is in the reduction of SO_X emissions. However, since both SO_x and NO_X reduction regulations are linked in the ECA areas, the NO_X potential of scrubber technology should not be discounted.

Method	Reduction Possible	Effect on Fuel Consumption	Cost relative to engine price	Operating Costs	Notes
Primary methods: late fuel injection timing, etc.	15% below IMO Tier I	Moderate	Up to 10% for 40% reduction in NO_x	Moderate	Well advanced development
Humid air motor	30-60%	Low	5-30%	Moderate	Water quality requirements if inject before air cooler
Direct water injection	40-50%	Low	10%	3%	Elevated water injection rates can result in excessive smoke and fuel consumption
Water-in-Fuel Emulsions	Up to 20%	Low	5%	5%	· Increased flow rates through fuel injections system · Can reduce smoke generation at low loads
EGR	50-70%				Limitations regarding fuel quality (low sulfur and ash content)
Scrubbers	5-10%		No	Moderate	Primarily designed to reduce SO_x
SCR	90%	None/possible decrease	15-20%	10% (Dependent on reagent price)	· Requires reagent and dosing system · Sensitive to fuel sulfur content · Temperature operating window is crucial · Installed before Turbocharger on 2-Stroke engines · Engine may be optimized for lower fuel oil consumption

Figura 1.9 *Summary of the characteristics of various NOx reductions technology*

1.5 The importance to investigate the high pressure SCR process

As already shown, starting from 2016, in a large part of world-wide coasts, the ECA, it will be active the Tier III regulation. Due to this, the large transport ships should adopt efficient abatement systems to meet the new emission limits.

Thanks to the marketing data provided by Yarwil, it is possible to estimate that about one thousand new two-stroke diesel engines are fabricated each year just for the marine market. The medium size of these engines is about 10 MW.

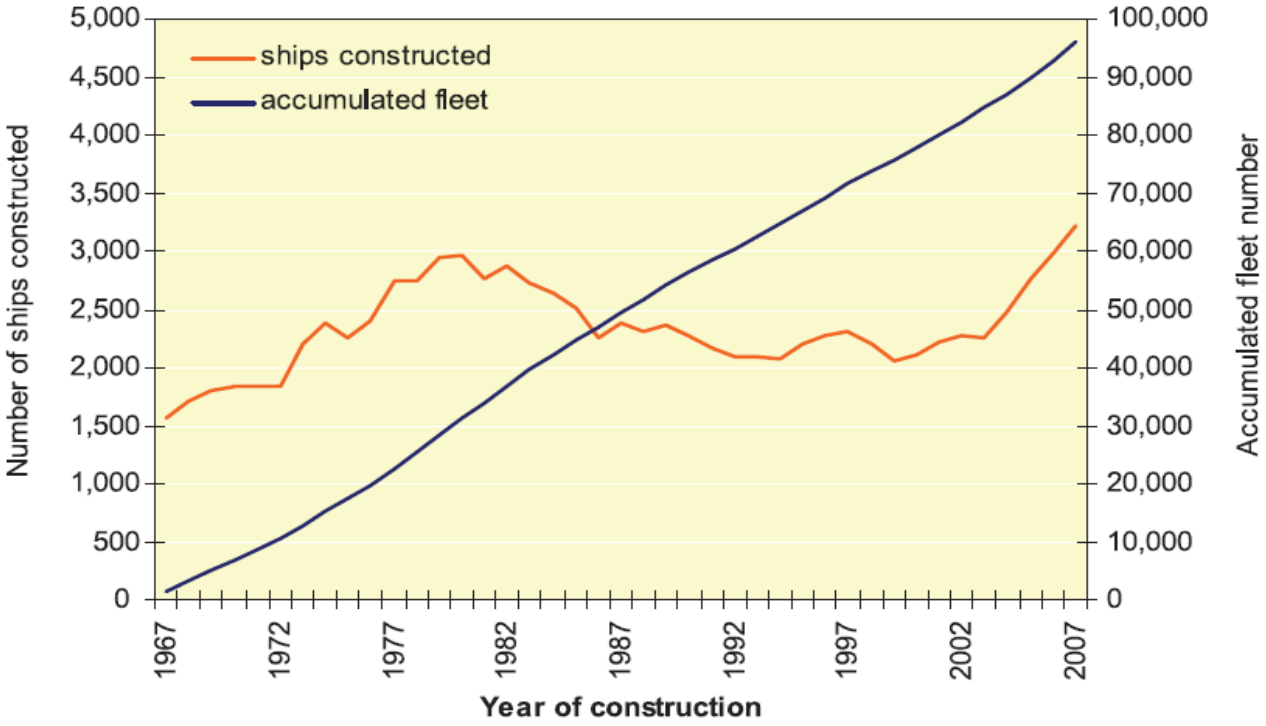

Figure 1.10 *Age profile of the world fleet*

The second IMO GHG study of 2009 clearly says: "Tier II NOx limits, i.e. 15–20% reduction from the current levels, can be achieved with modifications of the internal-combustion process. At present, reduction of emissions of NOx to Tier III limits (~80% reduction from Tier I) can only be achieved by selective catalytic reduction (SCR) post-treatment or by using LNG and lean pre-mixed combustion. These technologies are proven for four-stroke engines; however, experience with large two-stroke engines is limited." Today still, large two-stroke engines that have an SCR system installed are very few, and before coming into force of the Tier III in the ECA, probably 2016, very few projects of SCR application on two-stroke engines are predicted.

The introduction of a tax on NOx emissions from domestic shipping in Norway since 1 January 2007 has resulted in emissions from a significant number of engines being measured. These previously unpublished data were made available to the study by the Norwegian Maritime Administration. These data, together with data from the Lloyd's Marine Emissions study and from other MARINTEK measurement campaigns, were combined to produce a joint data-sheet of NOx emissions from existing ships. This data-sheet contains a total of 121 measurements, 96 of which are for medium-speed engines. The NOx data match fairly well the technical expectation, except for the MSD (Medium Speed Diesel) data derived from the combined Swedish Environmental Research Institute (IVL) and Lloyd's, that appear slightly high.

.The MARINTEK data collected for SSD, Slow Speed Diesel, are the base line of the present work.

Yarwil, in partnership with MARINTEK, tried to perform an SCR system pilot application on a two-stroke engine. The main problem to perform an SCR application in this condition is the fact it has to be located before the recovery of the mechanical energy; this kind of installation is called "Pre-Turbo SCR".

This pre-turbo installation is necessary to guarantee a sufficient high temperature of the tail gases, because after the turbocharge the temperature is lower than 200° C.

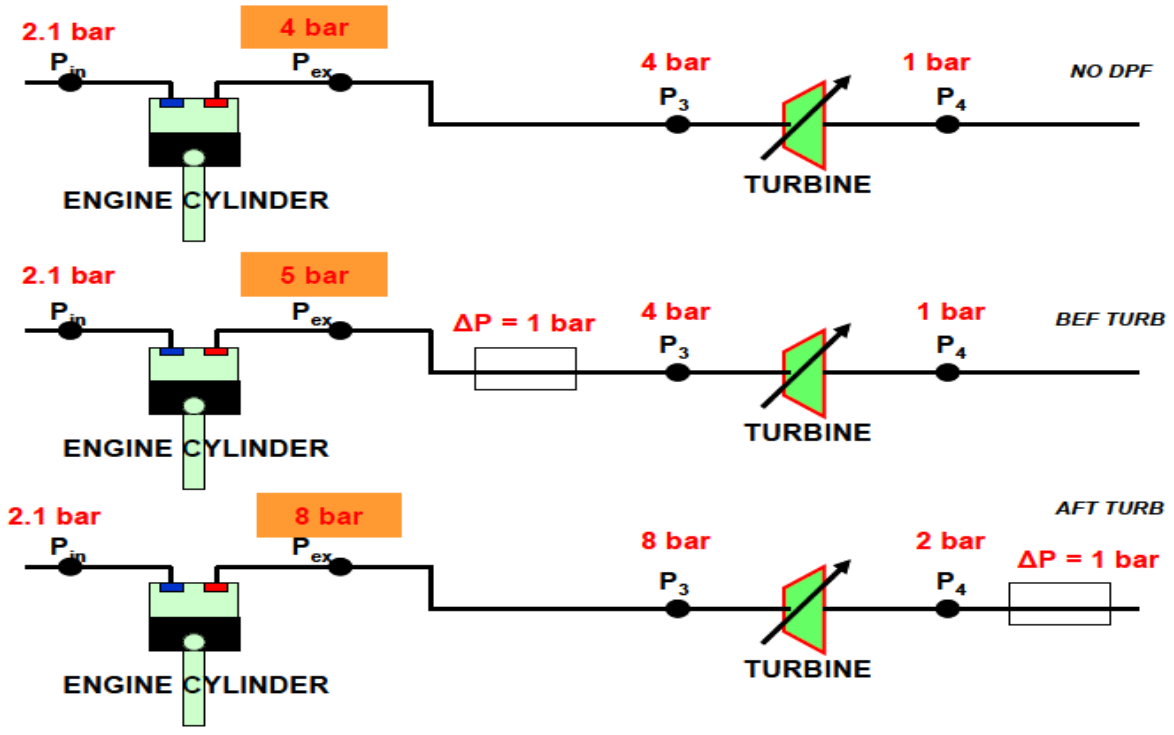

Figure 1.11 *Theoretical Impact of After treatment on Engine back pressure*

Since 1970, when the first SCR system was installed on a power plant, it was not required to investigate the effects of pressure on the SCR system, because it was not needed, as all the stationary sources that require an SCR system were operating at atmospheric pressure.

Starting from 2016 it will be required to install SCR systems on new ships that want to navigate in the ECA and probably in the upcoming years the Tier III will be extended also on Mediterranean Sea and by the coasts of China and Japan, so it will be necessary to start the investigation of the problem, to be prepared and to be able to supply the best solution in compliance with the new legislation.

Today Hitachi-Zosen, Johnson Matthey and D.E.C. Marine, say that they have installed a pre-turbo SCR system, high pressure-high temperature, that meets the Tier III regulations, but no data are available on literature about these DeNOx systems and the criteria used for taking in account the high pressure conditions.

Chapter 2

The SCR Chemicals

As already shown, the Tier III emission limits will be reached only by using advanced abatement systems; in particular the BAT about NOx abatement is the SCR process, reduction of NOx via ammonia or urea injection with a proper SCR catalyst. For this reason it is important to investigate and understand what happens on the SCR catalyst by a kinetic point of view.

2.1 SCR chemistry

The reduction of NOx occurs by reaction with NH3 (stored in the form of liquid anhydrous ammonia, aqueous ammonia, or urea) into N2 and H2O according to the following global reactions:

$$4NO + 4NH_3 + O_2 \rightarrow 4N_2 + 6H_2O \quad (R1)$$

$$6NO_2 + 8NH_3 \rightarrow 7N_2 + 12H_2O \quad (R2)$$

$$NO + NO_2 + 2NH_3 \rightarrow 2N_2 + 3H_2O \quad (R3)$$

Reaction (R1) is the most important one; it proceeds rapidly on the catalyst at temperatures between 250 and 450 °C in excess of oxygen and accounts for the overall stoichiometry of the SCR process. Since NO_2 generally accounts for only 5% of the NOx, reactions (R2) and (R3) play a minor role in the process. Four undesirable oxidation reactions can also take place:

$$4NH_3 + 5O_2 \rightarrow 4NO + 6H_2O \quad (R4)$$

$$4NH_3 + 3O_2 \rightarrow 2N_2 + 6H_2O \quad (R5)$$

$$2NH_3 + 2O_2 \rightarrow N_2O + 3H_2O \quad (R6)$$

$$SO_2 + ½\ O_2 \rightarrow SO_3 \quad (R7)$$

Reactions (R4)–(R6) imply the consumption of ammonia and result in a net reversal of the removal of NOx and in the formation of N_2O as a byproduct. These reactions are observed over SCR catalysts in the absence of NO in the feed, but they become negligible in the presence of NOx. The

ability to react selectively with NOx in excess oxygen has not been observed in the case of other simple reagents such as carbon monoxide and hydrocarbons. Hence the choice of ammonia as the unique reducing agent in the SCR process. Reaction (R7) is the SO_2 oxidation, promoted by the Vanadium content in the catalyst and responsible for the formation of salts like ammonium sulfate[43].

Now it will be discussed a general kinetic behavior of the SCR process; we will focus only on the Vanadium-based catalyst, but there are several studies on different types of catalyst like CuO-based or Fe_2O_3-based catalyst and also Zeolite catalyst[24]

2.1.1 Kinetics of the reactions

Several kinetic studies, mostly obtained under "real" conditions, have been reported for the SCR reaction. These are based on both merely empirical expressions (e.g. power-law kinetics) and/or mechanistic approaches (e.g. Langmuir-Hinshelwood or Eley-Rideal models). A detailed survey of the kinetic models developed for the SCR reaction is outside the aim of the present review. However, since several authors deducted mechanistic information from their kinetic models, in the following such results will be briefly discussed. The NO conversion rate for the SCR process can be supposed to depend on the concentrations of the reactants C_{NO}, C_{NH3} and C_{O2} , and also from the concentration of water, C_{H2O}, which is a reaction product and is also present in the feed under actual SCR conditions. Accordingly, the following empirical power kinetic equation can be used to model kinetic data:

$$r_{NO} = k_C C_{NO}^{\alpha} C_{NH3}^{\beta} C_{O2}^{\gamma} C_{H2O}^{\delta} \qquad \text{(E1)}$$

The reaction order with respect to NO, called α, has been measured by many authors to be equal to one on vanadia-based catalysts[11-14]. Working in excess of oxygen and in the absence of water vapor or with water contents above 5%, the rate dependencies from oxygen and water can be neglected. Under these conditions, according to Wong and Nobe [13] (for V_2O_5/TiO_2), working with NH3/NO = 1, then Eq. (E1) reduces to:

$$r_{NO} = k_C C_{NO} \qquad \text{(E2)}$$

According to some authors[19,30], working with a sub stoichiometric NH_3/NO ratio (as actually occurs in industrial reactors to minimize ammonia slip) the rate dependence from C_{NH3} become relevant. In this case, β values near 0.2 have been measured [15]. Conflicting data are reported on the reaction order with respect to oxygen, generally found in the range 0-0.5 which has however been neglected by many authors because, in practical conditions, oxygen is in large excess. In any case, most authors agree that oxygen is involved in the reoxidation of the catalyst in a Mars-van Krevelen or ``redox" type mechanism. If this is true, dioxygen does interact with neither NO nor NH_3, and this is also an important indication for the details of the reaction mechanism. Some authors like Lietti et al. [12] concluded that the slow step of the SCR reaction is or can be associated to the catalyst oxidation step by oxygen. Water is a product of the SCR reaction, and interacts strongly with the surface of the catalysts, and possibly allowing the retention of high oxidation state. All authors agree that water hinders the SCR reaction (negative value of δ) although this effect is no more evident, on industrial catalysts, for H_2O levels above 5% (v/v)[16]. The inhibiting effect of water has been interpreted as an effect of a competition of H_2O with NH_3 on the reaction sites.

The kinetics of the DeNOx SCR reactions over vanadia-based catalysts has been investigated by several authors[17-19]; most of the studies refer to steady-state conditions and have been successfully applied to the design of SCR reactors. As previously reported, an Eley–Rideal mechanism is generally accepted for the DeNOx SCR reactions, which implies the reaction between adsorbed NH_3 and gas-phase NO. A kinetic expression which would well fit the observed dependency of the rate of reaction on ammonia, NO, oxygen, and water is given by:

$$r_{NO} = kcC_{NO}\theta_{NH3} \quad \text{(E3)}$$

where kc is the intrinsic chemical rate constant, C_{NO} is the NO gas-phase concentration, and θ_{NH3} represents the surface concentration of ammonia. In Equation (E3) the influence of oxygen has been neglected: this is correct for O2 concentrations higher than 1 to 2% v/v, since above this level the rate of reaction is almost independent of the oxygen content. By hypothesizing that ammonia and water compete for adsorption onto the active sites and that adsorption equilibrium is established for both species, the following relations hold:

$$\theta_{NH3} = K_{NH3}C_{NH3}\theta_l \quad \text{(E4)}$$

$$\theta_{H2O} = K_{H2O}C_{H2O}\theta_l \quad \text{(E5)}$$

where K_{NH3} and K_{H2O} are the adsorption equilibrium constants for NH_3 and H_2O, respectively, C_{NH3} and C_{H2O} are ammonia and water gas phase concentration, respectively, and θ_l is the concentration of the vacant surface active sites. Considering the site balance equation

$$(\theta_{NH3} + \theta_{H2O} + \theta_I = 1) \quad \text{(E6)}$$

and substituting (E4) and (E5) in (E3) the following Rideal rate expression is eventually obtained:

$$r_{NO} = k_c \cdot K_{NH3} \cdot \frac{C_{NH3} C_{NO}}{(1+K_{NH3} C_{NH3} + K_{H2O} C_{H2O})} \quad \text{(E7)}$$

is appropriate in the case of typical SCR applications, where a sub stoichiometric NH3/NO feed ratio is employed to minimize the slip of unconverted ammonia. However, considering that water practically does not affect the rate of NOx removal in the concentration range of industrial interest, namely above H2O = 5% v/v the kinetic dependence of water can be neglected in Equation (E7) and the following simplified rate equation can be adopted for practical purpose

$$r_{NO} = k'_c \cdot K_{NH3} \cdot \frac{C_{NH3} C_{NO}}{(1+K_{NH3} C_{NH3})} \quad \text{(E8)}$$

Few studies concerning the kinetics of the ammonia oxidation reaction have been published. Most authors agree that water has a strong inhibiting effect on the reaction [18,11,20], thus resulting in a significant increase of the selectivity of the process at high temperatures. The following kinetic expression has been typically considered [21]:

$$r_{NH3\_ox} = k_{NH3\_ox} \cdot \theta_{NH3} \quad \text{(E9)}$$

2.1.2 An example of a detailed mechanism

Just to show a different way to approach the description of the SCR reactions, without using global kinetic equation, it could be interesting to show an hypnotized detailed (step by step) mechanism of reaction. The reaction mechanism of (R1) may consists of 24 steps, in the idea of the Authors reported in [23], and involves ammonia dissociative adsorption on the vanadium atom. NO from the gas phase attacks the NH_2 moiety to evolve to the products. The catalyst is thus reduced and reoxidized with O2 to complete the catalytic cycle. The vanadyl oxygen would participate in the activation of ammonia but would not be its adsorption site. Several authors have recently performed ab initio calculations on finite models to analyze the stability of proposed intermediates. Anstrom et al. [22] used a hydrated tetramer cluster [V2O5_3H2O]2, and found that ammonia stabilizes in the first step as NH4 + on two vanadyl units in a vanadia cluster model. Ammonium then reacts with NO in a series of steps to form an adsorbed NH_2NO species, which undergoes decomposition to products by a ‘‘push–pull’’ mechanism. The main steps of the mechanism (illustrated here in Fig. 2.1) are the following:

$$\mathrm{VOH + NH_3 + O{=}V \rightarrow V{=}O{-}HNH_3{-}O{=}V}$$
$$\mathrm{V{=}O{-}HNH_3{-}O{=}V + NO \rightarrow V{=}O{-}H_3NNHO{-}O{=}V}$$
$$\mathrm{V{=}O{-}H_3NNHO{-}O{=}V \rightarrow VOH{-}H_2NNO + HOV}$$
$$\mathrm{V{=}O{-}H_2NNO{-}HOV \rightarrow VOH{-}HNNOH{-}O{=}V}$$
$$\mathrm{VOH{-}HNNOH{-}O{=}V \rightarrow VOH{-}HONNH{-}O{=}V}$$
$$\mathrm{VOH{-}HONNH{-}O{=}V \rightarrow V{=}O{-}HOH{-}N_2{-}HOV}$$

Figure 2.1 *Main steps of SCR mechanism*

The oxidation of the adsorbate takes place at step 3; the catalyst is reduced during this process.The next Fig. 7 shows the 24 steps detected for the SCR reaction (R1). Twenty-four steps from the reaction scheme calculated by Jug et al. [24]. NONH2 is formed at steps 3, 9, 16 and 22 and next evolves toward NH–NOH (balanced redox reaction) and N2. O2 is adsorbed at step 13 to give adsorbed OOH intermediate.

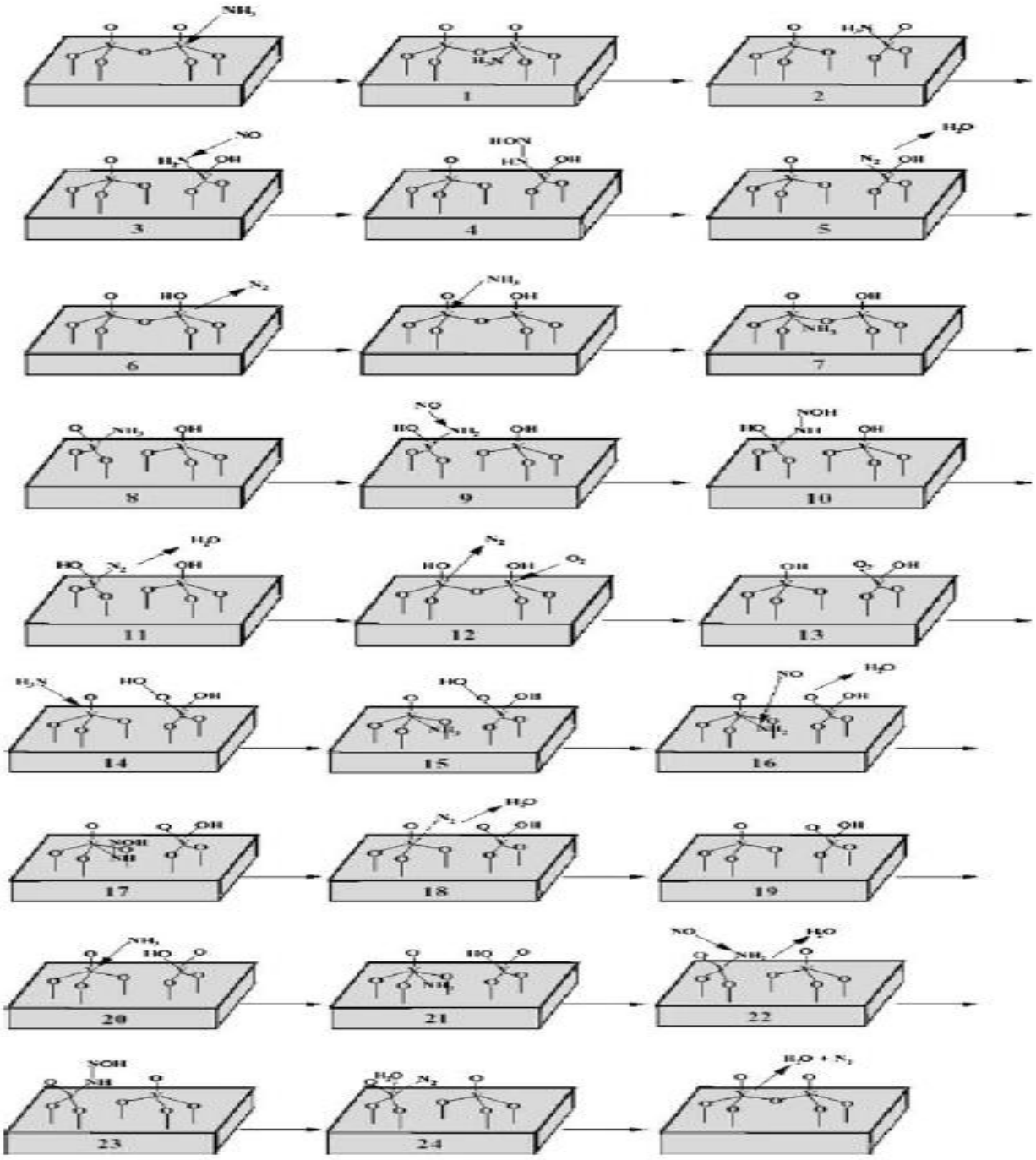

Figure 2.2 *The 24 hypothesized steps of SCR mechanism [23]*

kinetic data strongly suggest that ammonia reacts on all active catalysts from a strongly adsorbed state, whereas different opinions are available concerning the interaction of NO with the catalytic surface. To elucidate such aspects, the adsorption characteristics of the SCR reactants over V-based catalysts have been extensively investigated. It is considered the molecular adsorption of ammonia on the Lewis acid sites. Again, adsorption at the V and Ti sites is comparable, slightly larger than

that of molecular water but weaker than the dissociative one. At variance with water, the adsorption on the mixed cluster is smaller than that on pure titania cluster. The adsorption forming ONH_2 on V (with O transfer to Ti) and a hydroxyl group leads to the most stable structure as for that on V_2O_5. These adsorptions take place on terminal oxygen atoms bound to V atoms.

Heat of adsorption for the best adsorption modes on anhydrous $(TiO_2)_3$ and V_2O_5/TiO_2

Adsorbate	$N_\alpha - N_\beta$	Support	E_{ads} (kcal/mol)
NH_3: molecular on Ti	0	V_2O_5/TiO_2	49
NH_3: molecular on V*	0	V_2O_5/TiO_2	51.2
NH_3: molecular on Ti	0	$(TiO_2)_3$	45.8
NH_3: ONH_2 on V + OH on V*	2	V_2O_5/TiO_2	70.7

* There is an O transfer from V to Ti to avoid the dissociation of the 11A frame. The heat of adsorption includes the cost for the O migration. For the H adsorption energy, the reference energy is $1/2H_2$.

Figure 2.3 *The adsorption's activation energy on a commercial Vanadia-Titania catalyst*

The proposed model for NH3 adsorption is presented in the figure 2.4

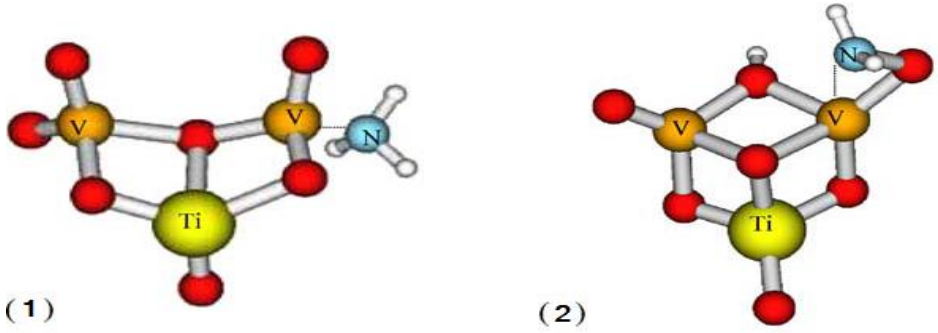

Figure 2.4 *Mechanism of adsorption for NH3[23]*

Since from 1998 Lietti et al. [25] studied the adsorption of ammonia over V-based catalysts and the transient kinetic. The dynamic adsorption-desorption of the SCR reactants (i.e. NH_3 and NO) in flowing He+1% v/v O2 has been investigated. A typical result obtained in the case of a rectangular step feed of ammonia performed at 220°C , over the V_2O_5-WO_3/TiO_2 model catalyst is presented in Fig.2.5

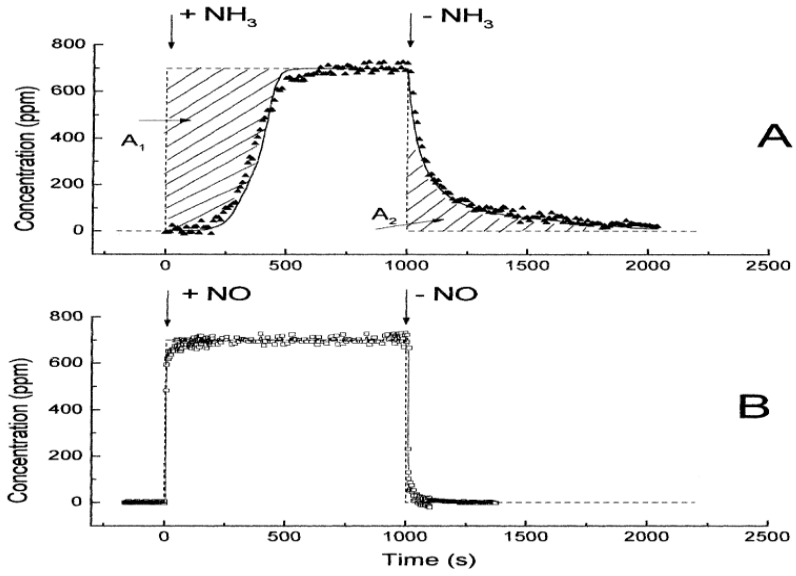

Figure 2.5 *Ammonia adsorption detected with delay time[26]*

Upon the NH_3 step addition (at t=0 s), the ammonia reactor outlet concentration slowly increased with time, approaching the ammonia inlet concentration (700 ppm) only after ≈500 s. This clearly indicates that ammonia is involved in adsorption -desorption processes at the catalyst surface. Along similar lines, upon the ammonia shut-off (t =1000 s) the reactor outlet NH3 concentration slowly decreases with time due to the desorption of previously adsorbed ammonia. Complete desorption of NH_3 is not yet achieved after 2200 s, as shown by the lower value of area A2 if compared with A1. This indicates that part of the pre-adsorbed ammonia is strongly adsorbed on the catalyst surface. The NH_3 dynamic adsorption-desorption experiments were also performed at higher temperatures, in the range 220-400°C. On increasing the catalyst temperature, the variations in the ammonia outlet concentration during the adsorption step are faster and the amount of ammonia adsorbed on the catalyst surface is reduced, in line with the increased rates of the adsorption-desorption processes and with the exothermicity of the NH_3 adsorption.

Chapter 3

The MARINTEK pilot engine: experiment and data collection

At the end of January 2012, Yarwil in cooperation with MARINTEK, The Norwegian Marine Technology Research Institut, which performs research and development for companies in the field of marine technology, made a four-days experimental campaign to test an application of SCR system in a "pre-turbo" configuration installed on a two-stroke engine.

3.1 The engine : Wichmann WX28 heavy fuel diesel 2-stroke engine

WICHMANN's commitment to the two-stroke loop-scavenged trunk piston concept was renewed in 1984 with the launch of its 295 kW/ cylinder WX28 engine (Figure 3.1). The simple 'valveless' approach had been proven in service by the Norwegian company's earlier AX, AXG and AXAG designs. The 280 mm bore/360 mm stroke WX28 covered an output band from 1180 kW to 4735 kW at 600 rev/min with four, five and six in-line and V8-, 10-, 12- and 16-cylinder models.

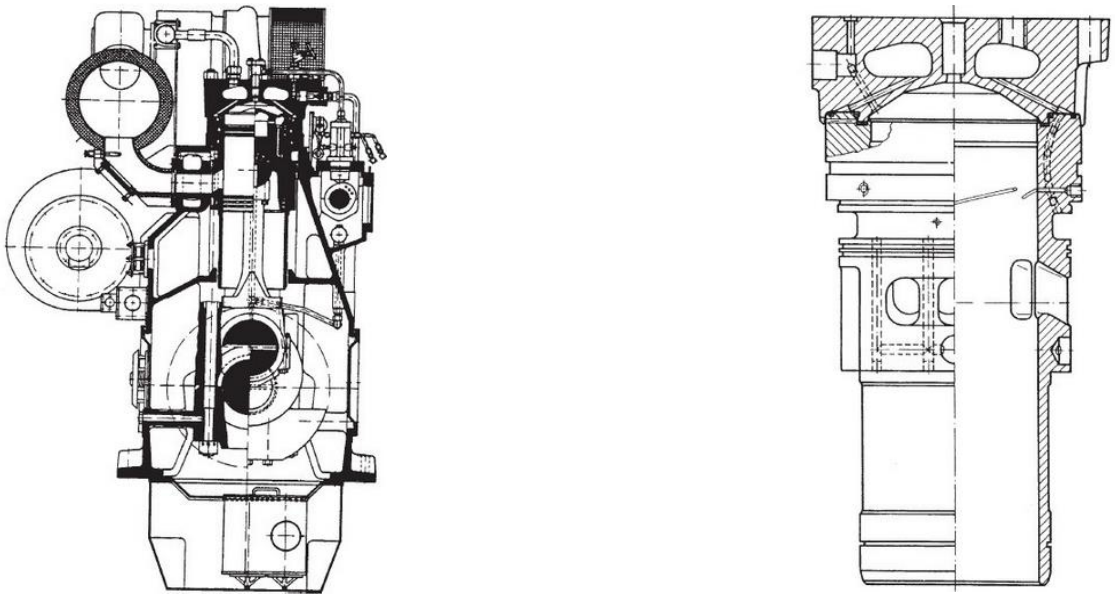

Figure 3.1 *Wichmann WX28L design and Bore-cooled cylinder liner and cover of Wichmann WX28 engine; separate cylinder lubrication is standard*

Development focused on low fuel and maintenance costs with high reliability. The engine was also claimed to be one of the lightest and most compact in its power class. The ability to operate on heavy fuel (180 cSt) under all conditions was another goal. A specific fuel consumption of 188 g/kWh resulted from enhanced scavenging and fuel injection systems, and a maximum combustion pressure of 140 bar is underwritten by rugged construction. The mean effective pressure is 13.5 bar.

The valveless cylinder cover is of simple construction, the lack of ducts for hot exhaust gas promoting uniform temperature distribution and low stress. Fastened by eight hydraulically tightened nuts, the cover can be removed in a few minutes and the piston withdrawn in 10 minutes. The connecting rod can be disconnected while leaving the big end bearing on the crankshaft; this feature reduces the necessary removal height. Wichmann stressed the overall simplicity of the engine and the impact on reliability and serviceability, citing fewer moving parts and hence fewer wearing parts. Separate cylinder lubrication—a standard feature—permits matching of the lubricating oil total base number to the fuel sulphur content. The oil is distributed over the cylinder surface by a hydraulic lubricator via four bores and quills.

Wichmann engines—including the earlier 300 mm bore/450 mm stroke AXAG design—found particular favour in the Norwegian fishing and offshore vessel propulsion sectors. A/S Wichmann became part of the Finland-based Wärtsilä Diesel group in 1986 and changed its name from Wärtsilä Wichmann Diesel in January 1994 to Wärtsilä Propulsion A/S (now Wärtsilä Propulsion Norway A/S). The Wichmann 28 engine, which remained in production until 1997, was released with the following specification:

Cylinder block: cast iron monobloc design with integrated crankcase, scavenging air receiver, water manifold and camshaft box; underslung type of crankshaft support.

Crankshaft: fully forged and machined in Cr–Mo steel; dimensionally laid out for 50 per cent power growth potential.

Cylinder liner (Figure 3.1): wear-resistant cast iron alloy; bore cooled with strong backed top section; balanced cooling water flow for efficient temperature control; separate cylinder lubrication through four quills.

Cylinder head: cast iron, valveless, simple design; bore cooled with strong backing to secure efficient cooling and low stress level.

Piston (Figure 3.2): oil-cooled composite design with cast iron skirt and steel crown; ring grooves hardened for low wear rate in heavy fuel operation; integrated small end bearing in full gudgeon pin length.

Connecting rod: drop forged and fully machined; separate large end bearing unit for easy piston withdrawal and low removal height.

Bearings: three-metal steel-backed type, interchangeable with main and crank journal.

Turbocharging: constant pressure system with auxiliary blower in series; the moderate speed auxiliary blower boosts the turbocharger effort to ensure an adequate air supply under all load conditions; the blower is engine driven via low pressure hydraulics using the engine lubricating oil and pump.

Fuel injection system: individual high pressure mono bloc pumps with built-in roller tappet; short high pressure pipes and temperature controlled nozzles for heavy fuel operation.

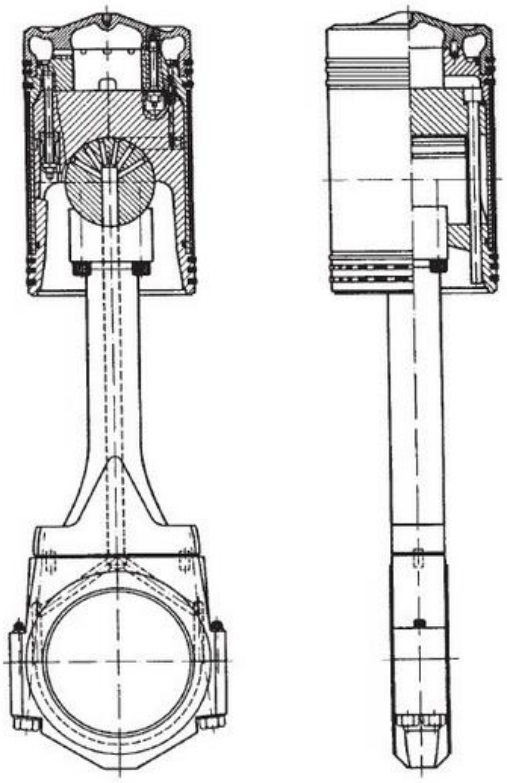

Figure 3.2 *Composite piston (high alloy steel crown, cast iron skirt and light alloy gudgeon pin support) and connecting rod of Wichmann WX28 engine*

Engine Speed	[rpm]	603
Torque	[Nm]	4733
BMEP	[bar]	13.4
Effective_eff	[%]	39.6
Turbine Speed	[rpm]	60340
Fuel Cons Diesel	[g/s]	17.55
Fuel Cons_s	[g/kWh]	211.3
Fuel Temp	[°C]	111.2
RootsBlaster Speed	[rpm]	1771
Power	[kW]	299

Table 3.1 *Engine test data WX28: Engine performance*

Figure 3.3 *The engine installed on the plan*

3.2 The MARINTEK test plan and Yarwil SCR system

The main scope of these experiments was to verify if the criteria used by Yarwil to design their SCR systems, specifically in terms of amount of catalyst and urea consumption, used so far in standard (atmospheric) conditions, can be used also for pre-turbo installations (under pressure).

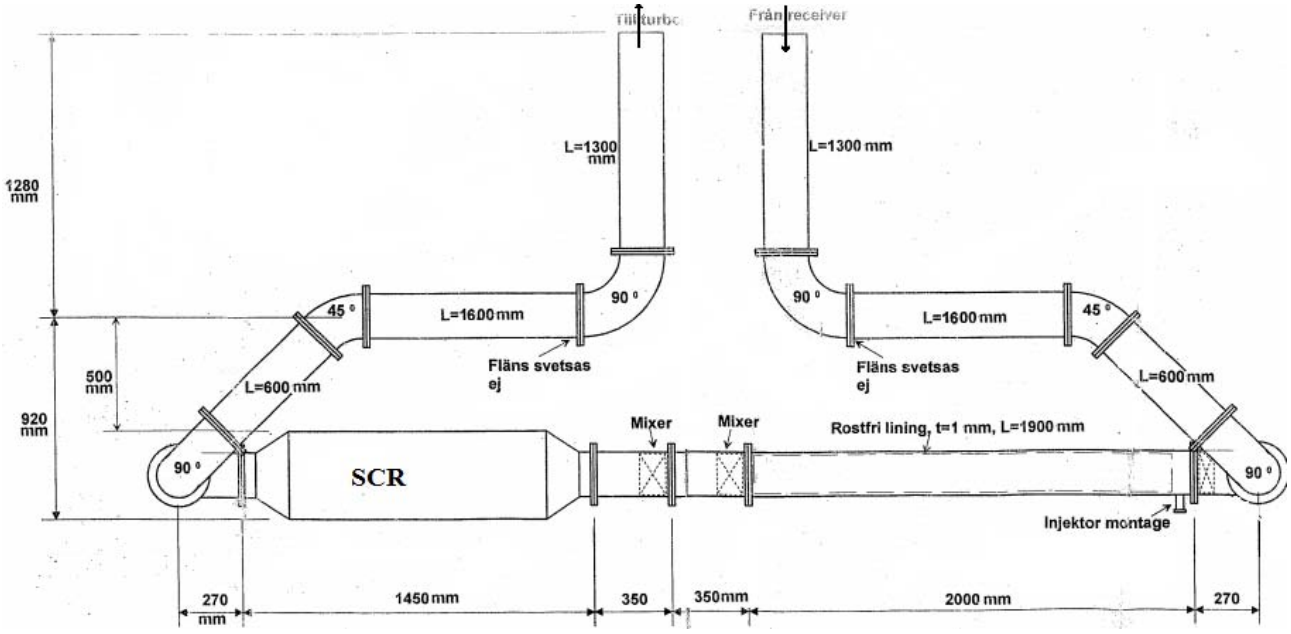

Figure 3.4 *Top view of the exhaust gas pipe, urea injection and SCR reactor*

As show in Figure 3.4, it was prepared a duct that provide 2.7 m available length between the Urea injection and the SCR system, and two static mixers to ensure a good distribution of ammonia in the pipe cross section.

The SCR reactor was sized using the "standard" equations provided by Yarwil. The reactor accommodates three modules in the cross-section and three modules in length, as show in the next figure

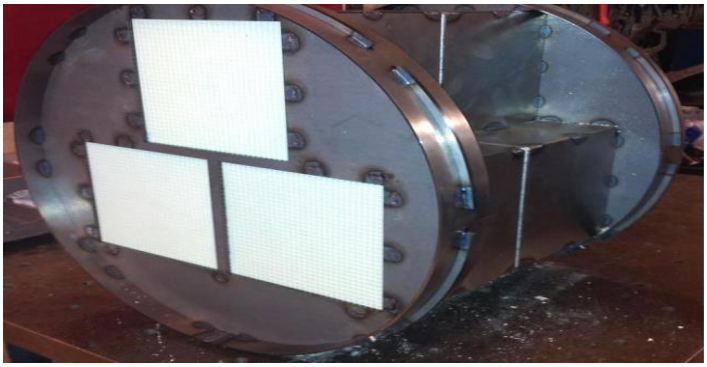

Figure 3.5 *The catalyst configuration*

3.2.1 The experiment: NOx Composition's values at different catalyst, configurations and engine loads

Yarwil intended to measure PM emissions, NOx emissions and temperature at the following engine loads:

- 60 %
- 75 %
- 100 %

In the following table it is possible to see the data collected from the engine manufacturer, compared with the data measured before the catalyst at the three different engine load. The gap between the two data is probably due to some inaccuracy during the measurement and to the different type of fuel used by the manufacturer to collect his data.

Engine Load	Power [kW]	Ex Flow Gas [g/s]	NOx conc. giv. [ppm]	NOx conc meas.[ppm]	Exhaust Temperature [°C]	Exhaust Pressure [bar]
60 %	180	505	1045	997	317	2.07
75 %	225	597	1033	990	354	2.4
100 %	299	734	1045	890	405	2.95

Table 3.2 *Data collected at the engine outlet*

The emission data were collected with the Horiba PG-250. The Horitiba PG-250 is a portable gas analyzer, that uses non-dispersive IR detection for CO, SO2 , CO2 and chemiluminescence (cross-flow modulation) for NOx [37]. Non-dispersive IR detection is based on electro-optically measuring of the gas concentration by the concentration's ability to absorb a specific wavelength in the infrared spectrum. The absorption indicates the concentration of certain gases. The weakness of such instruments is that many gases adsorb well in the infrared area and components may interfere in measurements as e.g. CO2 and H2O, and many others (SO2 , NO2) interfere with H2O.

For this reason we send the sample gas through a condensator removing the water vapour H2O before analyzed so the system get a dry air sample. As we don't know if NO2 and NH3 are cross-sensitive, and we will use the FTIR to measure the difference in NOx content between the two, sample.

Figure 3.6 *Horiba PG-250*

The data collected have a margin of uncertain, in particular compared with the emission baseline provided by the manufacturer .

Three different experiment settings were tested, with two different kind of catalyst, same amount of Vanadium content but different number of channels, and three different catalyst configurations for the 30x30 cells/module, one "standard" with three modules of 300 mm length each, and one with 12 modules of 60 mm each to see the effect of turbulence.

Experiment 1

This experiment was conducted with three layers of catalysts material, each one composed by three modules in the cross section, as shown in figure 3.5. The catalyst modules were provided by CERAM, one of the largest catalyst producer in the world. These modules have a quantity of vanadium equal to 1.25% v/v , and a specific area of 686m^2/m^3 that means 30x30 cells per module

The composition's data were collected after each layer, so for this experiment it is possible to see four values of NOx concentration, at the inlet of the catalyst, after 0.3 m (first layer), after 0.6 m (second layer) and at the end of the reactor, so after 0.9 m

The test was performed at the three different engine load to have the possibility to test different condition of temperature and pressure.

The data collected are shown in the next three figures of the reactor and the point of measurement:

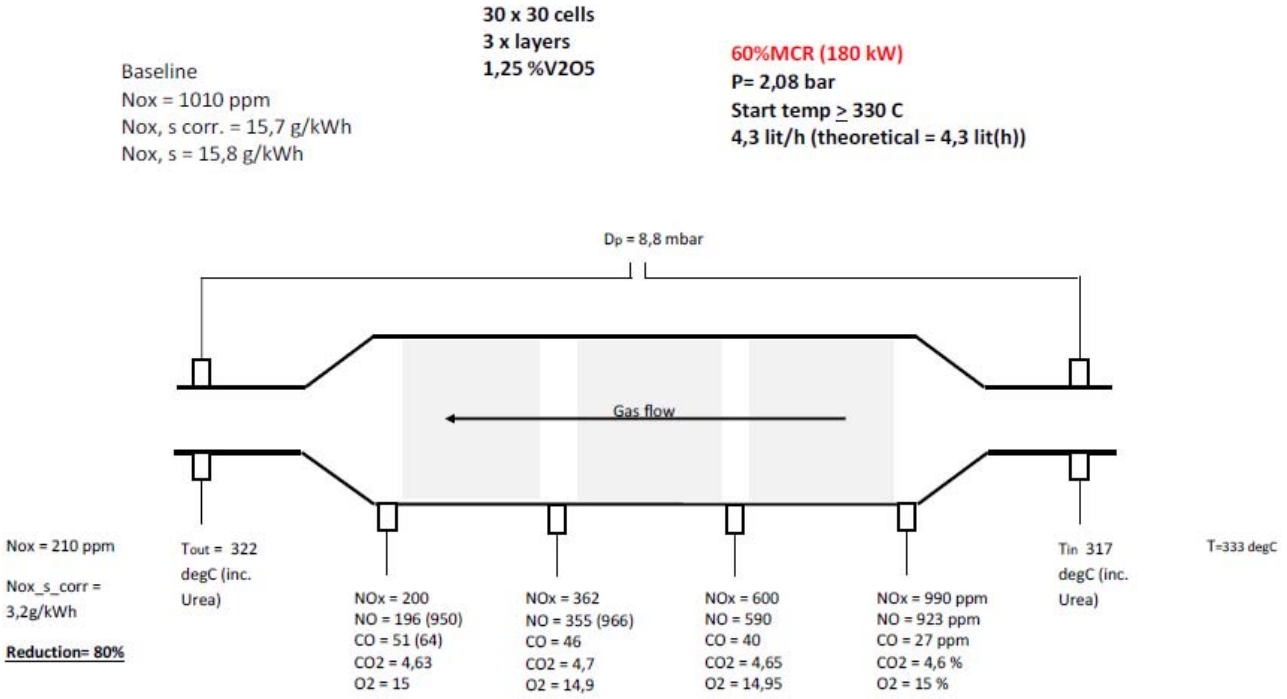

Figure 3.7 *Data collected at 60% engine load*

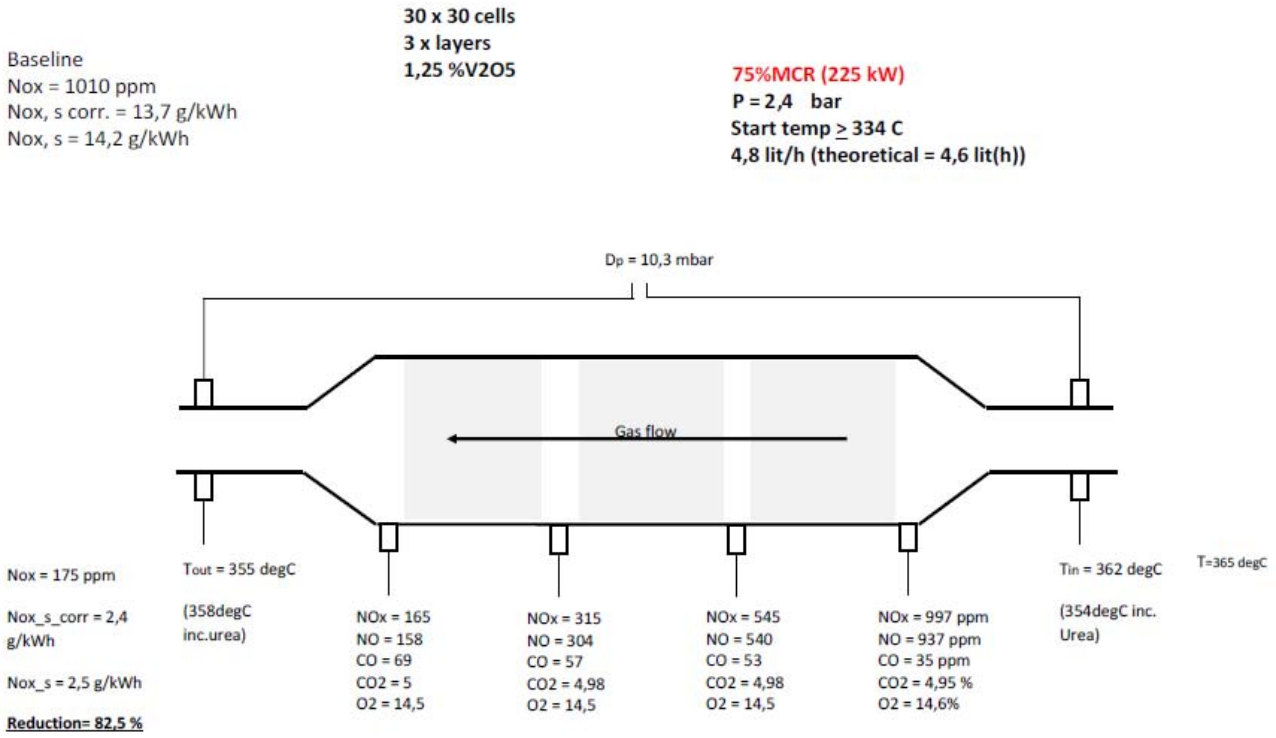

Figure 3.8 *Data collected at 75% engine load*

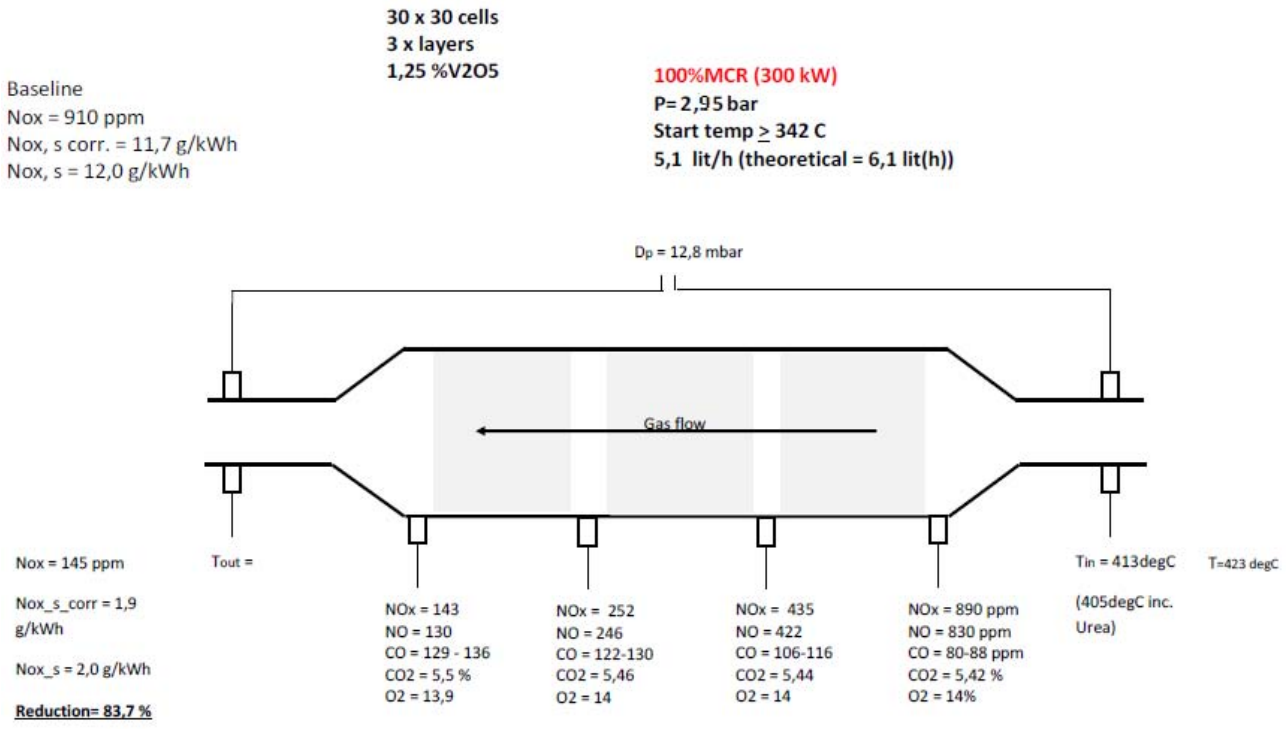

Figure 3.9 *Data collected at 100% engine load*

As easily shown in these figures, there are some inaccuracies in particular between the baseline(the baseline is shown in the high left corner) and the inlet data, and also between the data collected at

the end of the last catalytic layer and the data collected after the reactor. This was probably due to the different position of the instrument inside the duct and/or to the inaccuracy of some measurement. Nevertheless the inaccuracy in the amount of NOx is always less than 30 ppm.

Experiment 2

The second experiment was conducted on three modules in cross-section and three layers like the previous one, but in this case the catalyst used, also provided by CERAM, was a different type, the 40x40 cells per module that means a specific surface area of 801 m^2/m^3.

As easily shown in the next figures, that show the data collected, as expected there is more NOx conversion, due to the larger specific surface and to the less velocity inside the catalyst channel, that means larger residence time.

The data collected are shown in the next three figures of the reactor and the point of measurement:

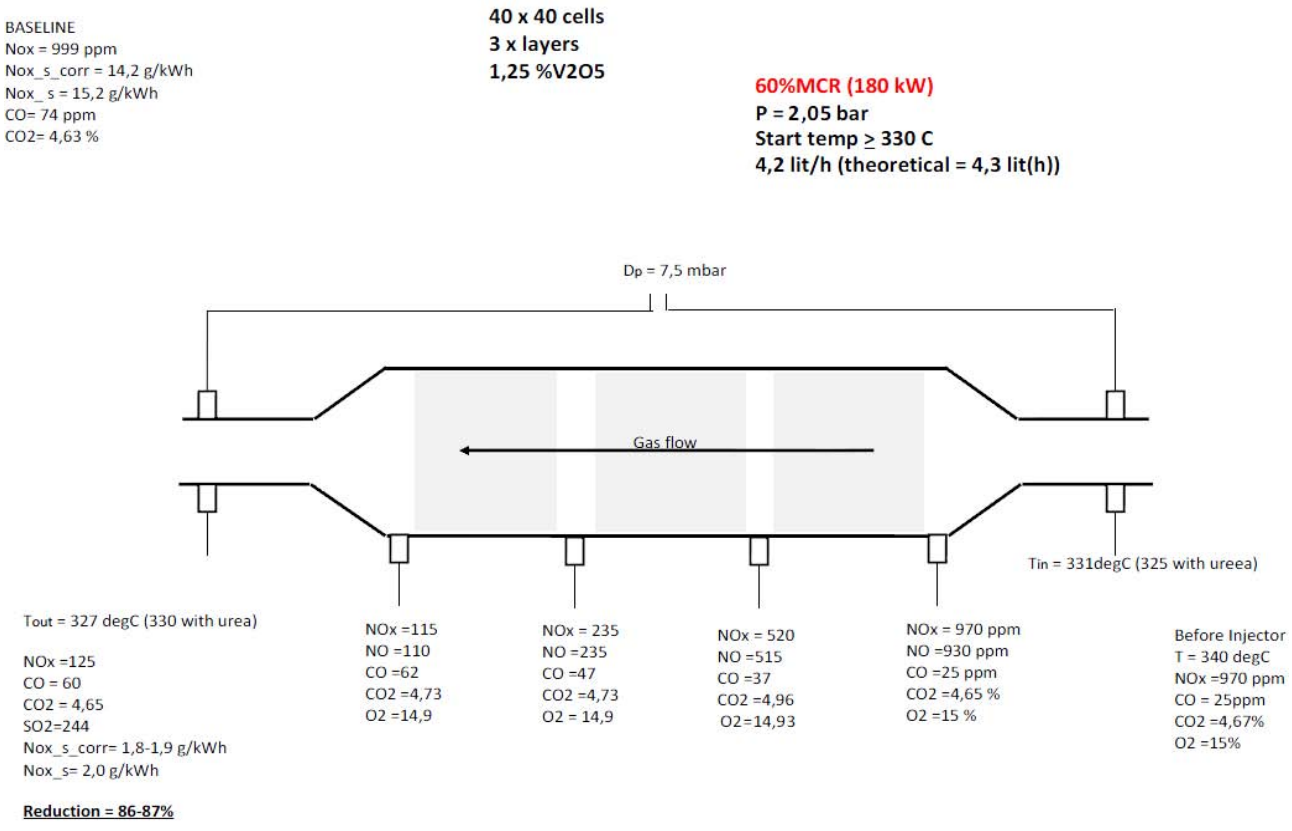

Figure 3.10 *Data collected at 60% engine load*

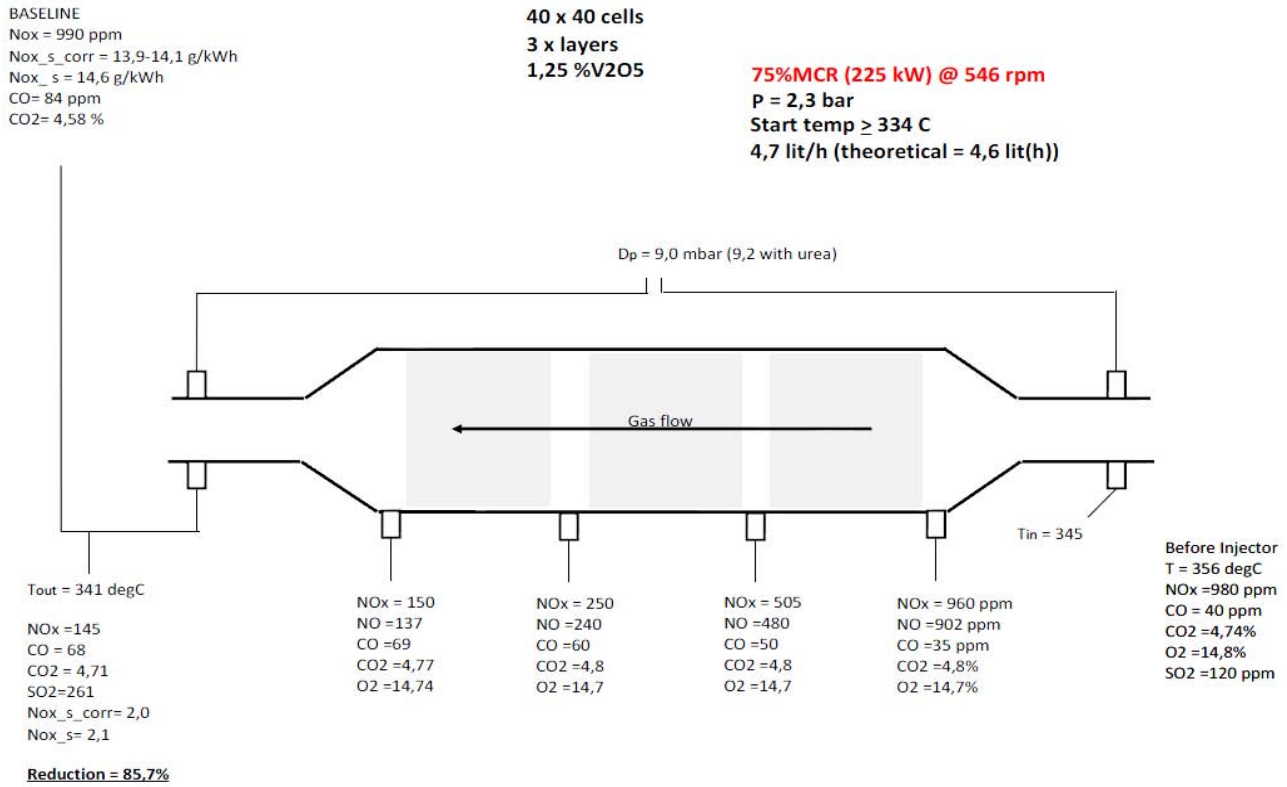

Figure 3.11 *Data collected at 75% engine load*

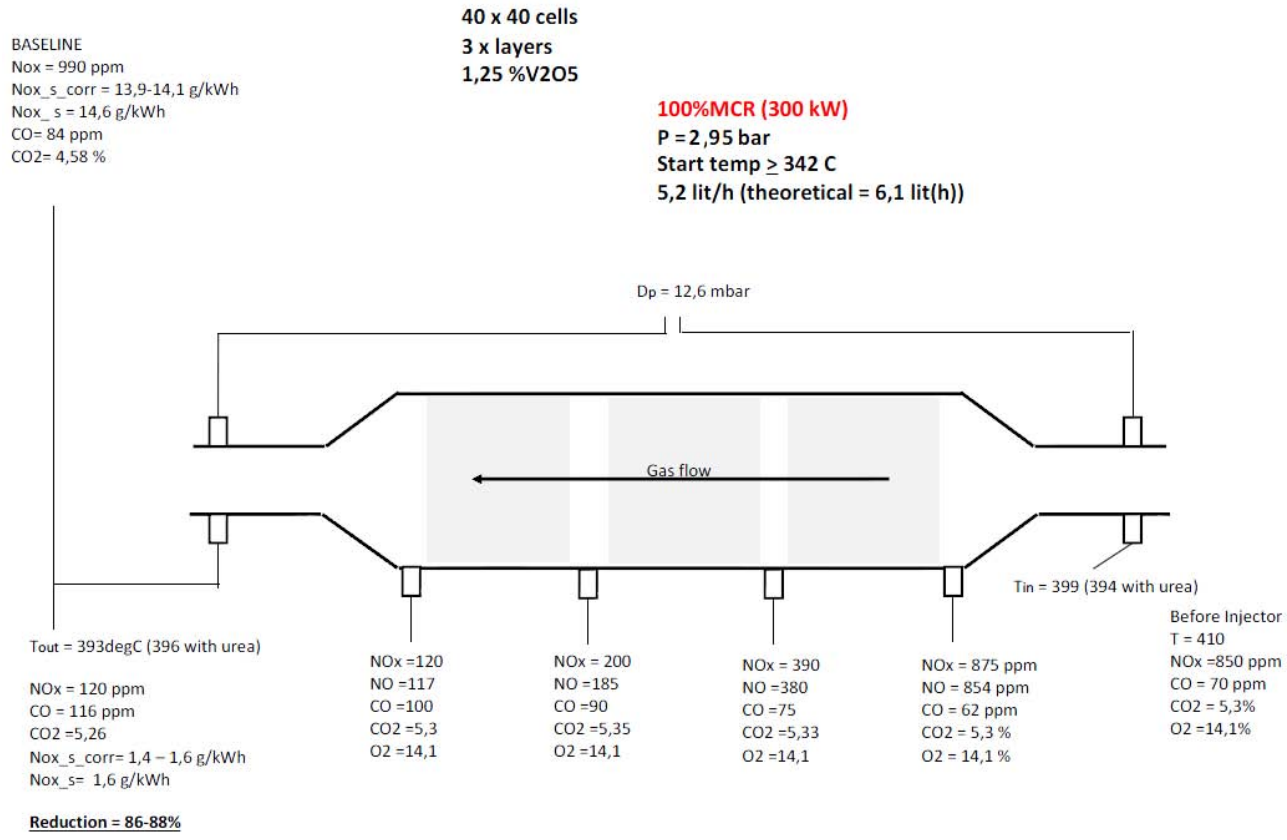

Figure 3.12 *Data collected at 100% engine load*

Also in these data it is possible to see some inaccuracies. Note that in all the experiments performed there was a problem with the SO_2 detector, so the data about the SO_2 concentration at the inlet of the reactor and the data of the $SO_2 \rightarrow SO_3$ conversion are not shown in the present work.

Experiment 3

The experiment 3 was performed with the same type of catalyst used for the experiment 1, so 30x30 cells/module that means a specific surface of 686 m^2/m^3. The only difference was the fluid dynamics configurations: the catalyst modules were broken in three thin layers of 60mm of length. This was done to try to improve the turbulence: in fact it is well known that inside the catalyst channel the flow is fully laminar, but the Yarwil researcher was thinking that a good way to generate turbulence could be to reduce the length of each layer, in order to not have a fully developed laminar flow inside the thin channel and to create a remixing after each layer.

In this experiment the data was collected every 2 layers, that means every 120 mm of catalyst. Just comparing the data, the researcher note that at 100% engine load the conversion was higher than the conversion at the same operating condition obtained with three standard catalyst layers.

The experiment was performed only at 75 and 100% of engine load.

The data collected and the points of measurement are shown in the next figures:

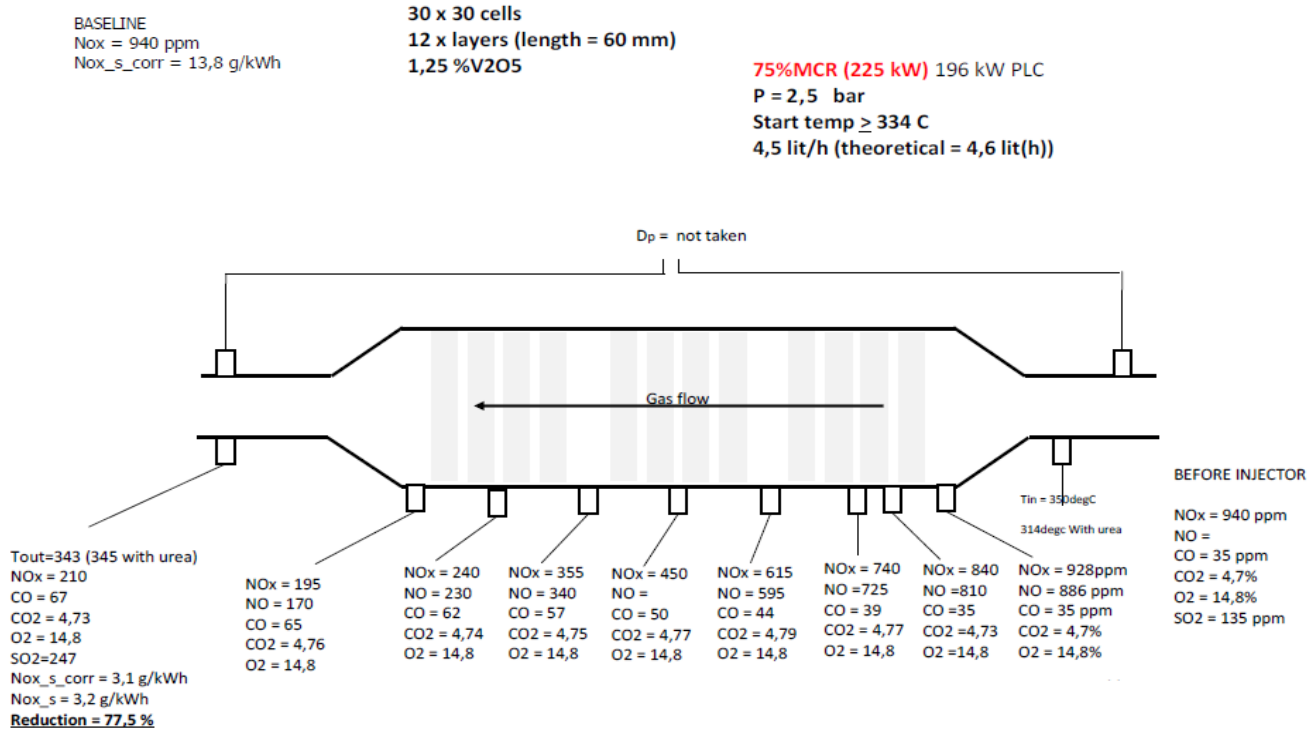

Figure 3.13 *Data collected at 75% of engine load*

As it is possible to see in the Figure 3.13 the conversion of NOx was lower than expected and also lower than the previous results (experiment 1)

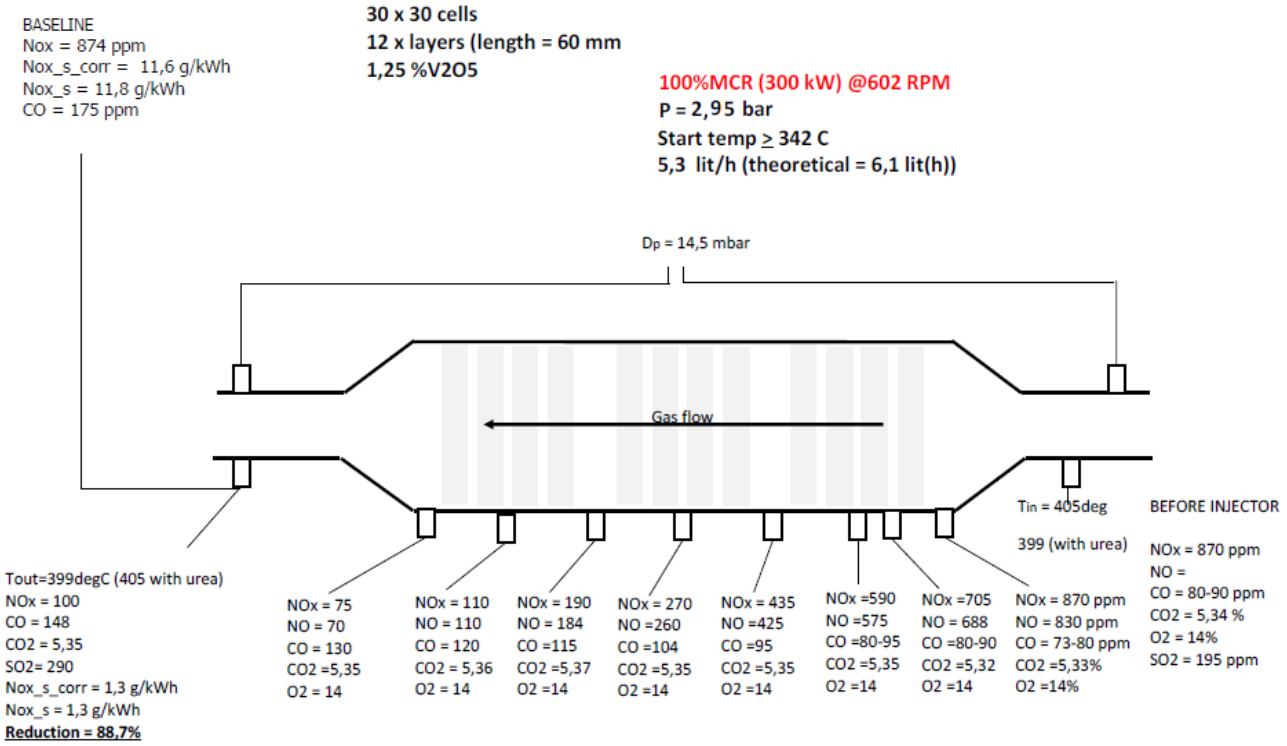

Figure 3.14 *Data collected at 100% engine load*

Chapter 4

Reactor models from literature

The approach to design and analysis of monolith SCR reactors customarily adopted in the early technical literature was based on simple pseudo-homogeneous models accounting only for axial concentration gradients. The effects of inter- and intra-phase mass transfer limitations were lumped into ‘‘effective’’ pseudofirst-order rate constants, such as k*NOx in Equation (E2), which were specific for each type of catalyst. Such constants actually varied not only with temperature, but also included dependences on the gas flow velocity, on the monolith channel geometry, and on the catalyst pore structure. Only from the beginning of the 1990s have efforts been devoted to a detailed chemical engineering analysis of monolithic SCR catalysts. All published modeling studies rely on a common set of basic assumptions:

(1) isothermal conditions: due to the small concentrations of NOx and NH_3 in the flue gases, typically of the order of hundreds of ppm, thermal effects associated with the de-NOx reactions are negligible for engineering purposes;

(2) laminar flow in the monolith channels: typical Reynolds numbers for industrial operation are below 1000-1500;

(3) isobaric conditions: negligible pressure drops are associated with laminar flow in straight monolith channels;

(4) negligible axial diffusion: convective transport is dominant under representative conditions;

(5) single-channel approach: if uniform conditions prevail over each cross-section of the monolith catalyst, modeling of a single monolith channel is adequate to represent the behavior of the whole SCR reactor.

However, published models differ in various aspects: (1) lumped (1D) versus distributed (2D, 3D) representation of the concentration fields; (2) account of interphase (gas/solid) and intraporous diffusional limitations; (3) developing versus fully developed laminar velocity profile; (4) nature of the rate expression for the de-NOx reaction; (5) inclusion of side reactions (SO2 oxidation, NH3 oxidation); (5) steady-state versus dynamic nature of the reactor model.

With the purpose to present a larger view of the models proposed in literature it can be interesting to describe 3 models:

4.1 The 1D models at Steady State

Buzanowski and Yang [44] first presented a simple one-dimensional analytical solution of the SCR reactor equations, which yields the NO conversion as an explicit function of the space velocity; unfortunately, this applies only to first-order kinetics in NO and zero order in NH3, which is not appropriate for industrial SCR operation. Lefers [45] reported a one-dimensional model of a SCR pilot plant, which, however, neglected the influence of internal diffusion. Beekman and Hegedus [46] published a comprehensive reactor model which includes Eley–Rideal kinetics and fully accounts for both intraand interphase mass transfer phenomena. Model predictions reported compare successfully with data. A single-channel, semi-analytical, one-dimensional treatment has also been proposed by Tronconi et al. [40]. The related equations are herein summarized as an example of steady-state modeling of SCR monolith reactors.

Dimensionless material balances for NO and NH_3 in the gas phase:

$$\frac{dC_{NO}}{dz*} = -4Sh_{NO}\left(C'_{NO} - C'_{NO,wall}\right) \tag{E10}$$

$$\alpha - C'_{NH3} = 1 - C'_{NO} \qquad @z* = 0 \quad C'_{No} = 1\,, C'_{NH3} = \alpha \tag{E11}$$

$$Sh_{NO} = 2.977 + 8.827(1000z*)^{-0.545}\exp(-48.2z*) \tag{E12}$$

Dimensionless material balances for NO and NH3 in the solid phase:

$$Sh_{NO} = \left(C'_{NO} - C'_{NO,wall}\right) = Sh_{NH3}\left(C'_{NH3} - C'_{NH3,wall}\right)\frac{De_{NH3}}{De_{NO}} \tag{E13}$$

$$Sh_{NO}\left(C'_{NO} - C'_{NO,wall}\right) = Da\left[C'^{2}_{NO} - Y_0^2 + 2(S_1 - S_2)\left(C'_{NO} - Y_0 - S_2 ln\frac{C'_{NO}+S_2}{Y_0+S_2}\right)\right]^{1/2} \tag{E14}$$

with

$$S_1 = \frac{De_{NH3}}{De_{NO}}C'_{NH3} - C'_{NO} \quad and \quad S_2 = S_1 + \frac{De_{NH3}}{De_{NO}}\frac{1}{K'_{NH3}} \tag{E15}$$

and

$$if\ S_1 \geq 0\,, Y_0 = 0; else\ Y_0 = -S_1 \tag{E16}$$

In Equations (E10)–(E16), concentrations of NO and NH3 are normalized with respect to the inlet NO concentration $C°_{NO}$, the dimensionless axial coordinate is z*=(z/dh)/ReSc (as **dh** being the hydraulic channel diameter), $Da=(k_{NO}D_{e,NO})^{1/2}dh/D_{NO}$ is a modified Damkohler number,

K_{NH3} $=K_{NH3}C°_{NO}$ is the dimensionless NH3 adsorption constant, Di is the molecular diffusivity of species i, De,i is the effective intraporous diffusivity of species i evaluated according to the Wakao–Smith random pore model [47]. Equation (E12) is taken from [50]. Equations (E14)–(E16) provide an analytical approximate solution of the intraporous diffusion–reaction equations under the assumption of large Thiele moduli (i.e., the concentration of the limiting reactant is zero at the centerline of the catalytic wall); the same equations are solved numerically in [30]. This model was successfully compared with laboratory data of NO conversion over commercial honeycomb SCR catalysts, as shown, for example, in Figure 4.1.

Notably, the effective diffusitivities of NO and NH3 were estimated from pore size distribution measurements, whereas intrinsic rate parameters were obtained from independent kinetic data collected over the same catalyst ground to very fine particles, so the model did not include any adaptive parameter. The model of [48] was later applied to evaluate the performance of an SCR catalyst with original composition [49]. More recently, Koebel and Elsener also compared on a fully predictive basis a similar model to experimental data of NOx conversion and NH3 slip obtained on a diesel engine

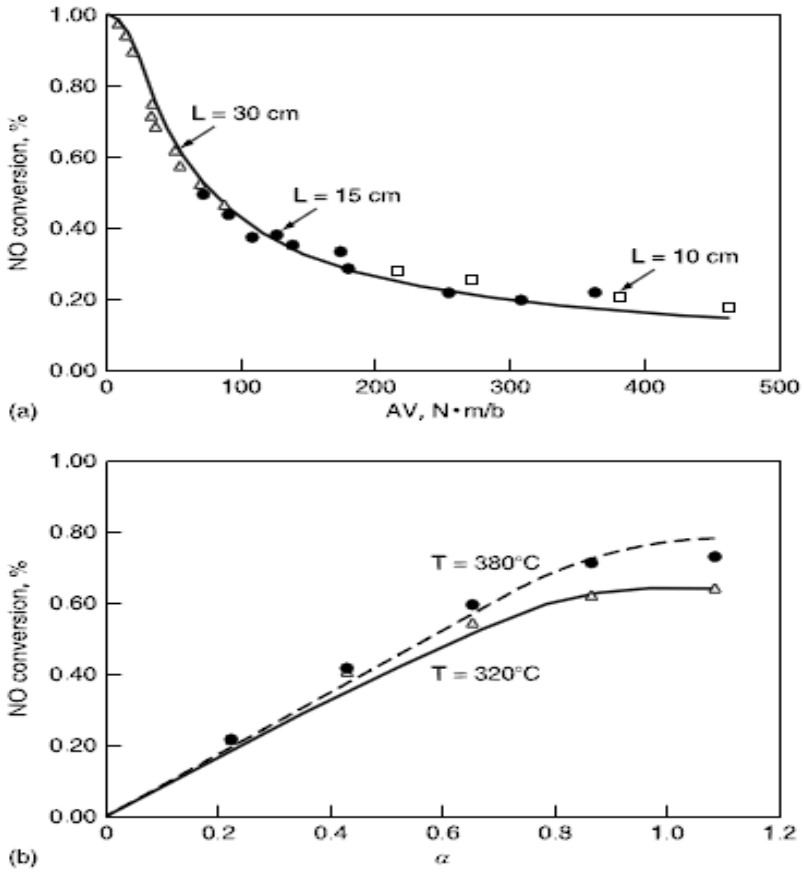

Figura 4.1 *Comparison of experimental and calculated effects of (a) monolith length and area velocity AV=volumetric flow rate/geometric surface area. Channel hydraulic diameter=6 mm, α=1.2, T=380°C, feed=500 ppm NO, 500 ppm SO2, 2% v/v O2, 10% H2O+N2. (b) α and T. Channel hydraulic diameter=6 mm, α=1.2, T=380°C, feed=550 ppm NO, 500 ppm SO2, 2% v/v O2, 10% H2O+N2. (From Tronconi, E., Forzatti, P., Gomez Martin, J.P., and Malloggi, S., Chem. Eng. Sci., 47, 2401–2406, 1992.)*

test stand [34]. In this case, the model was shown to describe qualitatively the performance of the SCR monolithic reactor, specifically with reference to the NOx conversion versus NH3 slip relationship; however, an exact quantitative match was found to be impossible. According to the authors, the reasons for the discrepancies may include unaccounted kinetic effects of the contaminants present in the diesel exhaust gases, uncertainties due both to the extrapolation of the kinetic parameters and to the measurement of the intraporous diffusivities, and the excessive simplification involved in the assumption of a pure Langmuir isotherm for NH3 adsorption. Recently, Ruduit et al. [50] have presented a three-dimensional steady-state model of a square-channel honeycomb SCR reactor for denitrification of exhaust gases from diesel engines. Such a model accounts for a few additional aspects previously neglected, namely hydrodynamic entrance effects and occurrence of direct NH3 oxidation as a side reaction. The latter point may be relevant for the correct prediction of the NH3 slip in commercial SCR reactors.

4.2 The Unsteady State 1D and 3D models

With the TRM, transient response method, the same used to show the delay in the NH_3 outlet that makes possible to measure the rate of ammonia adsorption, dynamics of the SCR reaction has been investigated as well. Accordingly, step feed experiments of NH_3, NO and O_2 have been performed, while keeping constant the concentration of the other reactants. They observed that The evolution with time of N_2 is specular to that of NO. After 300 s, the reactor outlet NO concentration (and hence the NO conversion) is virtually constant, whereas the NH_3 concentration is still increasing. This is a clear indication of the fact that the NO conversion does not depend on the ammonia surface coverage (θ_{NH3}) for θ_{NH3} values above a characteristic `critical' value.

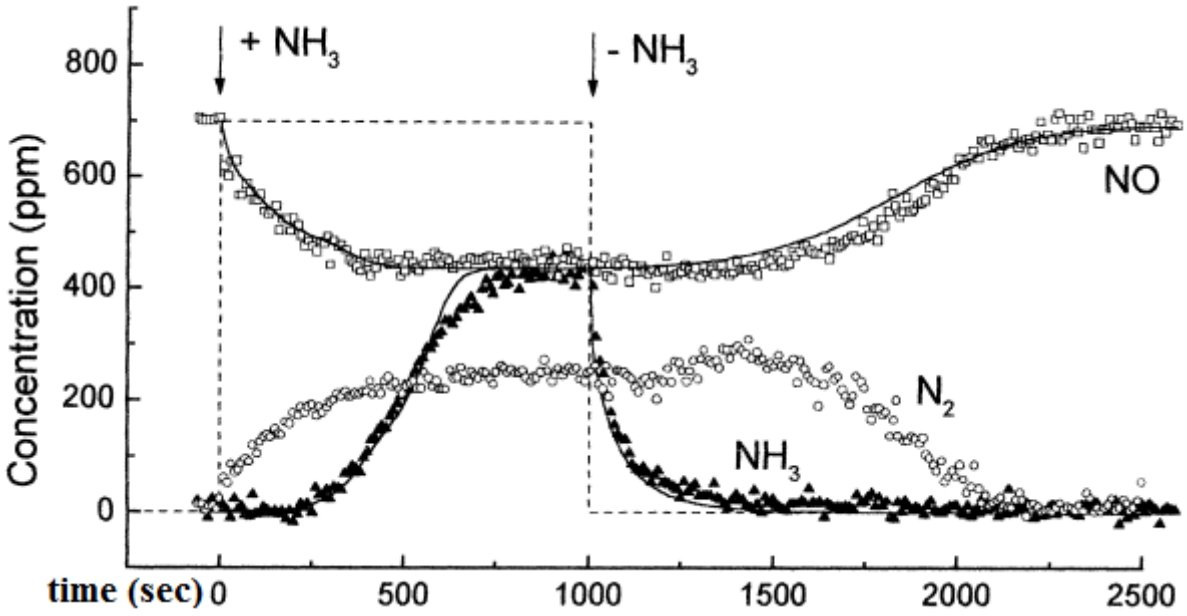

Figure 4.2 *Composition's data collected outlet the reactor*

A different transient behavior is observed upon the NH_3 shut-off (t=1000 s). Indeed whereas the NH_3 concentration dropped to zero, the NO concentration signal was not apparently affected; only after several minutes it began to increase up to the inlet concentration value. Again this indicates that the rate of the SCR reaction does not depend on NH_3 above a characteristic `critical' value. The fact that NO is consumed even in the absence of gas-phase ammonia suggests that a `reservoir' of adsorbed ammonia species available for the reaction is present on the catalyst surface. Similar results were obtained by performing the NH3 step-feed experiments at higher temperatures (280 and 350°C). In particular on increasing the reaction temperature: (i) the steady-state NO conversion is increased, (ii) the NH_3 and NO steady-state concentration levels are more rapidly reached; (iii) the `dead time' in the variation of the NO concentration that is observed upon the ammonia shut-off

is reduced. This results have been analyzed according to a dynamic one-dimensional heterogeneous PFR model and fitted by nonlinear regression to provide estimates of the relevant kinetic parameters. Under these hypotheses, the unsteady mass balance of NH_3 on the catalyst surface and of NH_3 and NO in the gas phase were written:

Unsteady mass balances of NH_3 on the catalyst surface (1) and of NH_3 (2) and NO (3) in the gas phase

$$\frac{\partial \theta_{NH_3}}{\partial t} = r_a - r_d - r_{NO} \quad (1)$$

$$\frac{\partial C_{NH_3}}{\partial t} = -v\frac{\partial C_{NH_3}}{\partial z} + \Omega(r_d - r_a) \quad (2)$$

$$\frac{\partial C_{NO}}{\partial t} = -v\frac{\partial C_{NO}}{\partial z} - \Omega\, r_{NO} \quad (3)$$

Figure 4.3 *Species balance with dynamic PFR model of reactor*

where C_{NH3} and C_{NO} represent the NH_3 and NO gas-phase concentration; r_a, r_d and r_{NO} the rate of adsorption, desorption and of NO consumption, respectively; ν is the interstitial gas velocity, z the reactor axial coordinate and Ω the catalyst NH_3 adsorption capacity. NH_3 adsorption occurs via a non-activated process, described by the rate expression:

$$r_a = k°_a \cdot C_{NH3} \cdot [1 - \theta_{NH3}] \quad \text{(E17)}$$

with k_a^0 is a constant. Lietti et al. also hypothesized an activated kinetic rate expression for desorption:

$$r_d = k°_d \cdot \left[\exp\left(-\frac{E_d}{RT}\right)\right] \cdot \theta_{NH3} \quad \text{(E18)}$$

Different dependence of E_d on θ_{NH3} have been used, including E_d =constant (Langmuir) and more complicate expressions that take into account the catalyst surface heterogeneity.

Also for SCR reaction different rate expressions have been tested, from (E3) to something that take in account the critical value for the NH3 surface concentration θ^*_{NH3}:

$$r_{NO} = k_{NO} \cdot C_{NO} \cdot \theta_{NH3}\left[1 - \exp\left(-\frac{\theta_{NH3}}{\theta^*_{NH3}}\right)\right] \quad \text{(E19)}$$

In this case the rate of reaction is considered independent on θ_{NH3} above a critical NH3 surface concentration value, as showed in the experimental data. The estimates of the kinetic parameters used in the data fit are

Parameters	V_2O_5–WO_3/TiO_2	V_2O_5/TiO_2
k_a^o (m^3/mol s)	0.614	0.820
k_d^o (l/s)	1.99×10^5	3.67×10^6
E_d^o (kcal/mol)	23.4	25.8
α	0.448	0.310
Ω (mol/m^3)	270	209
k_{NO}^o (m^3/mol s)	8.39×10^5	1.08×10^6
E_{NO} (kcal/mol)	14.2	16.0
$\theta^*_{NH_3}$	0.108	0.076

Figure 4.4 *Parameters value used in this model*

With the additional eq. for $E_d = E_d^0(1-\alpha\ \theta_{NH3})$.

The team led by prof. Pio Forzatti, University of Milan, had extensively studied the unsteady state SCR kinetic . In the 2000 and 2001 I. Nova et al. [26] use the same eq. model of [25], just add the ammonia oxidation rate equation in the dynamics balances.

$$\frac{\partial\theta_{NH_3}}{\partial t} = r_a - r_d - r_{NO} - r_{ox} \qquad \frac{\partial C_{NO}}{\partial t} = -v\frac{\partial C_{NO}}{\partial z} + \Omega_{NH_3} r_{NO}$$

$$\frac{\partial C_{NH_3}}{\partial t} = -v\frac{\partial C_{NH_3}}{\partial z} + \Omega_{NH_3}(r_a - r_d - r_{NO} - r_{ox}) \qquad \frac{\partial C_{N_2}}{\partial t} = -v\frac{\partial C_{N_2}}{\partial z} - \Omega_{NH_3}(r_{NO} + 0.5r_{ox})$$

Their results agree with those previously shown, almost the same values was obtained for all the parameters.

Chen-Tan Model

The model proposed by Chyi-Tsong Chen and Wei-Lun Tan, Department of Chemical Engineering, Feng Chia University, Taiwan, is one of the few models that apply 3D equations: This model use a simple kinetic and devotes much more attention to the fluid dynamic.

The reaction mechanism for the reduction of NO using NH3 over catalyst is described as previously but taking in to account just R1 and R5 (see 2.1.1), with the following rate equations:

$$r_1 = k_1 C_{NO} \frac{aC_{NH3}}{1+aC_{NH3}} \qquad \text{(E20)}$$

$$r_2 = k_2 C_{NH3} \quad \text{(E21)}$$

In the above expressions, the reaction constants are assumed to obey the Arrhenius law as follows:

$$k_i = A_i \exp(\frac{E_i}{R_g * T}) \quad \text{(E22)}$$

$$a = A_0 \exp(\frac{E_0}{R_g * T}) \quad \text{(E23)}$$

where Ei is the activated energy (J/mol), Rg is the gas constant (J/ mol K) and T the temperature (K); The transport phenomena through individual part are described as follows: **Inert portion**:

$$\rho \frac{\partial u}{\partial t} + \rho(u \cdot \nabla)u = \nabla \cdot [-Pl + \eta(\nabla \mathrm{u}) + (\nabla u)^T - \frac{2\eta}{3}(\nabla u)I] \quad \text{(E24)}$$

$$\frac{\partial \rho}{\partial t} + \nabla(\rho u) = 0 \quad \text{(E25)}$$

Note that (E24) describes the slightly compressible behavior due to the gas flow, and (E25) is the equation of continuity.

Catalyzed bed:

$$\left(\frac{\rho}{\varepsilon_p}\right)\frac{\partial u}{\partial t} + \left(\frac{\eta}{k} + Q\right)u = \nabla \cdot [-Pl + \left(\frac{1}{\varepsilon_p}\right)\left(\eta(\nabla \mathrm{u}) + (\nabla u)^T - \frac{2\eta}{3}(\nabla \mathrm{u})\mathrm{I}\right) \quad \text{(E26)}$$

$$\frac{\partial \varepsilon_p \rho}{\partial t} + \nabla(\rho u) = 0 \quad \text{(E27)}$$

$$\frac{\partial C_i}{\partial t} + \nabla(-D\nabla C_i + uC_i) = R_i \quad \text{(E28)}$$

(E26) is the Brinkman equation used to express the flow dynamics through the porous solid catalyst, while (E27) and (E28) are respectively the equation of continuity and mass transfer in the catalyst bed. Note that the Brinkman equation [38] is a generalization of Darcy's law that facilitates the matching of boundary conditions at an interface between the larger catalyst pores and the permeable medium. Besides, the mass-balance equations in (E28) are the diffusion-convection equations at unsteady state, where the term Ri corresponds to the species' net reaction rate, which is a function of the reaction rates and the reaction stoichiometry. In this paper we ignore the heat transfer in the reactor because the concentrations of reactants are extremely low and the energy

accumulation is insignificant [39]. Since the diffusion coefficient and gas viscosity are dependent of temperature and pressure, the following corrections are used [40]:

$$D = 2.695 \times 10^{-3} \frac{\sqrt{T^3(M_i+M_0)/(2\times10^3 M_i M_0)}}{P\sigma_i\sigma_0\Omega_D} \quad \text{(E29)}$$

$$\eta = 2.699 \times 10^{-6} \frac{\sqrt{T(1\times10^3 M)}}{P\sigma^2\Omega_V} \quad \text{(E30)}$$

where Mi and Mo are the molar mass (kg/mol), and σi and σo the diameters (m) of the gas species. Besides, P is the pressure (Pa) and Ω_D and Ω_V are collision integrals [40]. The nominal operating condition and physical properties of the SCR reacting system are listed in Figure 2.9. To this end, it should be mentioned that the proposed 3D dynamic model, which is quite different from the previous one- and two-dimensional steady-state models of monolith reactors [41] and the one-dimensional dynamic PFR model for SCR [42], can facilitate the investigation of the interior transport phenomena through porous catalyst and the spatial concentration distribution inside the SCR reactor.

Parameters	Physical meaning	Value	Unit
L	Length of reactor	0.1	m
L_c	Length of catalyzed bed	0.03	m
L_D	Diameter of the reaction tube	0.02	m
u	Inlet velocity	0.058	m/s
C_{NO}	Inlet NO concentration	330	ppm
NH_3/NO	NH_3-to-NO ratio	1	–
GHSV	Gas hourly space velocity	7000	h^{-1}
T	Operation temperature	573	K
p	Pressure	101,325	Pa
ε_p	Porosity	0.4	–
κ	Permeability	1×10^{-8}	m^2
R_g	Gas constant	8.3141	J/mol K

Figure 4.5 *The nominal operating condition and physical properties of the SCR reactor*

This model was solved by the authors using COMSOL Multiphysics and, for our purpose it results more complicated than other and less used and tested, so it doesn't appear a good idea to use a complicate model to extrapolate the data in different conditions, as higher pressure.

Yun-Kim Model

Another model, develop by Byoung Kyu Yun, Man Young Kim from Department of Aerospace Engineering, Chonbuk National University, show almost the same approach to the problem: they

need to find the workable reaction parameters for practical use for a commercial V2O5 SCR catalyst and to investigate the effects of such various parameters as the space velocity, O2 and H2O concentrations, and NO2/NOX and NH3/NOX ratios on the NOX conversion efficiency, using the same kinetic as shown by Lietti et al. [42].

Under the assumption that radial transport effects of a honeycomb- type catalyst are small compared to the heat transport in axial direction, the entire converter can be represented by one single channel. The effects taking place are convective, diffusive and conductive transport in the gas phase, mass and energy transfer through the boundary layer, diffusion and catalyst in the washcoat, and conduction in the solid phase. Neglecting radial gradients in the channel, transient and 1D (in axial direction) conservation equation suffice to describe the thermo- and fluid dynamic. The differential conservation equations for mass momentum and energy of a single channel can be written as shown:

$$\frac{\partial \rho_g}{\partial t} = \frac{\partial \rho_g \cdot v_g}{\partial z} \tag{E31}$$

The gas phase continuity, and the momentum conservation:

$$\frac{\partial P_g}{\partial z} = -A_D \cdot v_g \tag{E32}$$

Where A_D is the Darcy's constant, that can be described as

$$A_D = \varphi \cdot \frac{v_g}{2} \frac{\rho_g}{d_{hy}} \cdot \zeta \tag{E33}$$

d_{hy} is the hydraulic channel diameter and z is a friction coefficient. The factor 4 is called Fanning friction factor and takes into account deviations from round channel cross sections. The friction factor z is typically described as a function of the Reynolds Number Re and changes depending on the flow regime.

The species conservation equation is given by an equation that depend by the mass fraction of the species, the Deff, effective diffusive coefficient, given by the physical property Di and the morphological properties of the catalyst, as porosity and tortuosity.

The kinetic part was described by the rates of three reaction, the "standard SCR" (R1), the "fast SCR" (R2) and the partial oxidation of ammonia (R5). To describe this reactions were used the follow general formulas, with a nonlinear regression of the parameters:

$$Ri = \frac{Ai \cdot \exp(\frac{Ei}{RT}) \cdot \Pi_{REACTANT}}{Gi} \quad \text{(E34)}$$

Where Ai and Ei are the pre exponential factor and the activation energy for the Arrhenius expression and Gi take in accounts for the inhibition effects of the surface coverage of the species.

This model was used to simulate the effects of the operative variable and of the composition of the flue gas, as NO/NH_3 ratio or NO/NO_2 and the total amount of oxygen and water.

Nevertheless this model use a general expression for the rates of reaction, with the parameter fitted only on the data collected by the authors. A large part of the researchers that work in the SCR modeling agree to use the expression given by the work of the team of University of Milan, Forzatti, Tronconi et al. [11,12,16-19], maybe correcting the parameters if is used a different type of catalyst (means a different amount of Vanadia oxide).

Almost for the same reasons the other models that implement momentum equation were discarded

4.3 Selected Model for SCR pre-turbo application on marine two-stroke engines (1D+1D)

The main purpose of this work is to try to test a model, developed for atmospheric SCR application, under high pressure condition.

To do this safely, it was necessary to choose a consolidated reactor model, well known, that fit extremely well the experimental data previously collected in atmospheric pressure experimental campaign.

The selected model was the one nowadays used by prof. Tronconi and his team at the University of Milan and reformulated for steady state operations. It is called 1D+1D because it solves the species balances in two dimension, along the reactor and inside the pore.

A kinetic model of NH_3–SCR over V-based catalysts, developed and reported in [29,30] has been used for the estimation of the rate parameters by multi-response non-linear regression of data collected in the micro-reactor runs, based on a dynamic one-dimensional isothermal isobaric heterogeneous plug flow model of the test micro-reactor. The adopted kinetic scheme includes global steps for NH3 adsorption and desorption, NH_3 oxidation and NH_3–NO–NO_2 reactivity, as shown in figure 2.9

R.1	NH_3 adsorption	$S_2 + NH_3 \rightarrow S_2[NH_3]$	$r_{ads} = k_{ads} C_{NH3} (1 - \theta_{NH3} - \theta_{HNO3})$
R.2	NH_3 desorption	$S_2[NH_3] \rightarrow S_2 + NH_3$	$r_{des} = \exp\left[k_{des} - \frac{E_{des}}{RT}(1 - \alpha\theta_{NH3})\right]\theta_{NH3}$
R.3	NH_3 oxidation	$S_2[NH_3] + \frac{3}{4} O_2 \rightarrow \frac{1}{2} N_2 + 3/2\ H_2O$	$r_{ox} = \exp\left(k_{ox} - \frac{E_{ox}}{RT}\right)\theta_{NH3}\left(\frac{p_{o2}}{0.02}\right)^{0.275}$
R.4	Standard SCR	$NO + S_2[NH_3] + \frac{1}{4}O_2 \rightarrow N_2 + 3/2H_2O + S_2$	$r_{NO} = \exp\left(k'_{NO} - \frac{E_{NO}}{RT}\right) C_{NO}\theta_{NH3} / \left[\left(1 + K_{NH3}\frac{\theta_{NH3}}{1-\theta_{NH3}}\right)\left(1 + k_{o2}\frac{C_{NO}\theta_{NH3}}{p_{o2}^{1/4}}\right)\right]$
R.5	Fast SCR	$NO + S_2[HNO_3] + S_2[NH_3] \rightarrow N_2 + 2H_2O + NO_2 + 2S_2$	$r_{fst} = \exp\left(k_{fst} - \frac{E_{fst}}{RT}\right)\theta_{NH3}\theta_{HNO3}C_{NO}$
R.6	Nitrates formation	$2NO_2 + S_2[NH_3] \rightarrow N_2 + H_2O + S_2[HNO_3]$	$r_{amm} = k_{amm} C_{NO2}^2 \theta_{NH3}(1 - \theta_{NH3} - \theta_{HNO3})/\theta_{HNO3}$
R.7	Nitrates adsorption	$S_2 + HNO_3 \rightarrow S_2[HNO_3]$	$r_{ads\_nit} = k_{ads\_nit} C_{HNO3}(1 - \theta_{NH3} - \theta_{HNO3})$
R.8	Nitrates desorption	$S_2[HNO_3] \rightarrow S_2 + HNO_3$	$r_{des\_nit} = k_{des\_nit}\theta_{HNO3}$
R.9	NO_2 SCR	$S_2[NH_3] + \frac{3}{4}$ NO2 $\rightarrow$ 7/8 N_2 + 3/2 H_2O	$r_{NO2} = \exp\left(k_{NO2} - \frac{E_{NO2}}{RT}\right)\theta_{NH3}C_{NO2}$
R.10	N_2O formation	$S_2[NH_3] + S_2[HNO_3] \rightarrow N_2O + 2H_2O + 2S_2$	$r_{N2O} = \exp\left(k_{N2O} - \frac{E_{N2O}}{RT}\right)\theta_{NH3}\theta_{HNO3}$

Figure 4.6 *List of reactions and rate expressions which may be included in the kinetic model*

The model presented in this work, as said before, accounts also for intra-porous diffusion within the catalytic substrate. Taking into account this effect the model is able to simulate coated as well as

extruded catalysts. The intrinsic kinetics determined over the SCR catalyst in powdered form were incorporated into a 1D+1D mathematical model of SCR honeycomb monolith reactors.

The model assumes identical conditions within each channel of the honeycomb catalyst, with negligible axial dispersion and pressure drop.

Mass balance for a single monolith channel is provided by the following equations:

Gas phase (i = NO, NH_3) :

$$\frac{\partial Ci}{\partial z} = -\frac{4*L}{d*v} * Kmi * (Ci - Ci,w) \quad \text{(E35)}$$

Solid phase:

$$0 = Kmi * (Ci - Ci,w) + Reff,i \quad \text{(E36)}$$

Where Ci is the i-specie concentration in the bulk of the gas phase and Ci,w is the I concentration at the wall of the catalyst. The strong intra-phase diffusional limitations which can be present within NH3-SCR in monolith catalysts are accounted for by the following equations for diffusion reaction of the reactants in the intra-porous field (i.e. the catalytic monolith walls):

$$0 = Deff,i * \frac{\partial^2 Ci}{\partial x^2} + Sw^2 * Ri \quad \text{(E37)}$$

were *Ri* represents the volumetric intrinsic rate of formation of species *i*, Sw is the wall thickness and Deff is the effective diffusivity coefficient. Finally, the continuity between the external and the internal field at the gas/solid interface is granted by:

$$Reff,i = -\frac{Deff,i}{Sw} * \frac{\partial Ci}{\partial x}\Big|_w \quad \text{(E38)}$$

Accordingly, in addition to SCR rate parameters and reaction conditions the model requires the physicochemical, geometrical and morphological (porosity, pore size distribution) characteristics of the monolith catalyst as input data. Effective diffusivities, *Deff,j*, were evaluated from the morphological data according to a modified Wakao-Smith random pore model as specifically recommended by [31] for monolith SCR catalysts. The estimated values in the work of Tronconi et al. [32], of NO and NH3 effective intra-porous diffusivities were in the order of $5*10^{-6}$ m2/s. More recent works show slightly different values for the *Deff,j* coefficient. Based on the porosity and on gas-phase diffusivities computed as binary diffusivities in air according to the Fuller–Schettler–Giddings correlation, in the present thesis it has been calculated the value for the effective

diffusivities of NO, NO2 and NH3 at 200 °C were 4.2 $*10^{-5}$, 3.6 $*10^{-5}$ and 2.9 $*10^{-5}$ m2/s [33], respectively, that are one order of magnitude higher than the one calculated by Tronconi.

For our purpose not all the reactions shown in figure 2.9 are considered. For the first approach to the main problem, i.e. to find a good sizing criteria for SCR pre-turbo installations, it is sufficient to take in account the most important reactions. Thinking also that all the reactions that consider NO_2 (R6-R10 in figure 2.9) are not so important on marine installation, because there is not oxidation catalyst before the SCR system, so a large part of NOx are NO (≈ 95%).

The following reactions have been considered to describe the NH3 + NO + O2 reacting system ("standard" SCR):

NH3 adsorption-desorption: NH3 ↔NH3*

NH3 oxidation: 4NH3* + 3O2 → 2N2 + 6H2O

SCR reaction: 4NH3* + 4NO + O2 → 4N2 + 6H2O

The NH3 adsorption and desorption rates were fitted, in the work[31] by the following expressions, respectively:

$$r_{ox} = k_{ox}^{0} * \exp(-\frac{E_{ox}^{0}}{RT}) * (\frac{P_{O2}}{0.02})^{\beta} * \vartheta \quad \text{(E39)}$$

$$r_{des} = k_{des}^{0} * \exp[-\frac{E_{des}^{0}}{RT} * (1 - \alpha\vartheta)] * \vartheta \quad \text{(E40)}$$

Eq. (39) assumes non-activated adsorption of NH3 onto the catalytic sites, while Eq. (40) accounts for NH3 desorption from the heterogeneous catalyst surface, which is associated with a range of desorption activation energies [22]. α is a parameter for surface coverage dependence.

The rate of ammonia oxidation, observed at high temperatures, was fitted[31] by:

$$r_{ox} = k_{ox}^{0} * \exp(-\frac{E_{ox}^{0}}{RT}) * (\frac{P_{O2}}{0.02})^{\beta} * \vartheta \quad \text{(E41)}$$

As discussed below, an inhibition of NH3 on the SCR reaction can be observed. Therefore a competition between NO and ammonia in adsorbing onto the catalyst has been assumed, as also suggested in [33] and [34], and a two-sites Langmuir-Hinshelwood rate expression was adopted for the SCR "Standard" reaction [35]:

$$r_{ox} = k_{NO}^{0} * \exp(-\frac{E_{NO}^{0}}{RT}) \frac{C_{NO}\vartheta}{1+K_{LH}\frac{\vartheta}{1-\vartheta}} * (\frac{P_{O2}}{0.02})^{\beta} \quad \text{(E42)}$$

It should be emphasized that simplified models (e.g. surface reaction models) omitting to describe in details the complex dynamics of NH3 diffusion/ adsorption/ desorption/ reaction and the mass transfer limitations, are expected to yield significant errors under certain operating conditions, especially in the case of extruded catalysts. This point is illustrated by the simulation result shown in Figure 4.2

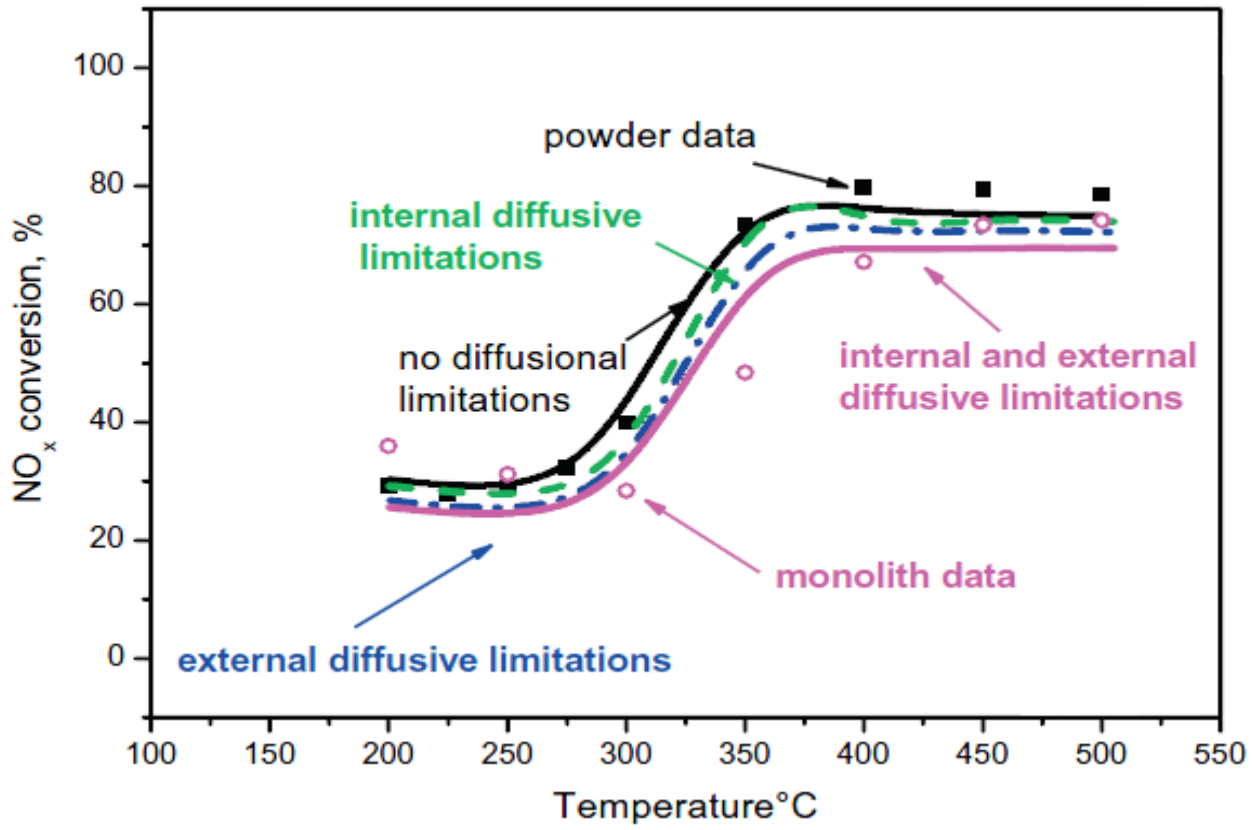

Figure 4.7 *Comparison between different reactor model and experimental data for NOx conversion2*

In order to validate the simulation model under real application conditions, engine test bench experiments were conducted by the team of prof. Tronconi in Milan. The performance of different SCR catalyst sets has been measured on a heavy duty engine test bench. The NO2 levels were negligible since no oxidation catalyst was present. Urea was used to provide NH3, while great attention was given to have a sufficient residence time within the exhaust gas stream for the complete conversion to NH3 before the SCR catalyst. Overall, a set of about one hundred

experiments have been performed. Extruded monoliths with 300 cpsi, a wall thickness of 0.32 mm and a monolith diameter of 5.66" were used for all catalyst sets. Other parameters like monolith length and the number of catalysts have been varied in order to increase or decrease the catalyst volume. Three catalyst volumes (25L, 32L and 43L) were tested.

During each experimental run the temperatures and emissions were measured with a sampling time of 2 Hz before and after the catalyst system, using a range of analyzers: chemiluminescence spectrometer for NO and NO2 and a diode laser spectrometer for NH3. A typical result of a test bench experiment is represented in Figure 4.3. At the beginning of the experiment the engine runs on constant load and speed. After 120 seconds the urea dosing starts which results in a increasing NOx conversion after the SCR catalyst. The urea dosing was kept at a constant rate during the measurement. After 250 seconds, when the NH3 storage capacity is approaching its limit, NH3 slip behind the catalyst can be measured. Typically, the experiment runs until total NOx conversion or steady state is established.

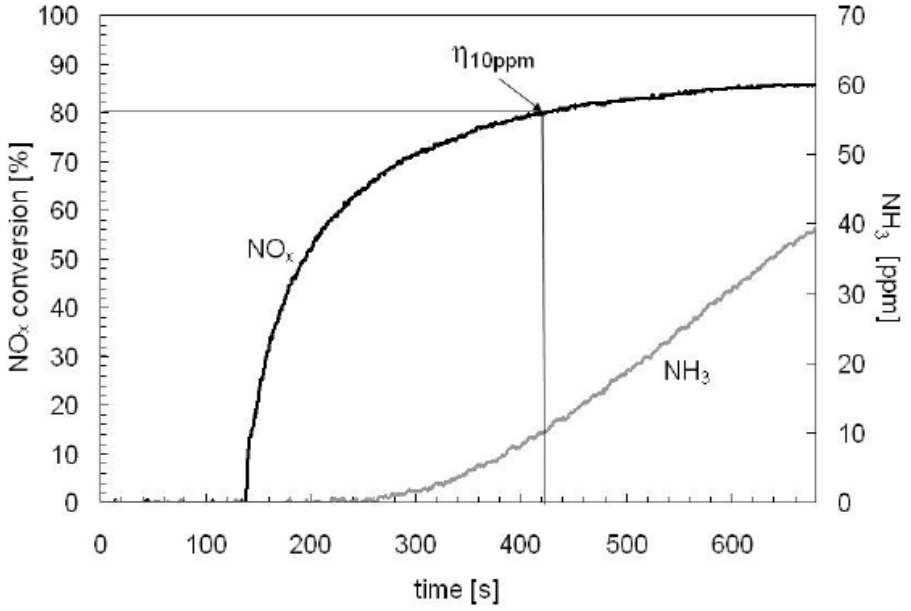

Figure 4.8 *Engine test bench measurement of NOx conversion and NH3 slip at 255 °C, mexhaust = 771 kg/h for an 25L SCR catalyst with 300 cpsi and a = 1.18*

Chapter 5

Results and Discussion

In this section it will be discussed the application of the model previously presented (Chapter 4). First the model predictions will be investigated over a broad range of conditions and prevailing resistances identified. Then, experimental data at the high pressure condition will be compared with model predictions, with specific attention will be given not only to the results obtained using our model but mainly to the limitation that the model show and its future development

5.1 Numerical Implementation of the model selected

The model selected is implemented in a Matlab R2012b code. The first part of the code, see APPENDIX, gives to the model all the data required: data about the reactor as length of the catalyst, number of modules and type of modules (number off cells per module), the cell hydraulic diameter and so on. Then we introduce the data about the operative conditions as Temperature, Pressure and the amount of gas flow rate in kg/h, and then the model calculate the physics properties of the gases as density, viscosity and velocity of the gas.

To calculate the density of the gas has been used the ideal equation of gases, considering that the over pressure of the engine will be never exceed the 6-7 bar, so it is always assumed that the compressibility factor of the gases will be always 1 in that condition (please note also that the temperature is always higher than 300°C)

The information required by the model to calculate the flow dynamic of the gas are: the gas velocity, which requires just the density and the geometry of the catalyst, the gas viscosity and the diffusive coefficient of the species considered by the model.

To calculate the viscosity it has been used the Sutherland' law that can be expressed as

$$\mu = \mu_0 (T/T_0)^{1.5} \cdot \frac{T_0+S}{T+S} \qquad \text{(E43)}$$

Where μ_0 , T_0 and S are the parameters of the equation tabulated for each species. Due to the large amount of Nitrogen in the exhaust flow gas, the properties of air has been considered as a good approximation.

To calculate the diffusivity coefficient at 1atm and 200°C was used the correlation of Fuller, Schettler, and Giddings as suggested in the article [44]. The correlation is the following:

$$D_{NO\_Air} = 10^3 \cdot T^{1.75} \cdot \frac{\left(\frac{1}{MW_{NO}}+\frac{1}{MW_{Air}}\right)^{1/2}}{P\cdot\left(V_{NO}^{\frac{1}{3}}+V_{Air}^{\frac{1}{3}}\right)^2} \quad \text{(E44)}$$

Where the Vi are tabulated. This correlation shows a good agreement also with the Chapman-Enskog solution of the Boltzmann equation that takes in the account the collision integral of the single particle and the Griskey correlation proposed by several of academic book as "Transport Phenomena and Unit Operations"[55]

$$D_{NO\_Air} = 1.8583e-7 \cdot \frac{\left(T^3\cdot\left(\frac{1}{MW_{NO}}+\frac{1}{MW_{AIR}}\right)\right)^{\frac{1}{2}}}{P\cdot\sigma^2\cdot\omega} \quad \text{(E45)}$$

Where ω and σ are tabulated for each gas and temperature.

All these properties are used to calculate the dimensionless number as

$$Re = \frac{\rho v d}{\mu} \qquad Sc = \frac{\mu}{\rho D_{NO-air}} \quad \text{(E46)}$$

And the property of intra-phase and external mass transfer, the effective diffusivity coefficient and the overall mass transfer coefficient Km

$$D_{NO,eff} = D_{NO\_air}\cdot\frac{\varepsilon}{\tau} \qquad Km = Sh\cdot\frac{D_{NO\_air}}{d} \quad \text{(E47)}$$

As shown, to calculate the effective diffusivity coefficient are needed some morphological properties of the catalyst, as the porosity and the tortuosity. The porosity of the catalyst has been measured by myself to be equal to 75%, that agree with the commercial data found from catalyst producers such as Johnson Matthey, Nano and Ceram. Some literature information about the catalyst tortuosity were found and this terms is about 2-2.3 for commercial catalyst [52].

About the external mass transfer coefficient, a lot of correlation have been studied. One of the most used, and suggested in the article [40] is the equation (E12), see chapter 4, that represent an approximation due to the similarity with the Nusselt number for laminar flow in a square channel.

In fact in the article [52] suggested by prof. Tronconi the term used as Sh at infinite length is equal to the Nusselt number at infinite.

The correlation selected to be used in this model is an experimental correlation, found to fit the data collected in a typical SCR catalyst by Santos et al. [54] A. Santos and his Team studied the problem of the Mass Transfer limitation on the SCR system since from 1998 and they tested on their pilot engine a lot of correlation trying to fit the experimental data. After a lot of study about that they propose an appropriate correlation, with the same form of the theoretical correlation but with the parameters found with empirical data, that has been used in the model:

$$Sh = 1.2824 \cdot \left(\frac{d}{L} \cdot Re \cdot Sc\right)^{1.079} \tag{E48}$$

This correlation is used specifically to describe the NOx mass transfer in a commercial SCR catalyst, and appears the best one to fit the experimental data given by Yarwil and MARINTEK, and gives good agreement with the literature data and other industrial data on SCR stationary application, that we found thanks to the support of AIRLIFE s.r.l.

After the definition of all the data and the physical and fluid dynamic properties of the gas and of each species the program start to solve the equations before shown (E35-E38). The Third part of the program solve the material balances for the two species (NO and NH_3) in the gas phase, the 2 differential equations (E35) and the two algebraic (E36) that in Matlab code are expressed as

```
ADE = [     -A * kmNH3(d,L,Re,Sc,Dnh3) * (Cnh3-Cnh3w)
            -A * kmNO(d,L,Re,Sc,Dno) * (Cno-Cnow)
            kmNH3(d,L,Re,Sc,Dnh3)*(Cnh3-Cnh3w)+rates(1)
            kmNO(d,L,Re,Sc,Dno)*(Cno-Cnow)+rates(2)];
```

In these equations rates represent the equation (E38) that is solved in another function appositely created, called “catalystpore” in the code. This section has to solve the diffusivity phenomena inside the catalyst pores and also the kinetic equation that express the terms of consumption of the reactant (E37).

To solve this part it has been used the Newton-Raphson method to linearize the kinetic equations and the Finite Difference method to solve a system of partial differential equation of second order with some appropriate boundary condition: in particular it was imposed that the concentration at the

inlet of the pore at a certain Z is equal to the concentration of the i-specie at the wall at the same Z, value that is calculated in the first part of the program.

The second boundary condition that was imposed is the symmetry between two channel, so that the profile at the end of the pore is flat.

To solve this system of equation with those boundary condition the program need as input data the process conditions, as T, P, the wall concentration for each coordinate, the value of the physical properties and of the morphological properties of the catalyst, and at the end the matrix with all the stoichiometric coefficients and the expression for the kinetic rate equations, for example the Arrhenius equations and the values of the parameters as the activation energy and the pre-exponential factor.

As results the model calculate the profile of concentration at bulk and at the wall of the gas phase in the main channel and the profile of the reactant inside the pores. A typical results of the model is shown in the next figures

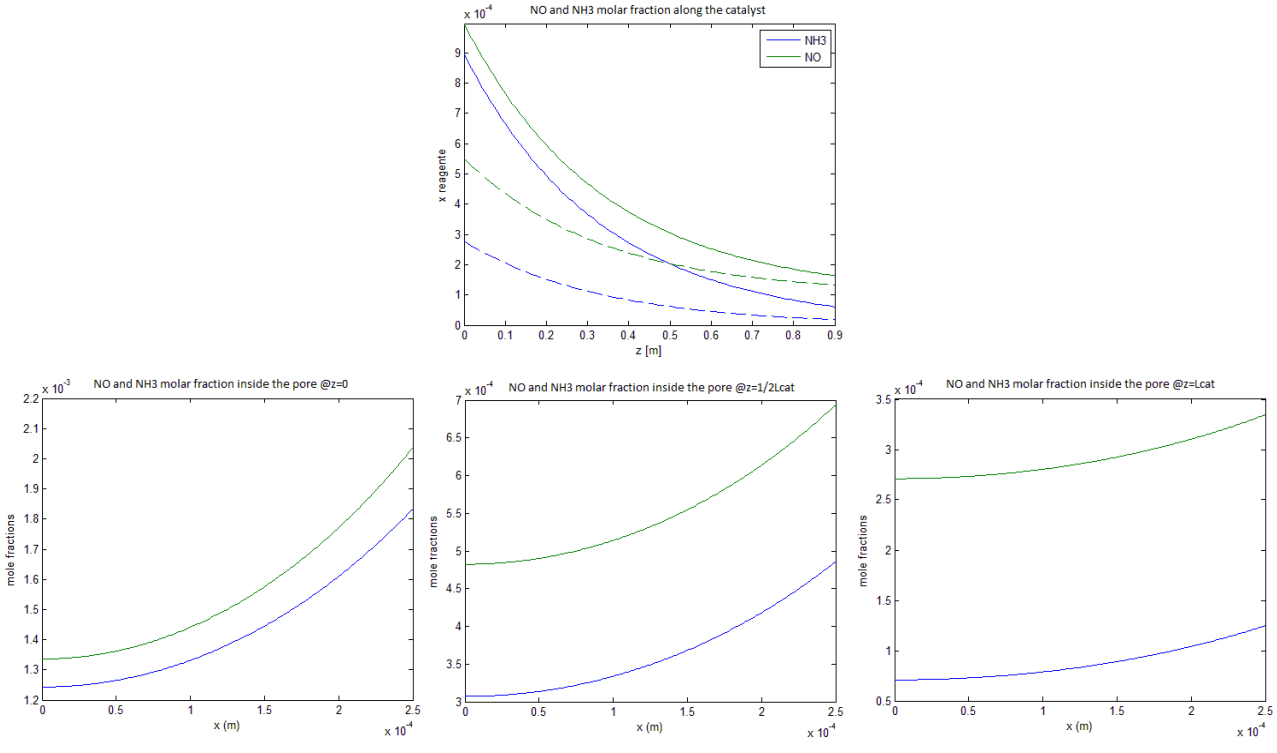

Figura 5.1 *NO and NH_3 molar fraction along the catalyst and inside the pores at three different values of coordinate z*

5.2 Model prediction and sensitivity analyzes

After the implementation the model has been used to calculate the possible behaviors of the SCR reactor in a wide range of operative conditions, to make possible to describe the effect of temperature and pressure onto the process and try to better understand what are the dominating phenomena and the weight of each resistance in the SCR process.

5.2.1 The effect of the Mass Transfer parameters

The first thing that the author has investigated in this model is the effect on the conversion of the mass transfer parameters as the effective diffusivity coefficient D_{eff} and the overall mass transfer coefficient Km, for fixed conditions of NOx inlet concentration and volume of the catalyst, using the data given by Yarwil about the MARINTEK experiment and, so ~1000 ppm of NOx and a catalyst compose by 3 modules 30x30 cells (hydraulic diameter ~4.3 mm and a wall thickness of ~0.5mm) for 900mm of total length. The results obtained by this study are shown in the following figure:

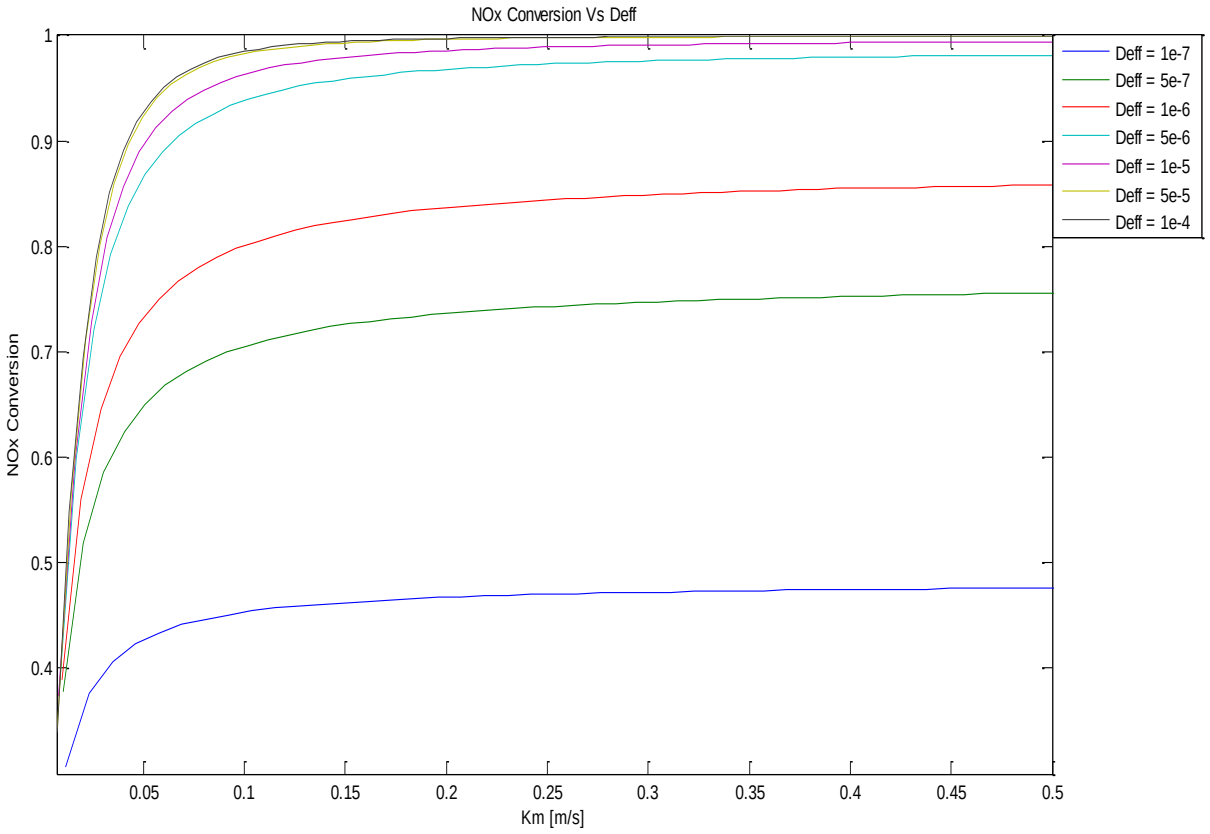

Figura 5.2 *NOx conversion Vs External Mass Transfer coefficient at different values of effective diffusivity coefficient*

As easily shown the process is affected by Mass transfer control for a wide range of values of both the two parameters, Km and D_{eff}. Only for values of Km > 0.15 m/s and $D_{eff} > 10^{-5}$ the process is controlled by the kinetic reactions. Using the same study it is possible to find the three areas of controlling regime, as shown in figure 5.2. This is a general study, not affected by the different possible correlation used to find the Km coefficient and the D_i property.

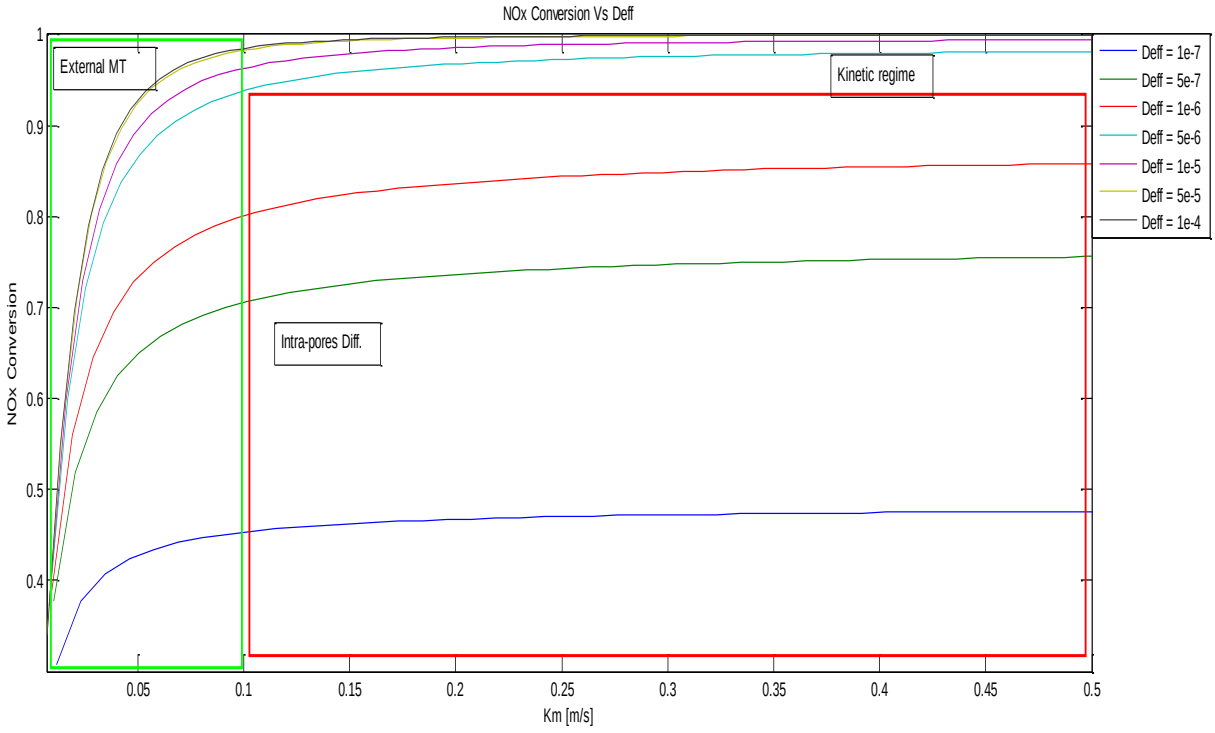

Figura 5.3 *Controlling regime areas (**green** external Mass Transfer, **red** Intra-porous diffusion and the kinetic) given by the correlations used in the model*

Using the correlation shown before it has been conducted a study on the controlling regime using the resistance definitions given by [55].

$$R_{ext} = \frac{1}{Km} \tag{E49}$$

$$R_{int} = \frac{R_{\Omega 2}}{3.5 \cdot D_{eff}} \tag{E50}$$

$$R_{kin} = \frac{1}{K(T) \cdot R_{\Omega 2}} \tag{E51}$$

Where $R_{\Omega 2}$ is the is the effective wall thickness (or effective transverse diffusion length) . This study shows that in industrial applications, due to the temperature and pressure, also for the pre-

turbo data available for this study, the controlling regime is the external mass transfer (~60-70% of R_{tot})It is important to know, before showing the results of this sensitivity study, the main influence of Pressure and Temperature on this model. As shown in section 4.3 and in the previous one, the model selected is a compromise between something fully kinetic, that takes in account only the chemistry of the SCR process, and something mainly physics, that use a simpler kinetic but a detailed description of fluid dynamic.

Probably to better describe the pressure dependence a more physic model will be used in the future but at the present time a model that require a computational fluid dynamic is not something needed by Yarwil, and, for the author, is not well tested as the kinetic part of the problem, that has been studied since 1980, so, for our purpose and to be safe during the calculation at high pressure, the model selected appear a good approximation of the fluid dynamic part and describe well the kinetic part, without going into detailed mechanism that will require a really complicated model. The approach used in this work is to believe the kinetic part of the model, confirmed by the fact that the data shown in the reference [31], are perfectly reproducible.

The comparison between the data of the literature and the value obtained with the code develop for this work (for the code see APPENDIX) is shown in the next figure, made again with Matlab:

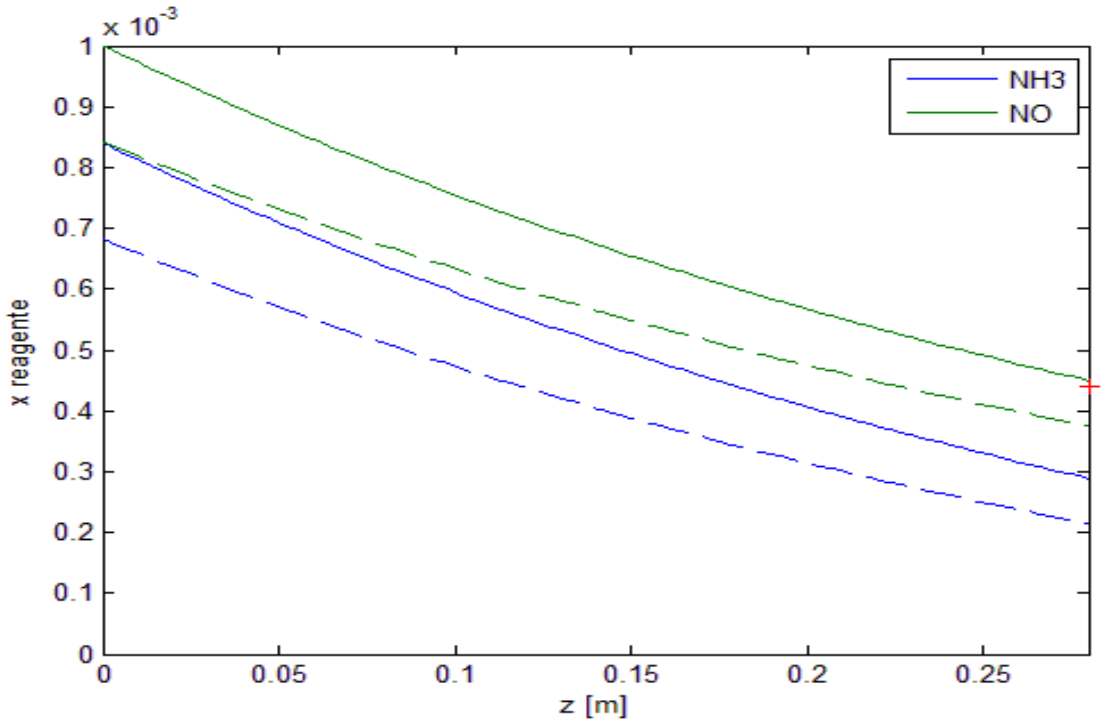

Figure 5.4 NO and NH3 molar fraction along the catalyst channel. Comparison between the model implemented (GREEN LINE) and the point of NO amount at Steady State shown in the article (RED +)

In the selected model the pressure influence in particular the physical aspects: in fact the pressure influence the gas concentration, the gas velocity, the gas density and the gas diffusive coefficients.

$$C_i = \frac{x_i \cdot P}{R \cdot T} \tag{E52}$$

$$\rho = \frac{P \cdot MW_{mix}}{R \cdot T} \tag{E53}$$

$$v = \frac{V}{(d_h^2 \cdot n)} = \frac{Mg}{\rho \cdot (d_h^2 \cdot n)} = \frac{Mg \cdot R \cdot T}{P \cdot MW_{mix} \cdot (d_h^2 \cdot n)} \tag{E54}$$

$$D_{i-AIR}(T,P) = D_{i-AIR}(To,Po) \cdot \left(\frac{T}{To}\right)^{1.75} \cdot \left(\frac{Po}{P}\right) \tag{E55}$$

The impact of pressure for the viscosity is minor, and the viscosity correction for pressure is less than 10% for the gases in our calculation for pressures up to 500 psi (34.5 bar).

Now it is to see the real effects of the pressure on the proposed model: as it is possible to see, the model take in to account two different effects if the pressure is more than atmospheric; one of this effects, that can be called “kinetic effect’, is the increase of the reactant concentration, even using simply the ideal gas law to describe the system. This effect simply increase the rates of reactions, that become fasters (it is not always true, i.e. in case of SCR reaction there is a inhibition effect of ammonia concentration, so if this terms increase with the pressure, the rate of SCR reaction will decrease).

The second effect, that can be called “physics effect”, regards the physical properties of the gas phase: increasing the pressure the density of the gas will increase , the velocity and the diffusivity coefficient will decrease.

Considering all this pressure dependence it is important to analyze what are the controlling phenomena:

The first simulation was conducted at fixed residence time, based on the practical experience, t=0.1s; In this condition it has been studied the Variations with temperature and pressure of the relative resistance defined as R_i/R_{tot} the results are shown in the figures 5.4

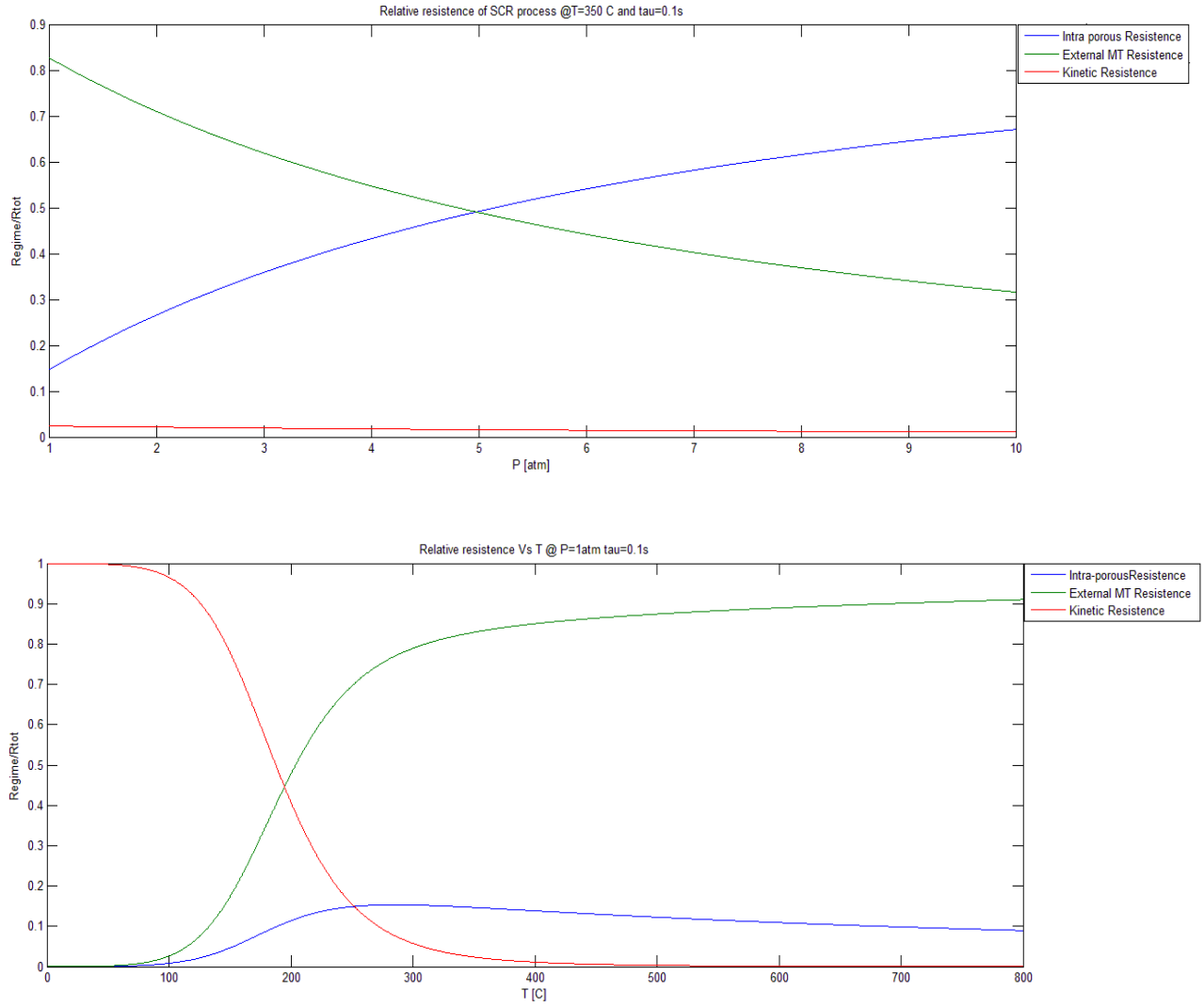

Figure 5.5 *Relative resistance versus Pressure and Temperature at fixed residence time*

If the residence time and the volume of the catalyst, section (3 modules 30x30 cells) and length (900mm) , are fixed it is possible to see the effect of pressure and temperature. Otherwise in this case the gas flow rate [kg/h] has to be changed to maintain constant the velocity at different T and P.

Typical values of the resistance, calculated using the data given by Yarwil and so for SCR system under pressure, are about ~60% of total resistance for external mass transfer, ~35% for the internal mass transfer and the residual for the kinetic resistance.

One of the undesired effects of this simulation is that, increasing the pressure but maintaining constant the velocity, increase linearly the Reynolds number (E49,E53). This involves that for high pressure the external mass transfer is facilitated by the higher Re and, as it is possible to see in the

first part of figure 5.4, for high pressure the controlling phenomena become the intra porous mass transfer.

Normally this conditions never happen in real applications because high pressure always means less gas velocity, so the Reynolds number is more or less constant, around a value of 1500 (typical value calculated with the data given by Yarwil).

With the same criteria, maintain the velocity and the residence time constant, other two sensitivity studies have been conducted: NOx Conversion against pressure at different values of temperature and NOx conversion against temperature at different values of pressure; the results are shown in the figure 5.5:

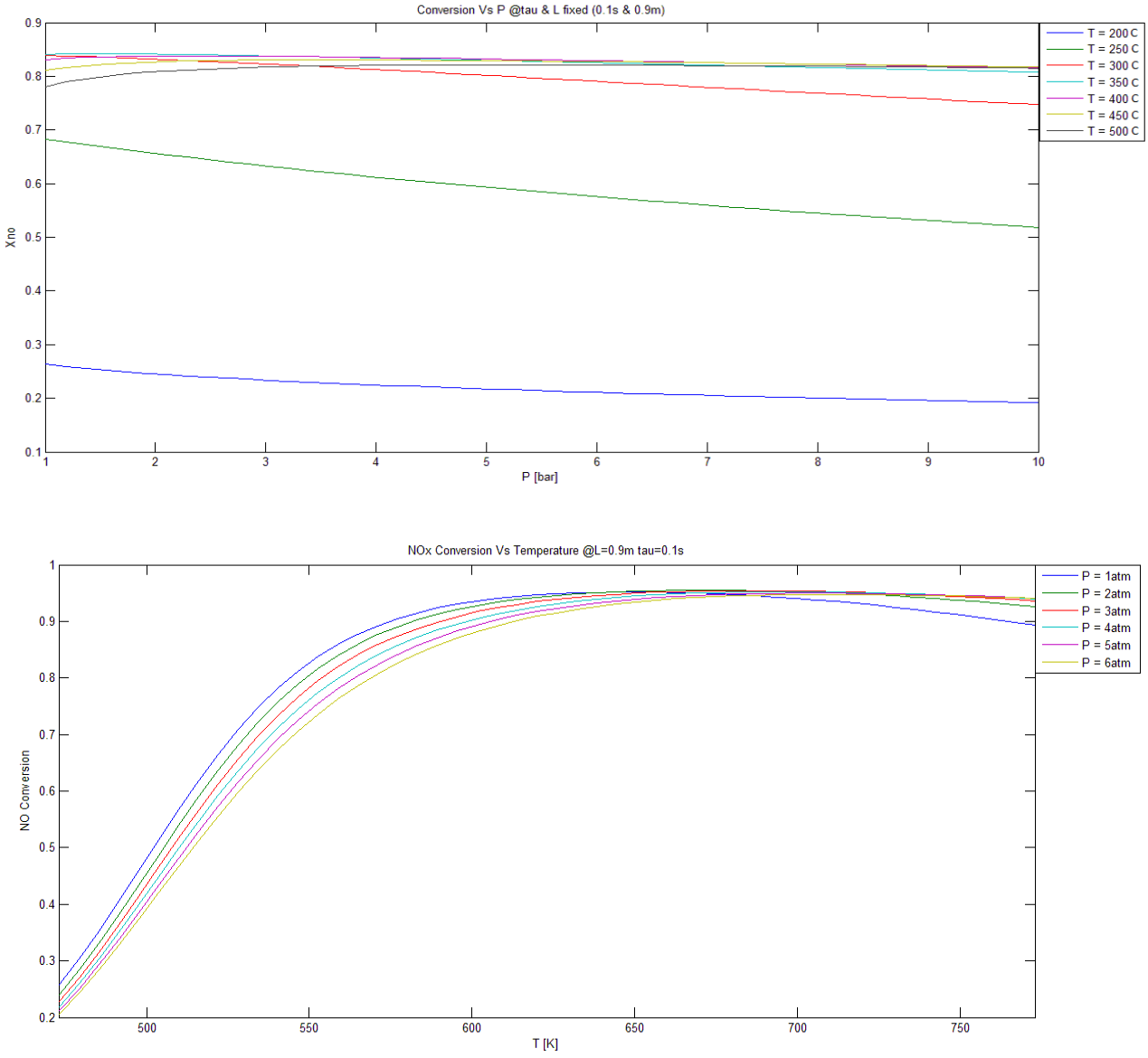

Figure 5.6 *NOx Conversion Vs Pressure (a) and Temperature (b)*

As shown, the increasing of pressure has a little inhibition's effect on the NOx conversion. This effect is better shown in the second part of the figure, that present the conversion against the temperature. In this case it is shown that, at the same temperature, the curve at higher pressure has less NOx conversion. Also in the first part of figure 5.5 it is possible to see, for the curves at higher temperature, less NOx conversion values, due to the fact that at those temperatures would also important the amount of ammonia involved in the oxidation reaction. Also these graphics, in particular the first of figure 5.5, don't show the real inhibiting effect of the increasing of pressure, because, as a collateral effect of maintaining the residence time and the velocity constant, as told before, there is an increasing of the Reynolds number and a benefit on the external mass transfer, that is the controlling regime in all the simulations made with real data.

Due to this problem, it has been done another study on the controlling regimes and the NOx conversion without the constraint of the fixed residence time. But this study, as it will be shown in the next figures, doesn't catch the inhibiting effect of pressure again: this is due to the fact that, fixed the gas flow rate (kg/h) higher pressure means lower volumetric flow rate and also, with fixed geometry of catalyst, lower gas velocity and higher residence time. Due to this, the increasing of pressure show an increasing of the conversion just because the gases stay inside the reactor for longer time.

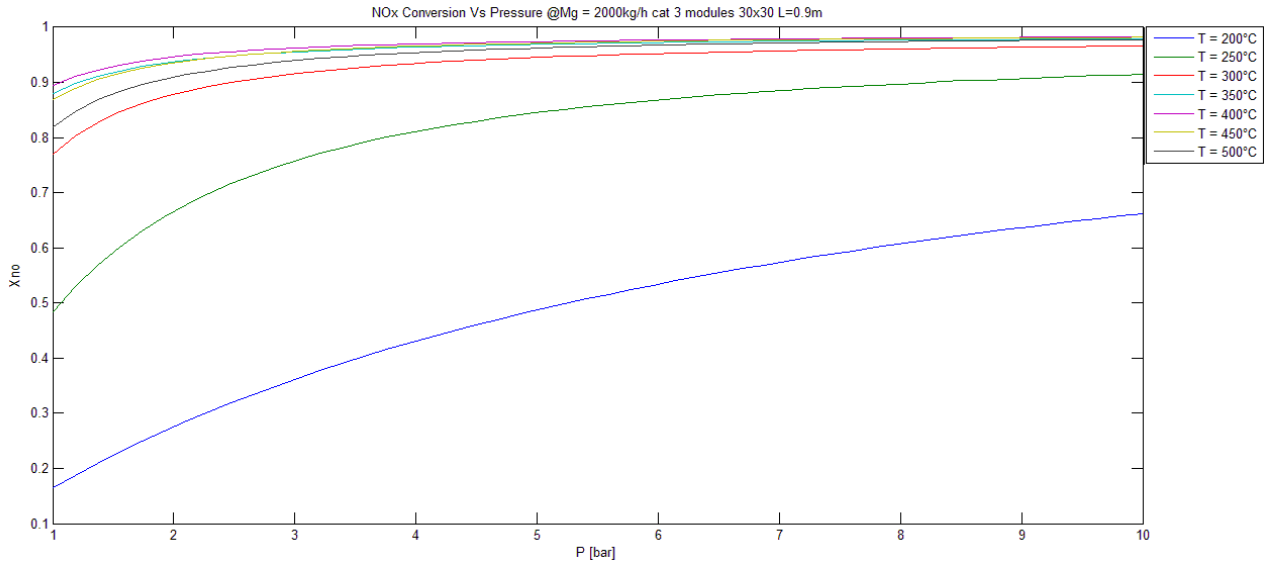

Figure 5.7 *NOx conversion against pressure at fixed Mg = 2000Kg/h and Lcat = 0.9m*

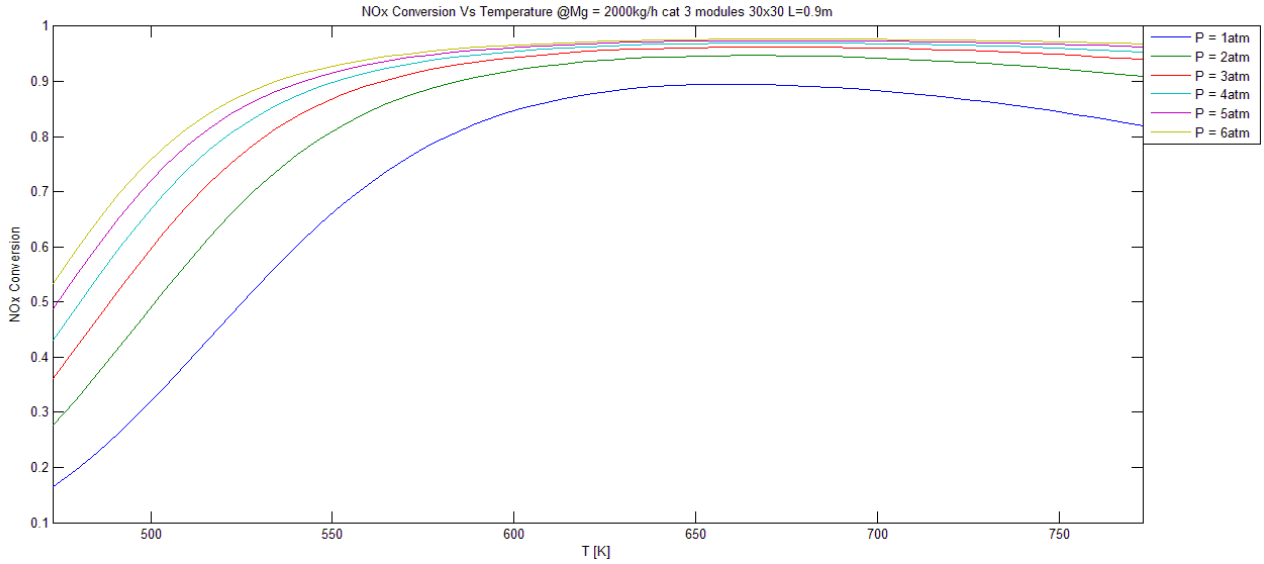

Figure 5.8 *NOx conversion against Temperature at fixed Mg = 2000Kg/h and Lcat = 0.9m*

Therefore, the best way to understand the effect of the pressure on the mass transfer is to see directly the curve of the single terms

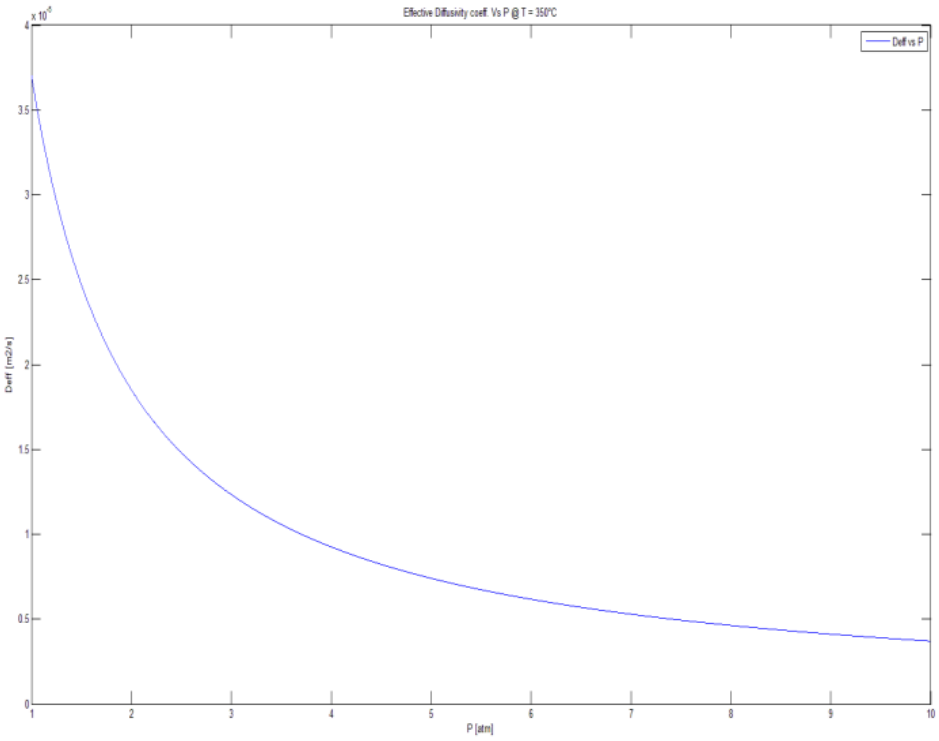

Figura 5.9a *Deff against pressure*

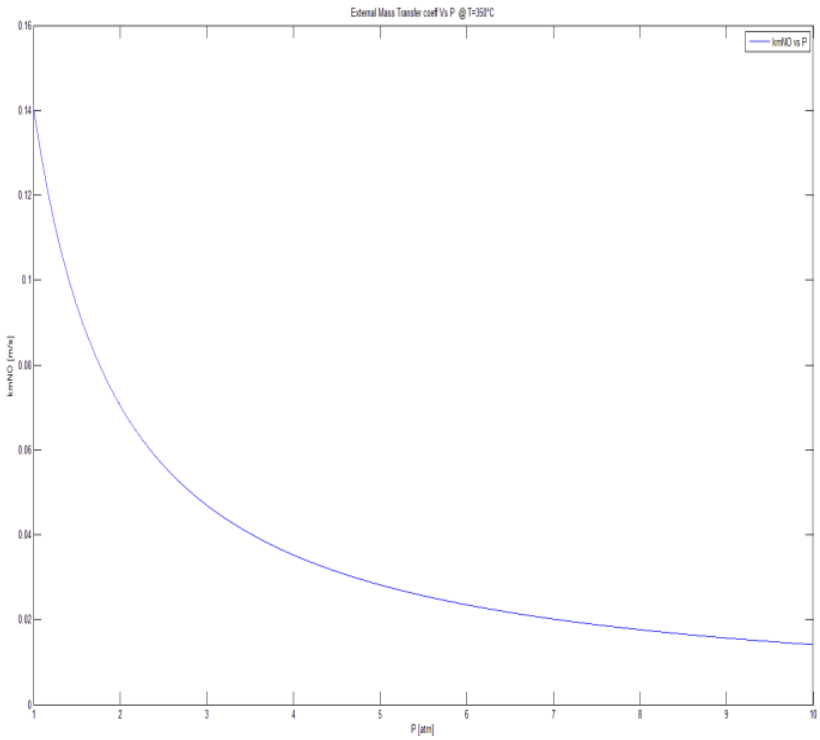

Figure 5.9b *Km against the pressure*

The two figures show the effective diffusivity coefficient and the external mass transfer coefficient against the pressure keeping all the other values fixed that means changing the flow rate to keep constant the Re number and the Sc. As it is clearly shown the pressure has a strong inhibiting effect on the two transfer phenomena.

With the same approach it has been study the trend of the conversion against the length of the reactor. During these studies it has been encountered almost the same problem: keeping fixed the residence time the Reynolds number increase linearly with the pressure, but otherwise if the residence time is not kept fix the increasing of pressure cause an increasing of the residence time that means an increasing of the conversion just due to the fact that the gas has more time to react and diffuse into the catalyst.

Nevertheless the results obtained are interesting to see the effect of the operative variables onto the NOx conversion; in this case the first results presented is conversion against the catalyst length at different values of pressure

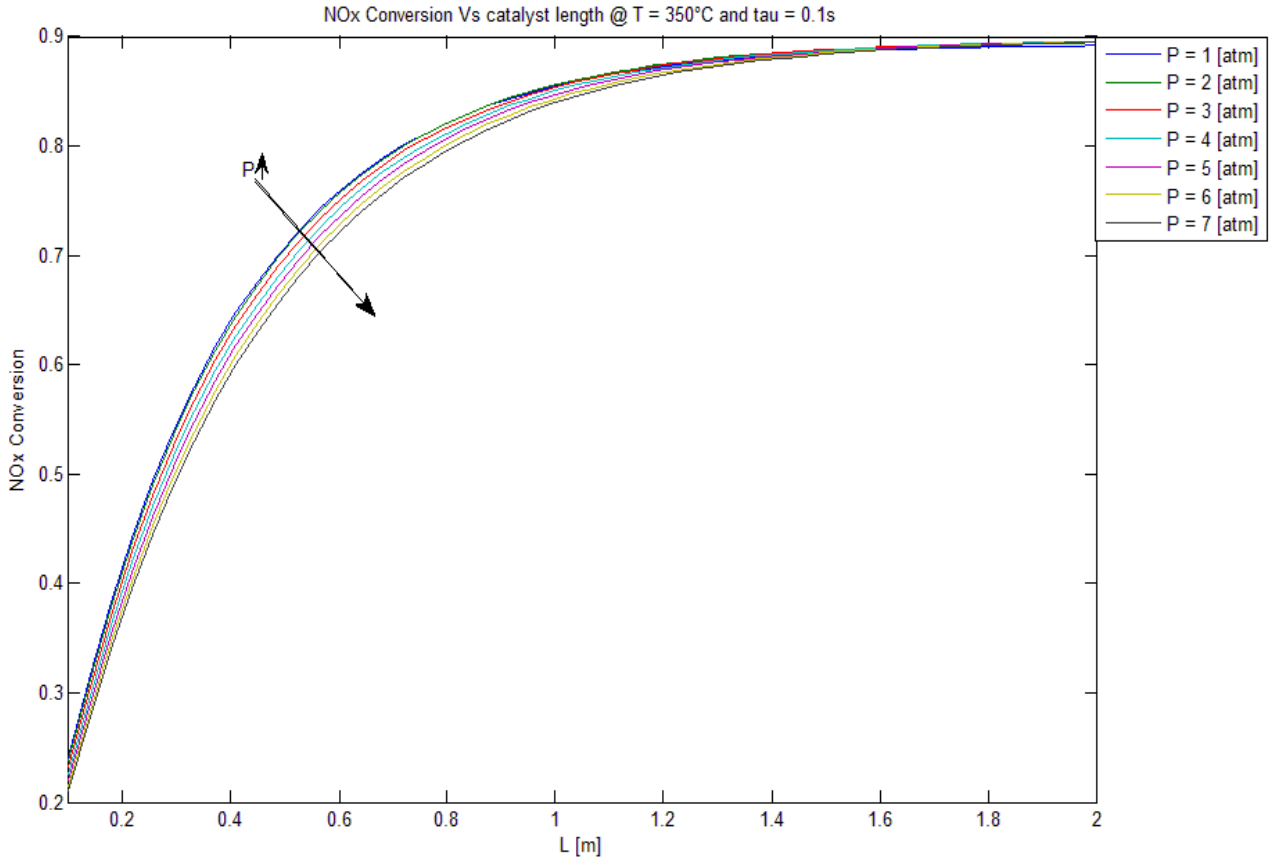

Figure 5.10 *NOx conversion against the length of the catalyst at fixed T = 350°C tau =0.1s and NH3/NO = 0.9*

This simulation was made in under stoichiometric condition, (NH_3/NO = 0.9) as it is possible to see the maximum NOx conversion is 90%. Again in this case the increasing of pressure doesn't show a huge decreasing of conversion, and this effect disappear when the reagent are almost finished.

The second study on the NOx conversion versus the length of the catalyst show the curves at different temperatures keeping constant the pressure (atmospheric) and the residence time. In this case it is is possible to see clearly the benefit to operate at temperature in the range of 350-400 °C. For higher temperature the NOx conversion decrease due to the competition of the oxidation reaction. Under 300 °C the temperature is not higher enough to ensure good conversion.

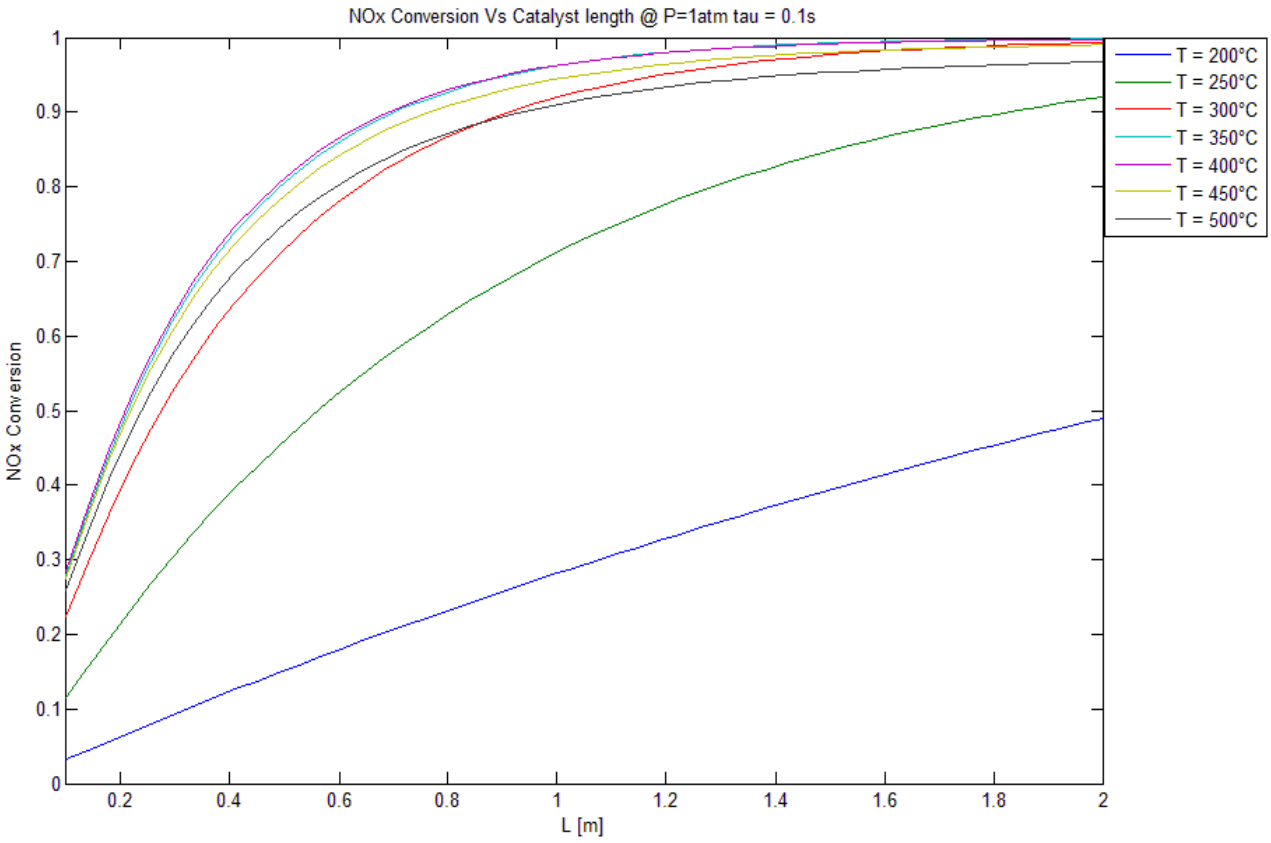

Figure 5.11 *NOx Conversion Vs catalyst length at different temperature and at fixed tau =0.1s and P=1atm*

As in the previous page the same study were conducted keeping fixed the gas flow rate to 2000 kg/h. In this case the residence time is not more fixed and it is possible to see again a positive effect of an increasing of pressure and also a little bad effect of the temperature, as increasing the temperature also increase the gas velocity that means less time given to the reactant to stay in contact with the catalyst.

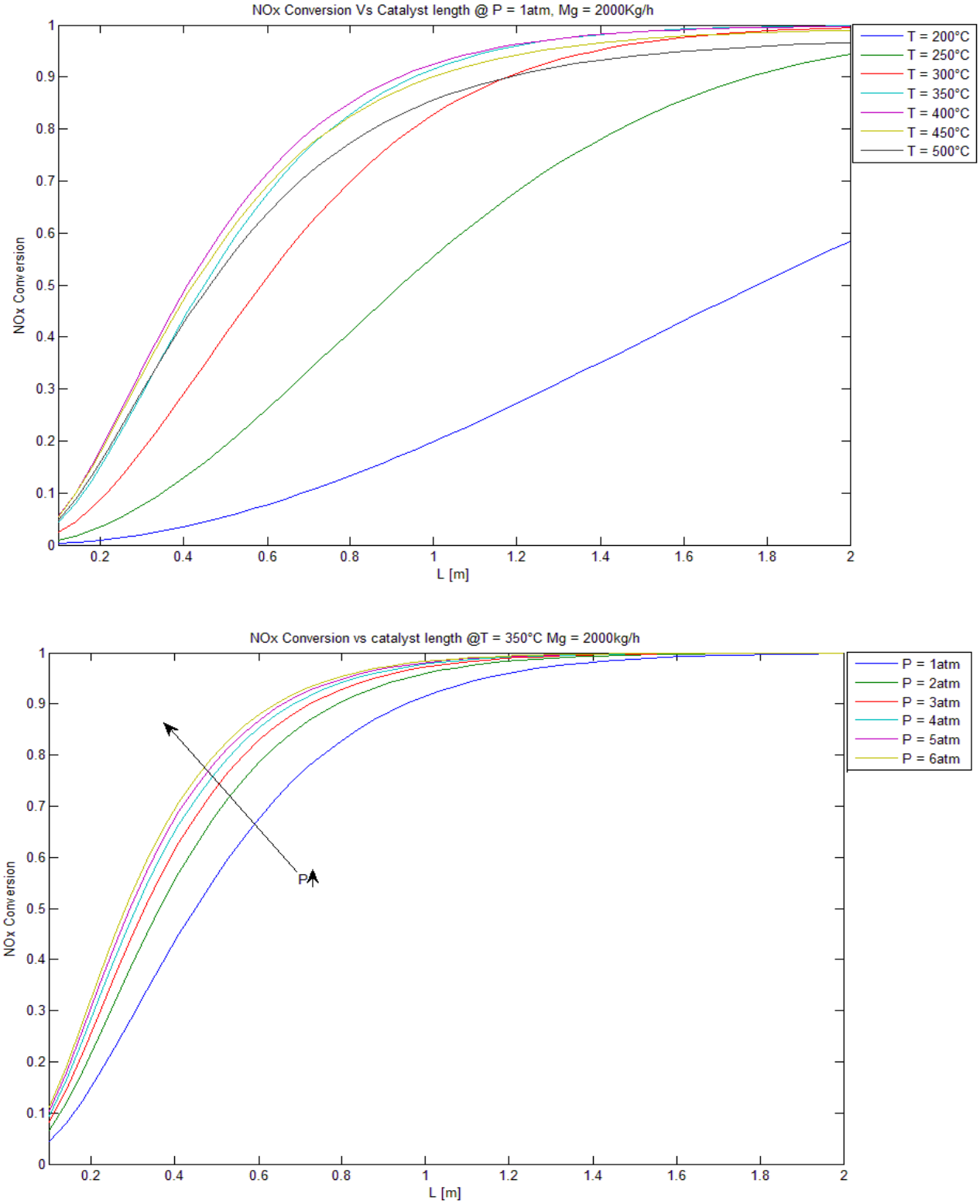

Figure 5.12 *NOx Conversion against catalyst length at different values of temperature and pressure keeping constant the Mg = 2000Kg/h*

The last study was made to try to show the negative influence of an increasing of pressure on the SCR system. In this case it was kept constant not only the values of the residence time, but also has been changed the value of the catalyst length to follow the variation of the gas velocity. In this study the results is clearly show in the next figure

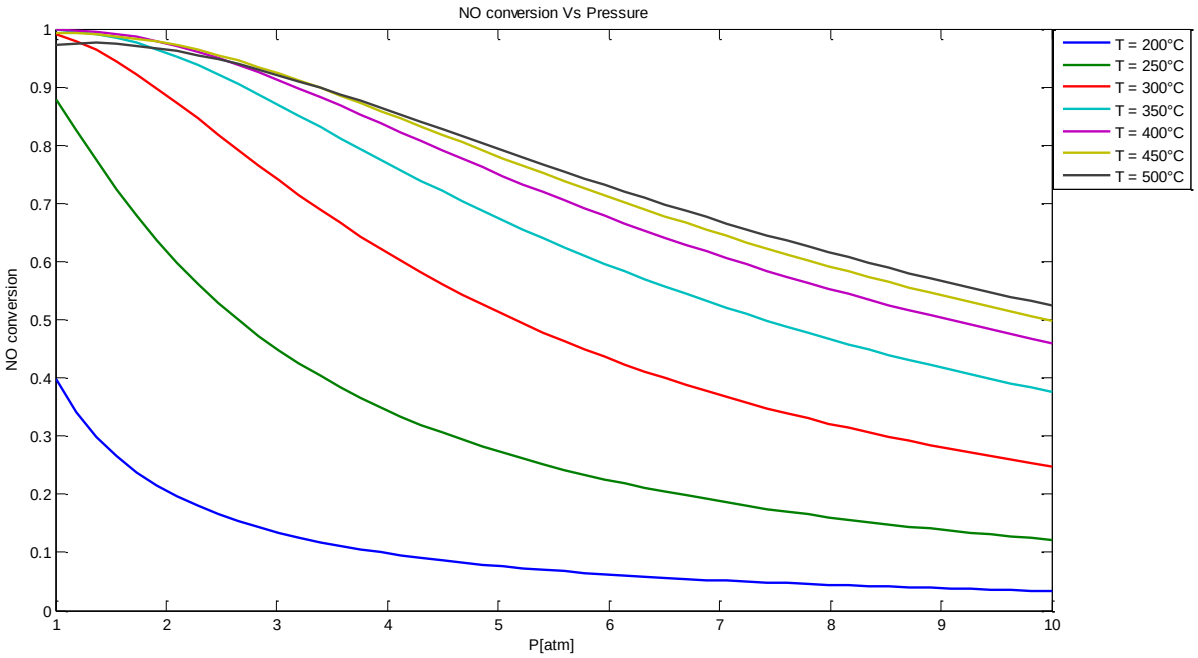

Figura 5.13 NO conversion Vs pressure @Mg and tau fixed

In figure 5.11 it is shown the negative influence of the pressure due to the effect shown in figure 5.8.

5.3 Comparison between the experimental data and the Yarwil sizing criteria

After the data collection, the researcher tried to compare these data with what was expected: it is important to note that the SCR system used in the experiments was sized to reach some values of NOx emission. These values were not reached for the test system, so the first phenomenon that was noticed was the less NOx conversion for a pre-turbo system

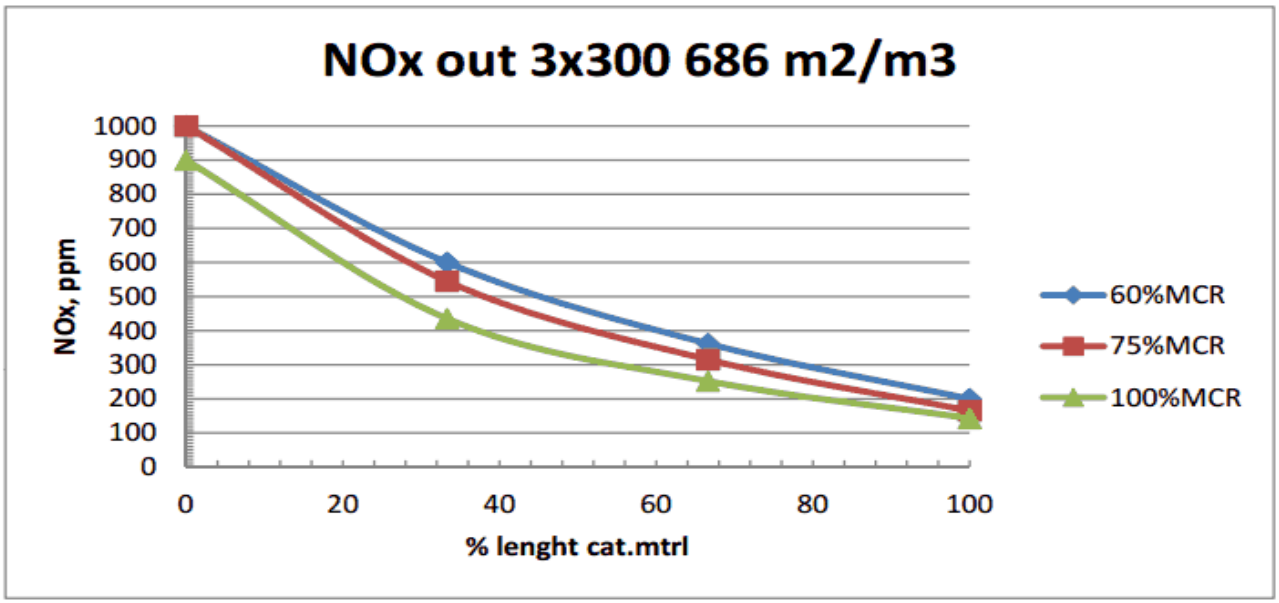

Figure 5.14 *NOx fraction along the catalyst*

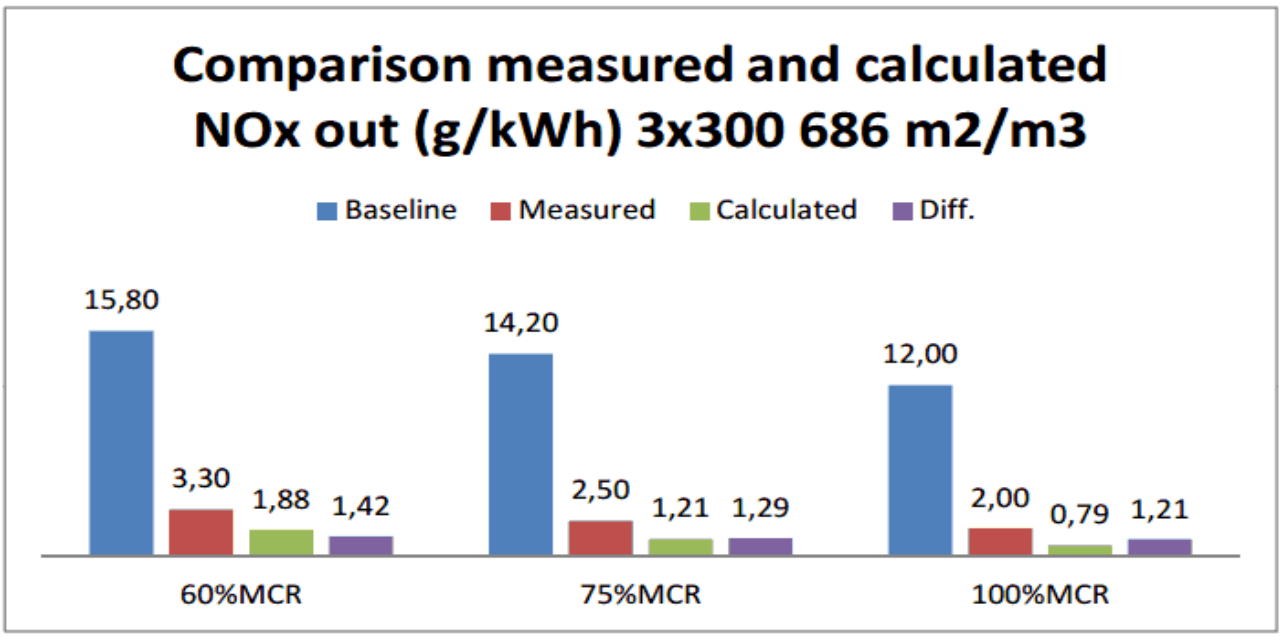

Figure 5.15 *Comparison between the data obtained, the baseline and the expected value of NOx outlet*

The previous figure shows the main point of the results obtained by the Yarwil researchers: there is a significant drop of the performance of the catalyst respect on what the mathematical model, successfully used by Yarwil to design a lot of "standard" SCR systems (means after-turbo, operating at atmospheric pressure), predicts to have as NOx emission.

The same results was obtained for the experiment 2 and 3:

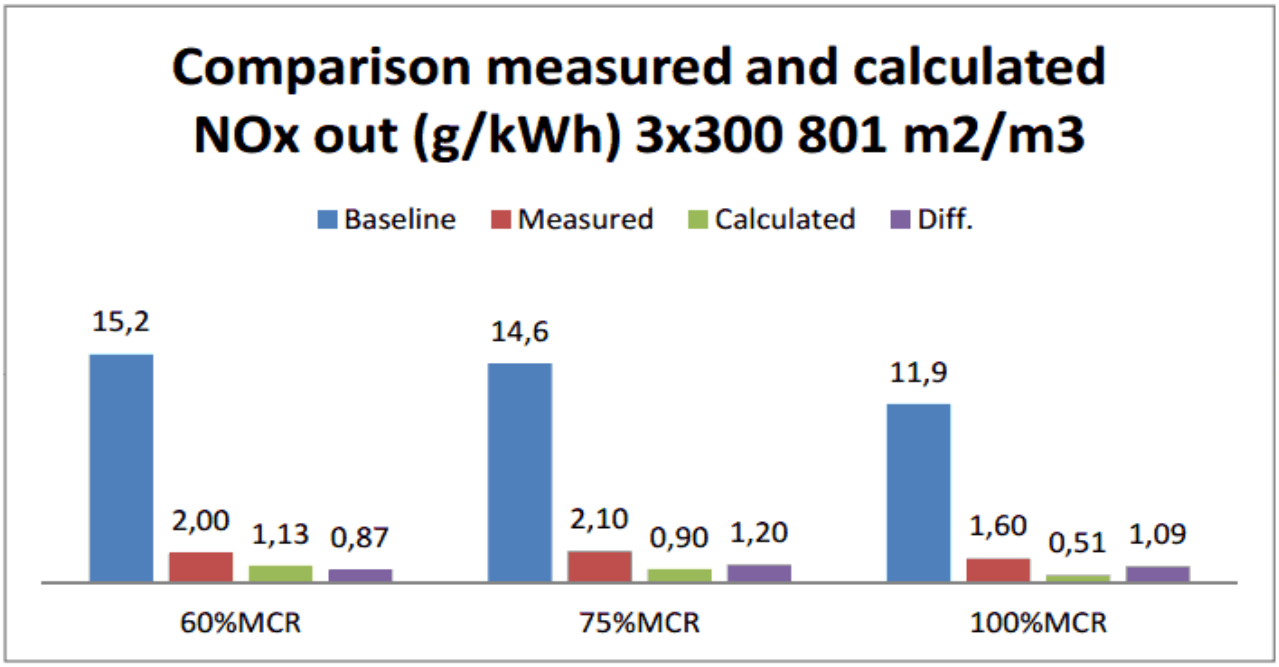

Figure 5.16 *Comparison between the data obtained, the baseline and the expected value of NOx outlet for 40x40 cat*

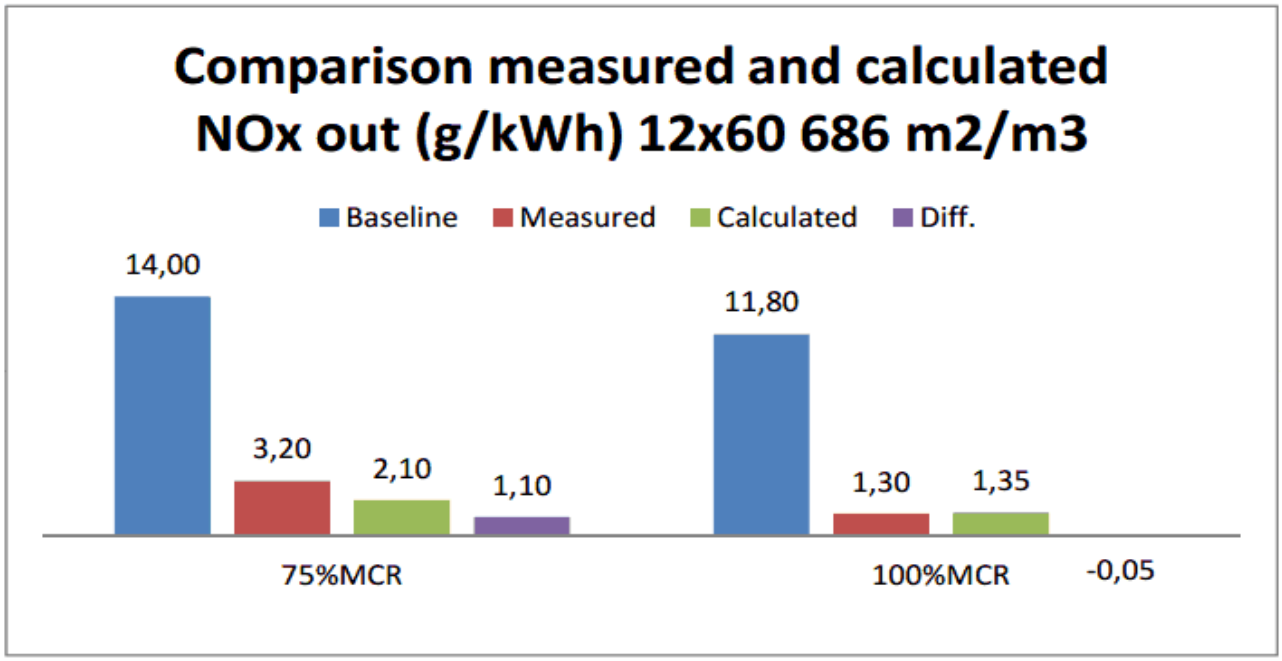

Figure 5.17 *Comparison between the data obtained, the baseline and the expected value of NOx outlet for 30x30 cat*

As said before the test performed with 12 modules of 60mm each present the higher conversion of NOx at 100% engine load, the unique that respect the prevision of the mathematical model.

Comparing the experimental results with the sizing equation normally used by Yarwil, they try to fit a correction factor that can be used to size the SCR pre-turbo installation; They got a K factor, a correction factor, that, multiply for the standard sizing equation, fit the experimental data, as shown in the next figure 3.19:

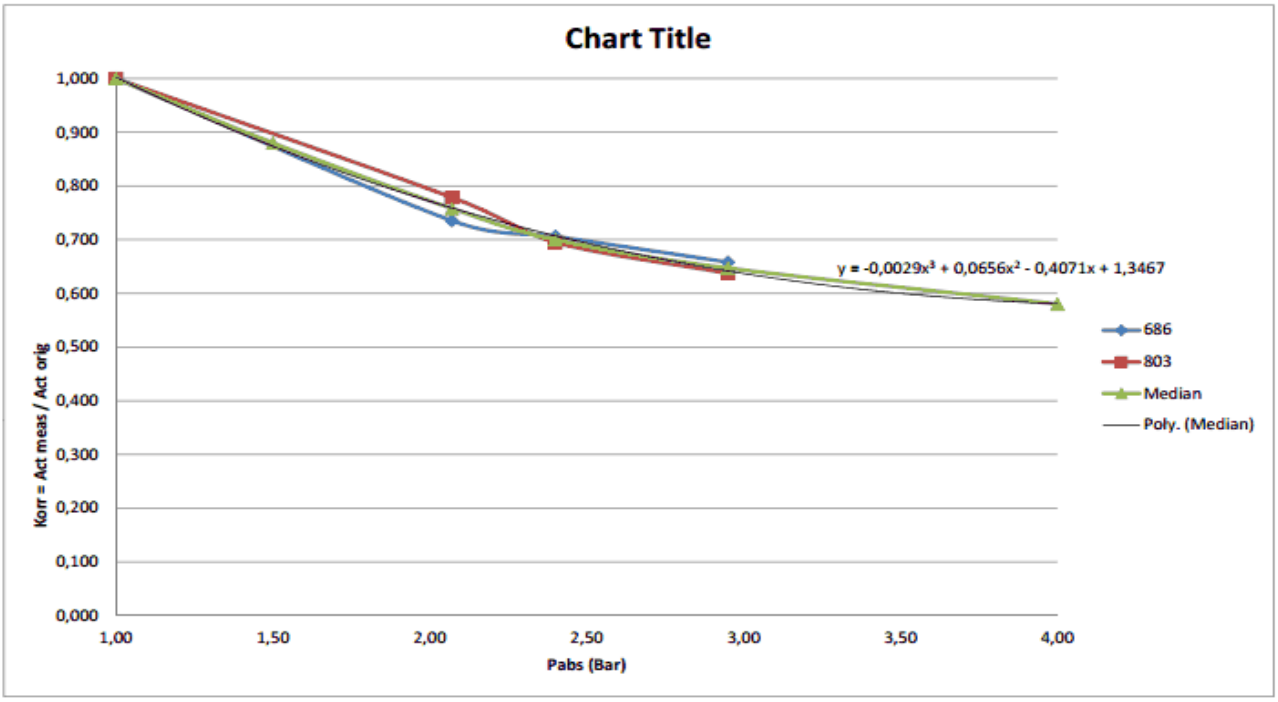

Figure 5.18 *The polynomial that follow the K correction factor for the 6 experiments*

In their opinion, using the midpoints between the two curves, constructed by connecting the three experimental points, they made a median curve, that connects the three midpoints, and they fitted this median curve with a 3rd degree polynomial to try to extrapolate the correction factor also outside the experimental range.

This way to approach the problem is fully empirical and, in the opinion of the author, will work only for the system subject to the experimental campaign. In fact there is a lot of phenomena that can't be explained only in "linear way" using a K correction factor and obtained something like SCR SYSTEM UNDER PRESSURE = K * STANDARD SCR SYSTEM.

5.4 Comparative analysis of the YARWIL design criteria and the presented model, and required improvements

As shown in the previous section, the Yarwil design criteria overestimates the NOx conversion. On the contrary the model developed for the present work shows the tendency to underestimate the conversion. The comparison between the experimental data given by Yarwil/MARINTEK and the model is shown in the next figures, both for the 30x30 modules and for the 35x35 modules

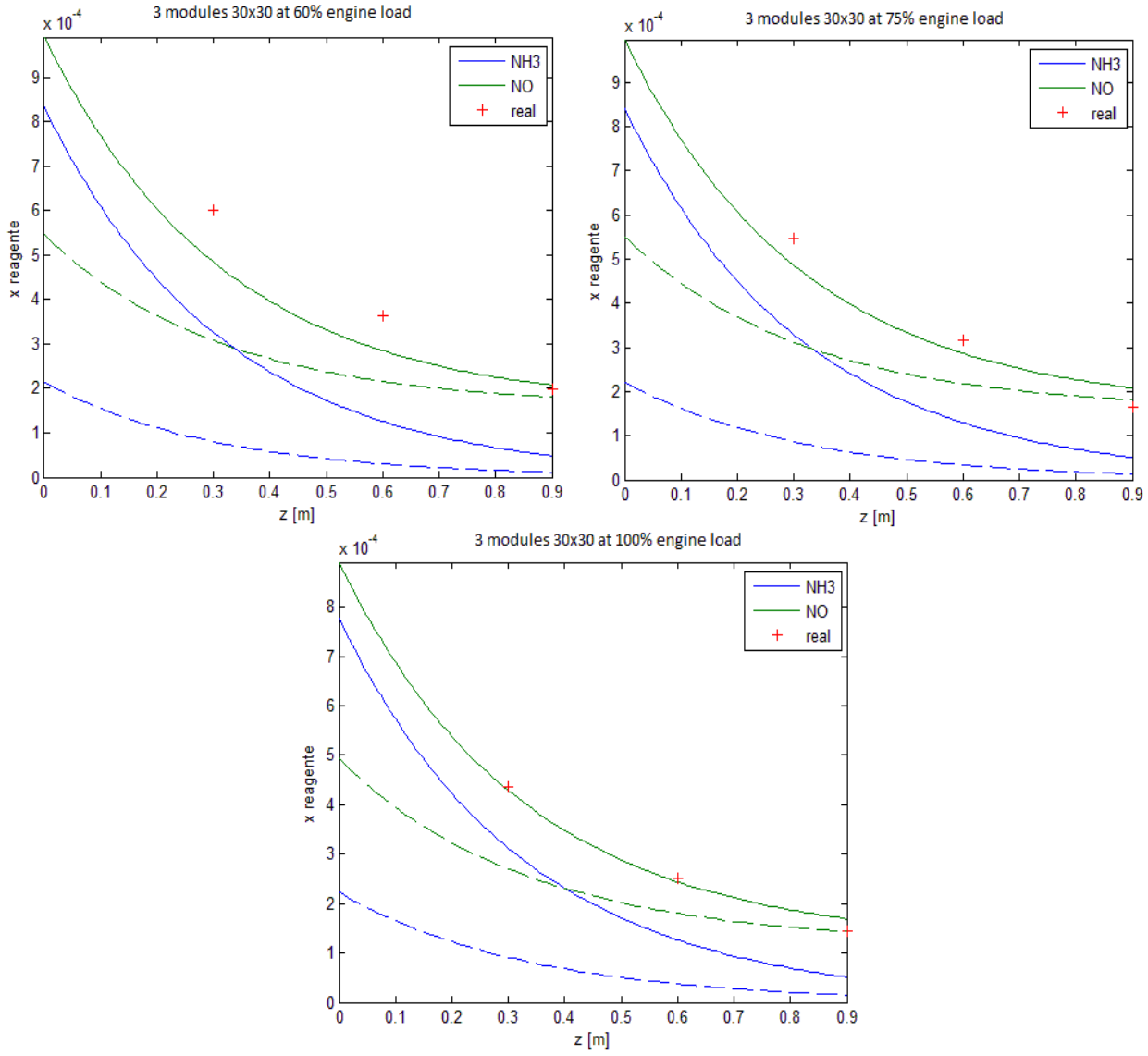

Figura 5.19 *Comparison between the experimental data* **(+RED)** *and the NOx molar fraction along the catalyst (***GREEN LINE***) for the catalyst configurations 3 modules 30x30 cells at three different engine loads*

As shown, it was taken in to account a below-stoichiometric amount of ammonia, that comes from the calculation based on the data of urea injection given by Yarwil and assuming an incomplete

conversion of urea (no data are available on this point) of 80-85%, in agree with some commercial data given by Yarwil and AIRLIFE.

The same has been done in the case of 3 modules of 35x35 cells

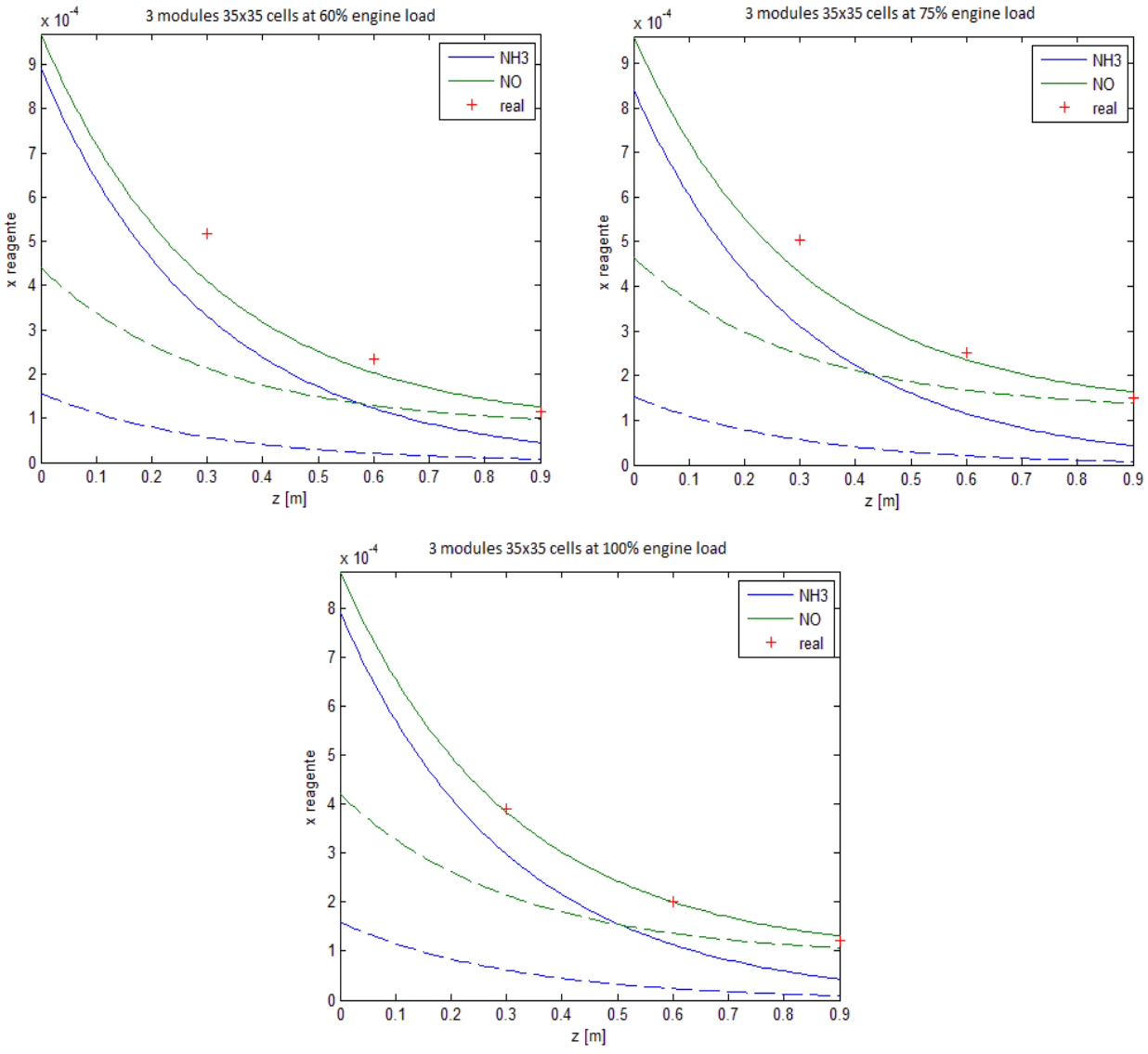

Figura 5.20 *Comparison between the experimental data* **(+RED)** *and the NOx molar fraction along the catalyst (***GREEN LINE**) *for the catalyst configurations 3 modules 35x35 cells at three different engine loads*

As it is possible to see the model shows the tendency to underestimate the NOx conversion compared with the experimental data. The comparison between the Yarwil design tool and the

present program is shown in the next two figures: as before shown there is a good description of the SCR process under pressure as good description of the experimental data.

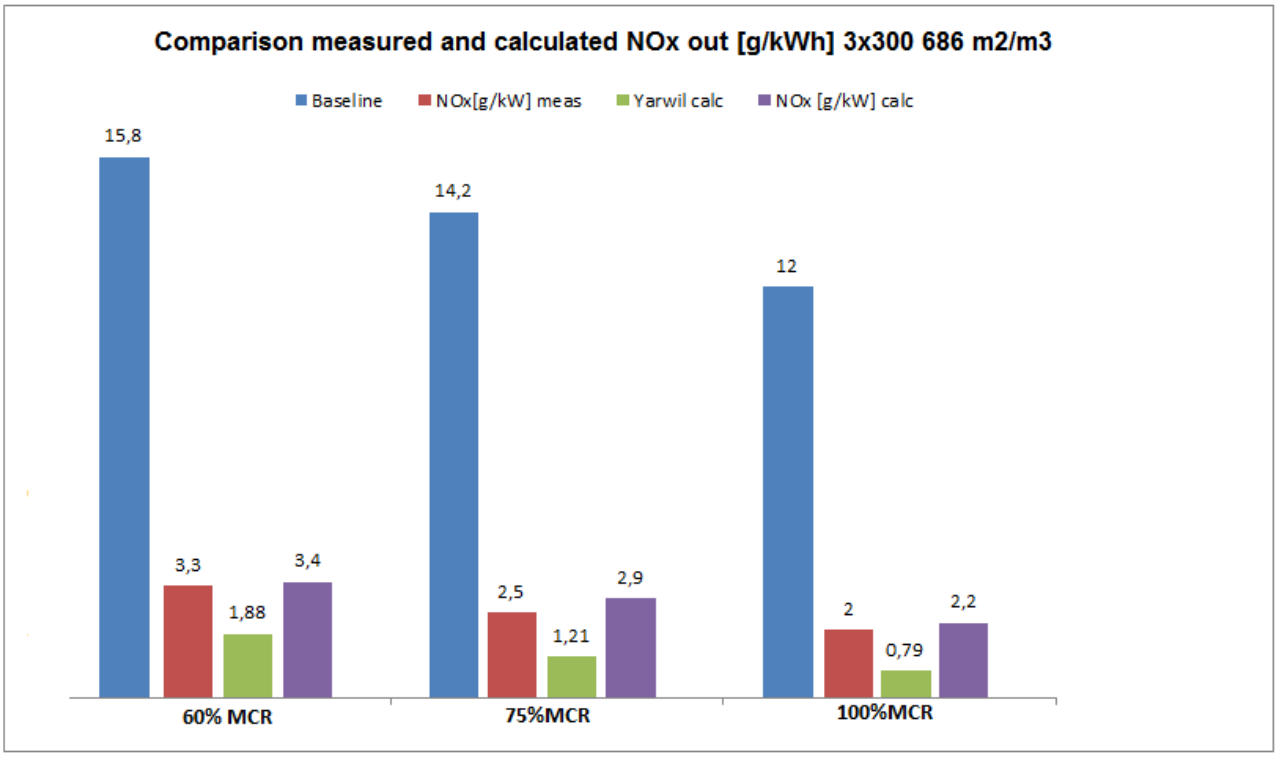

Figura 5.21 *Comparison between Measured outlet (RED) Yarwil criteria prediction (GREEN) and model prediction (VIOLET) for the 30x30 cells per module (686 m2/m3)*

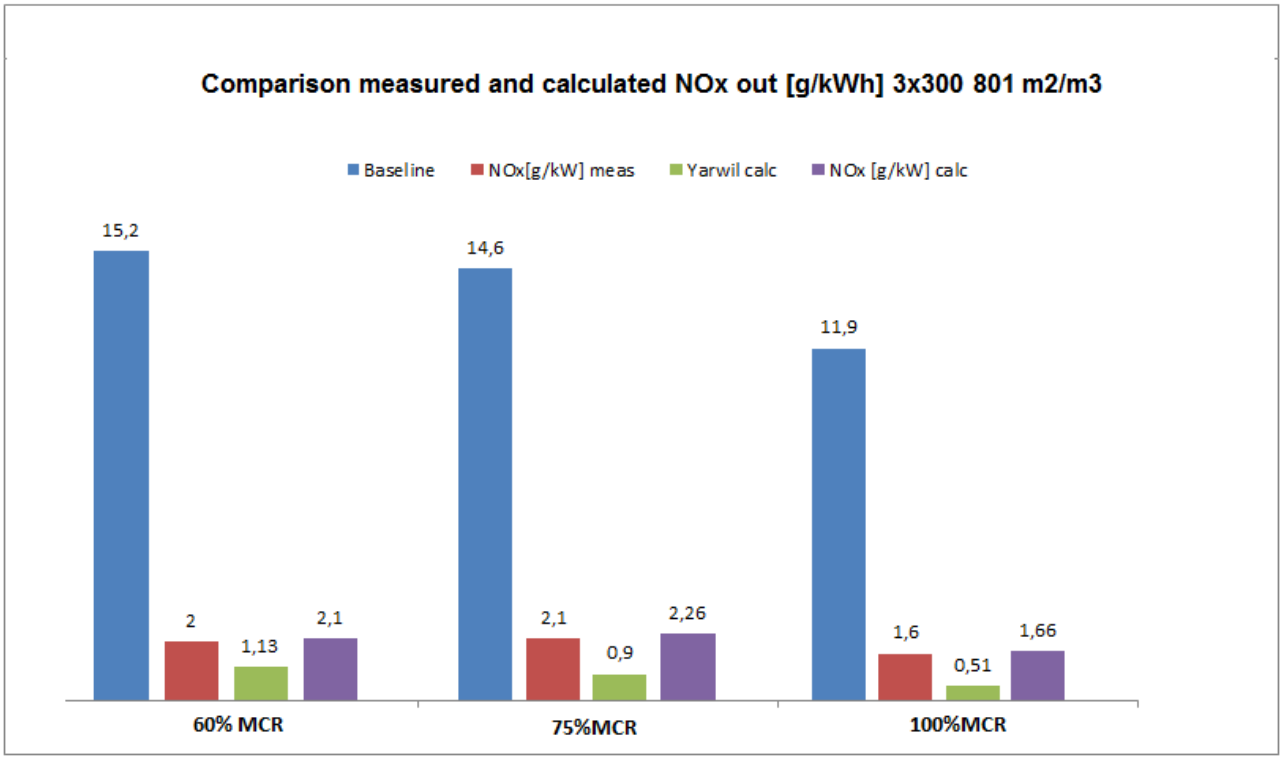

Figura 5.22 *Comparison between the experimental data, the Yarwil design criteria and the design criteria born in this work, for 801 m2/m3 (35x35 cells)*

The main difference between the two models born to describe the SCR process, is the description of the mass transfer. The sizing criteria used by Yarwil, as the large part of industrial criteria, use a pure kinetic approach, with a pseudo first-order kinetic that assume in the tool the form of a polynomial equation, typically of $3^{rd} - 5^{th}$ order. These equations can be expressed as:

$$Activity = A \cdot T + B \cdot T^2 + C \cdot T^3 + D \cdot T^4 + E \cdot T^5 + F \qquad \text{(E56)}$$

And the coefficient are fully empirical. This implies that the equation can be used safely only inside the operative conditions in which the parameters were calculated. When someone try to calculate the necessary amount of catalyst in a different set of operative conditions, then the equations could make some mistakes. If the conditions are different almost for the temperature or the NOx inlet concentrations, probably the equations, expressed as a polynomial, could be able to describe the system and then give to the operator a good approximations of the required amount of catalyst.

However, as for pre-turbo SCR applications, if we change a parameter (operating condition) that is not simulated in the model, as the pressure on the Yarwil standard model, then a fully empirical approach can't give good results, as long as the empirical parameters of the model itself would not be re-calculated on changed operating conditions.

In fact, on the standard model used by Yarwil, the pressure change would only have an influence on reagent's concentration, and therefore, as long as the pressure increase, the reaction velocity would increase as well, and the model would provide a (false) result of less catalyst volume required.

Otherwise a theoretical approach, as the model presented in this work, can describe the SCR systems independently from the operating conditions, as long as we try to describe all the phenomena, both chemical and physical, that could be affected by changing the operating conditions.

This can be translated in a good way to correct the present criteria industrially used, i.e. to compare, for a large number of real SCR applications, the results obtained by the standard tool and by the present model, and then to try, each time, to find some correlations between the two criteria and, maybe, to find some correction factor that can include the pressure variations, that can be added to the polynomial equations.

Conclusion

This work was created to better understand how the pressure can influence the SCR system. As shown in the Chapter 1, the SCR applications on marine engines, in general, and on two-stroke marine engines mainly, will increase tremendously starting from coming into force of the Tier III, that could happen in the 2016 or maybe afterwards, depending on the worldwide agreement between the various countries and also on the global economic situation.

To catch this aim, the first step was the selection of an appropriate model. This step implies that all the terms presented in the model, in particular the kinetic parameters, were not studied for the type of catalyst, in terms of Vanadia and other promoters as Tungsten and Molibden content, and operating conditions on which the model was applied in the present study.

A lot of studies were conducted to better describe the SCR process, since the 1990's, but unfortunately, at least in the part of literature studied for this work, no one has describe the kinetic equations as a function of the vanadium oxides content, but all the different authors that decide to conduct a study, with the purpose to describe the SCR kinetics, simply performed their experiment and regress the kinetic parameters using each time a different form of the equations.

As shown in Chapter 2, the SCR process can be described in almost three ways: fully chemical, using the micro-kinetic proposed by some authors, but for which is difficult to find all the parameters and to understand exactly the mechanism proposed; the second one is a full fluid dynamic approach: in this case the authors proposed to solve directly the equations associated to the flow regime, but they consider the simplest approach to the kinetic part, as first order kinetic in NO concentration and just one reaction, that is what is needed to be introduced in the fluid dynamic codes. The third way is the one that was selected for this work, trying to describe in simple way the fluid dynamic part, as the transport phenomena in the gas phase and inside the catalyst's pores, and at the same time to be quite accurate describing the kinetic part, although in the present work just four SCR reactions are considered.

The model selected present these characteristics but shows also some limitations: the first one, as said before, regards the kinetic parameters. Some studies conducted on this model on real data at low temperature and atmospheric pressure show that the kinetic used in this model is quite slow. Probably the parameters were regressed on a low-vanadia content catalyst, ~1.5% vol/vol, but

unfortunately no information are available about this issue. This is however interesting because, also with slow kinetic, the process appear controlled by the mass transfer phenomena, so using a more active catalyst would not add benefit to SCR pre-turbo applications.

It would then remain, as important advice for future works, the possibility to make an experimental campaign, maybe better on laboratory scale and using powder of catalyst, to describe the kinetic parameters as a function of the vanadia content, making experiment on different type of catalysts with different load of vanadium oxides.

Another point that, as author's opinion, has to be investigated, is the use of mass transfer correlations. Of course the use of these correlations is always an approximation of the phenomena, but during the present study it appears strange that the large part of the correlations proposed by several authors in the past 20 years, shows always an underestimation of the mass transfer coefficient Km. As told before, the best correlation was an empirical correlation, found in particular for NO in a SCR catalyst installed not after a laboratory reactor but after a pilot engine, so really in similar conditions compared with the conditions simulated in the present work. Also for this reason, the author's point of view is conservative by using this correlation to study the under pressure applications.

As shown in section 5.2, the model was used to make some simulation of the SCR reactor, also in extreme operating conditions (from 200 °C to 500 °C and from 1 to 10 bars). The results were not always as expected. The main problem showing the negative effect of the increasing of pressure on the NO conversion was the combined effect of pressure onto the mass transfer parameters (both external and intra-porous) and onto the density/velocity of the gas.

Keeping fix the residence time inside the catalyst, figures 5.5 5.9-10, it has been shown a slightly negative effect of an increasing of pressure: this was due to the fact that increasing the pressure the intra-porous diffusion is hindered, but at the same time the Reynolds number, that contributes to evaluate the external mass transfer coefficient, increase linearly with the pressure if the velocity is kept constant (necessary if the length of the catalyst is constant to kept fixed the residence time)

At the same time we conducted the same studies keeping fixed the gas flow rate Mg [kg/h] . In this case, figures 5.6-7 5.11, the negative effect of the pressure on the mass transfer is exceeded by the increasing of the residence time due to the fact that increasing the pressure, at fixed Mg, decreases the gas velocity.

For this reasons, the phenomena have to be studied for each case, using real input data and it was not possible to find a single design criteria as a function of the pressure. Future studies can be done to catch this aim, and therefore the present work can be a good starting point to find the better way to design the catalyst. At the present time the model, in particular the numerical implementation of the model, can be easily used to basically design an SCR reactor but, for the author, more experimental data will be needed to validate the model. Also the physical properties description could be more accurate .

For future works it will be interesting also to better understand the side reactions of the SCR process. As shown in section 4.3, the model can describe also the ammonium bi-sulphate deposition. It can be implemented, with more data, and eventually combined with the sulphur content in the flue gases. If these upgrades will be done, the model can also predict the amount of ammonium bi-sulphate formation and deposition, in addition to calculate the amount of active sites of the catalyst involved in the ammonium salt adsorption that are not available for ammonia and SCR reaction.

In the same context, it can be also evaluated the effect of the pressure on sulphur dioxide oxidation: in fact it is well known that the sulphur oxidation will occur inside the catalyst. For this reason, because an increasing of pressure system will decrease the diffusivity coefficient, it can be favorable to avoid the sulphur oxidation and to prevent the formation of ammonium salts.

Other studies can be conducted on the mechanical side of the problem: as shown in this work, an increasing of pressure has a negative effect on the mass transfer coefficient. The intra-porous mass transfer is not something that can be changed without change the catalyst morphology: a catalyst with more porosity or with a particular structure of the pores, likewise the tri-modal pores catalysts made by Haldor-Topsoe, may facilitate the internal mass transfer; the external mass transfer, that results to be a phenomenon that gives the higher resistance to the process in pre-turbo applications, is a function both of physical properties and of the fluid dynamic regime: an increasing of the Reynolds number can be an advantage to increase the external mass transfer coefficient.

Otherwise it is well known that the gases inside the channel can’t go faster than 9-10 m/s to avoid mechanical degradation of the catalyst and very high pressure drops. A detailed study on this topic can show the limit condition that can help the mass transfer coefficient without damaging the catalyst structure and without having a penalty on the pressure drop, especially in this kind of application (pre-turbo) whereas the flue gas pressure will become energy in the turbo-charger.

References

1. http://www.chemistry.wustl.edu/~edudev/LabTutorials/Water/FreshWater/acidrain.html

2. www.ghgonline.org

3. www.cgrer.uiowa.edu

4. J.W. Miller, H. Agrawal, and B. Welch (2009).”Measurement of Emissions from the Main Propulsion Engine (MAN B&W 11K90 MC-C) on a Panamax Class Containership. Riverside, CA” : University of California, Riverside.

5. MARISEC. Environmental Performance. [Online] naked ideas, den 20 November 2010. http://www.marisec.org/shippingfacts/environmental/atmospheric-pollution.php.

6. J. Corbett, J. Winebrake, E. Green, P. Kasibhatla, V. Eyring, and A. Lauer. 24, Newark, Delaware (2007). “Mortality from Ship Emissions: A Global Assessment”; American Chemical Society, Environmental Science and Technology, Vol. **41**, ss. 8512-8518.

7. UNCTAD. Review of Maritime Transport 2009. Geneva : United Nations Conference on Trade and Development, 2009.

8. C. Wang, J. Corbett, and J. Firestone. 9, Newark, Delaware, (2007).”Modeling Energy Use and Emissions from North American Shipping: Application of Ship Traffice, Energy, and Environment Model”; American Chemical Society, Environmental Science and Technology, Vol. **41**, ss. 3226-3232.

9. http://www.imo.org/ourwork/environment/pollutionprevention/airpollution/pages/nitrogen-oxides

10. http://www.lr.org/sectors/marine/Services/environmental/future-fuels/eca/index.aspx

11. J. Svachula, L.J. Alemany, N. Ferlazzo, P. Forzatti, E. Tronconi, F. Bregani (1993), “Selective reduction of nitrogen oxides (NOx) by ammonia over honeycomb selective catalytic reduction catalysts”, Ind. Eng. Chem. Res. **32**, 826.

12. L. Lietti, P. Forzatti, F. Bregani (1996). “Steady-state and transient reactivity study of TiO_2-supported V_2O_5-WO_3 de-NOx catalysts: relevance of the vanadium-tungsten interaction on the catalytic activity”, Ind. Eng. Chem. Res. **35**, 3884.

13. W.C. Wong, K. Nobe (1984). “Kinetics of NO Reductionwith NH_3 on “Chemical Mixed” and Impregnated V_2O_5-TiO_2 Catalysts”. Ind. Eng. Chem. Prod. Res. Dev. **23**, 564.

14. L.J. Pinoy, B.G. Massart, L.H. Hosten (1995), "Proceedings of the First World Congress on Environmental Catalysis", Pisa, SCI, Rome, p. 215.

15. M. Turco, L. Lisi, R. Pirone, P. Ciambelli (1994), "Effect of water on the kinetics of nitric oxide reduction over a high –surface-area V_2O_5-TiO_2 Catalysts"; Appl. Catal. B **3**, 133.

16. P. Forzatti, L. Lietti (1996), "Recent advances in de-NOxing catalysis for stationary applications", Heterogeneous Chem. Rev. **3** 33.

17. Odenbrand, C.U.I., Bahamonde, A., Avila, P., and Blanco J. (1994). "Kinetic study of the selective reduction of nitric oxide over vanadia–tungsta–titania/sepiolite catalyst", Appl. Catal. B, **5**, 117–131.

18. Tufano, V. and Turco, M. (1993), "Kinetic modelling of nitric oxide reduction over a high-surface area V2O5–TiO2 catalyst", Appl. Catal. B**, 2**, 9–26.

19. Svachula, J., Ferlazzo, N., Forzatti, P., Tronconi, E., and Bregani, F. (1993),"Selective reduction of nitrogen oxides (NOx) by ammonia over honeycomb selective catalytic reduction catalysts", Ind. Eng. Chem. Res., **32**, 1053–1060.

20. Lietti, L., Nova, I., and Forzatti, P. (2000), "Selective catalytic reduction (SCR) of NO by NH3 over TiO2-supported V2O5–WO3 and V2O5–MoO3 catalysts", Topics Catal., **11/12**, 111–122.

21. Nova, I., Lietti, L., Tronconi, E., and Forzatti, P.(2000), "Dynamics of SCR reaction over a TiO2-supported vanadia–tungsta commercial catalysts", Catal. Today, **60**, 73–82.

22. M. Anstrom, N.-Y. Topsøe, J.A. Dumesic (2003), "Density functional theory studies of mechanistic aspects of the SCR reaction on vanadium oxide catalysts", J. Catal. **213**, 115–125.

23. K. Jug, T. Homann, T. Bredow (2004), "Adsorption of small molecules on the anatase(1 0 0) surface", J. Phys. Chem. A **108** 2966–2971.

24. G. Busca, L. Lietti, G. Ramis, F. Berti (2008), "Chemical and mechanistic aspects of the selective catalytic reduction of NOx by ammonia over oxide catalysts: A review", Appl. Catal. B. **18**,1-36

25. L. Lietti, I. Nova, E. Tronconi, P. Forzatti (1998), "Transient kinetic study of the SCR-DeNOx reaction", Catal. Today **45**, 85-92

26. I. Nova, L.Lietti, E. Tronconi, P. Forzatti (2000)," Dynamics of SCR reaction over a TiO2-supported vanadia–tungsta commercial catalyst"; Catalysis Today **60**, 73–82

27. http://www.theguardian.com/environment/2009/apr/09/shipping-pollution

28. I. Nova, C. Ciardelli, E. Tronconi, D. Chatterjee, M. Weibel,(2009), "Unifying redox kinetics for standard and fast NH_3-SCR over a V_2O_5-WO_3/TiO_2 catalyst", AIChE J. **55** 1514–1529.

29. I. Nova, C. Ciardelli, E. Tronconi, D. Chatterjee, B. Bandl-Konrad (2006), "NH3-SCR of NO over a V-based catalyst: Low-T redox kinetics with NH3 inhibition", AIChE J. **52** 3222–3233.

30. Beeckman, J.W. (1991), "Measurement of the effective diffusion coefficient of nitrogen monoxide through porous monolith-type ceramic catalysts", Ind. Eng. Chem. Res., **30**, 428–430.

31. D. Chatterjee, T. Burkhardt, B. Bandl-Konrad, T. Braun, E. Tronconi, I. Nova and C. Ciardelli (2005), "Numerical Simulation of Ammonia SCR-Catalytic Converters: Model Development and Application"; **01**-0965 SAE International

32. M. Pia Ruggeri, I. Nova, E. Tronconi, (2012), "Experimental and modelling study of the impact of interphase and intraphase diffusional limitations on the DeNOx efficiency of a V-based extruded catalyst for NH_3-SCR of Diesel exhausts"; Chemical Engineering Journal **207–208** 57–65

33. M. Koebel, M. Elsner, (1998), "Selective catalytic reduction of NO over commercial DeNOx-catalysts: experimental determination of kinetic and thermodynamic parameters" Chem. Eng. Sci., **53**, 657-669.

34. Koebel, M. and Elsener, M.(1998), "Selective catalytic reduction of NO over commercial deNOx catalysts: comparison of the measured and calculated performance", Ind. Eng. Chem. Res., **37**, 327–335.

35. I. Nova, C. Ciardelli, E. Tronconi, D. Chatterjee, B. Bandl-Konrad, (2004)," SCR-DeNOx for diesel engine exhaust after treatment: unsteady-state kinetic study and monolith reactor modeling", Chem. Eng. Sci. **59**(22), 5301-5309

36. Horiba Systems. Pg-250 info sheet. Webpage, 05 2010.

37. Durlofsky L, Brady JF, (1987)." Analysis of the Brinkman equation as a model for flow in porous media". Physics of Fluids;**30**:3329–41.

38. Zuercher S, Pabst K, Schaub G. (2009), "Ceramic foams as structured catalyst inserts in gas-particle filters for gas reaction – effect of backmixing"; Applied Catalysis; **357**:85–92.

39. Dhanushkodi SR, Mahinpey N, Wilson M. (2008); "Kinetic and 2D reactor modeling for simulation of the catalytic reduction of NOx in the monolith honeycomb reactor". Process Safety and Environment Protection; **86**:303–9.

40. Tronconi E, Forzatti P, Martin JPG, Mallogi S.(1992); "Selective catalytic removal of NOx: a mathematical model for design of catalyst and reactor"; Chemical Engineering Science ;**47**:2401–6.

41. Ciardelli C, Nova I, Tronconi E, Konrad B, Chatterjee D, Eckl K,(2004). "SCR-DeNOx for diesel engine exhaust aftertreatment: unsteady-state kinetic study and monolith reactor modeling". Chemical Engineering Science **56** 5301–9.

42. L. Lietti, I. Nova, S. Camurri, E. Tronconi, P. Frozatti (1997), "Dynamics of the SCRDeNOx reduction by transient-response method", AIChE Journal **43** 2559-2570.

43. O. Kröcher, M. Elsener, E. Jacob (2009), "A model gas study of ammonium formate, methanamide and guanidinium formate as alternative ammonia precursor compounds for the selective catalytic reduction of nitrogen oxides in diesel exhaust gas", Applied Catalysis B: Environmental, Volume **88**, Issues 1–2, Pages 66-82

44. Y. H. Li, S. C. Kong. (2008) "Diesel combustion modelling using LES turbulence model with detailed Chemistry". Combustion Theory and Modelling Vol. **12**, 2.

45. Buzanowski, M.A. and Yang, R.T. (1990), "Simple design of monolith reactor for selective catalytic reduction of nitric oxide for power plant emission control", Ind. Eng. Chem. Res., **29**, 2074–2078.

46. Lefers, J.B., Lodders, P., and Enoch, G.D. (1991), "Modelling of selective catalytic denox reactors: strategy for replacing deactivated catalyst elements", Chem. Eng. Technol., **14**, 192–200.

47. Beeckman, J.W. and Hegedus, L.L. (1991), "Design of monolith catalysts for power plant nitrogen oxide emission control", Ind. Eng. Chem. Res., **30**, 969–978.

48. Wakao, N. and Smith, J.M. (1962), "Diffusion in catalyst pellets", Chem. Eng. Sci., **17**, 825–834.

49. Tronconi, E., Beretta, A., Elmi, A.S., Forzatti, P., Malloggi, S., and Baldacci, A. (1994); "A complete model of SCR monolith reactors for the analysis of interacting NOx reduction and SO2 oxidation reactions", Chem. Eng. Sci., **49**, 4277–4287.

50. Bahamonde, A., Beretta, A., Avila, P., and Tronconi, E., An experimental and theoretical investigation of the behavior of a monolithic Ti–V–W–Sepiolite catalyst in the reduction of NOx with NH3, Ind. Eng. Chem. Res., **35**, 2516–2521, 1996.

51. Roduit, B., Baiker, A., Bettoni, F., Baldyga, J., and Wokaun, A. (1998), "3-D modeling of SCR of NOx by NH3 on vanadia honeycomb catalysts", AIChE J., **44**, 2731–2744.

52. Tronconi, E. and Forzatti, P. (1992), "Adequacy of lumped parameter models for SCR reactors with monolith structure", AIChE J., **38**, 201–210.

53. P. S. Metkar, V. Balakotaiah , M. P. Harold (2011), “Experimental study of mass transfer limitations in Fe- and Cu-zeolite-base NH3-SCR monolithic catalysts”, Chem. Eng. Sci. **66** 5192–5203

54. A. Santos, M.Costa (2008), “Analysis of the mass transfer controlled regime in automotive catalytic converters”, International Journal of Heat and Mass Transfer **51** 41‑51

APPENDIX 1: FIRST PART OF THE MODEL MATLAB SCRIPT

```
% function = SCRreactor
%dati del reattore

L = 0.9;                              % lunghezza reattore, m
T = 273+350;                                                % K

d = 4.29e-3;                            % diametro canale, m
a = 4/d;                              % area specifica, 1/m

% Calcolo delle Concentrazioni in ingresso dai dati sul
motore
%-------------------------------------------------------------
--------------
n = 900*3;                                      %numero canali
P = 1*100000;                                        % Kg/s2*m
R = 8.314;                                % Kg*m2/(s2*K*mol)
MW = 29;                                               % g/mol
rho = P*MW/(R*T);                                       % g/m3
Mg = 2151*1000;                                           %g/h
V = Mg/rho/3600;                % volumetric flow rate, m3/s
v = V/( d^2 * n)                          % gas velocity, m/s

NOxIn = 997e-06;                                              %
VolNOx/VolTOT
VolNOxIn = NOxIn*V;
% m3/s
MNOxIn = VolNOxIn*P/(R*T);
% mol/s
CNOxIn = MNOxIn/V
% mol/m3
Ct = P/(R*T);
%----------------------Calcolo CNH3-------------------------

VolSol = 4.8;                                          %Lit/h
soluzione 40% urea
rhoSol = 1.3;
%Kg/Lit
Msol = VolSol*rhoSol/3.6;
%g/s
Murea = Msol*0.4;
%g/s
Nurea = Murea/60;
%mol/s
```

```
NNH3 = Nurea*0.85*2;                    %conversione stimata
urea 70%  mol/s
CNH3In = CNOxIn*1.1;
% mol/m3
%-------------------------------------------------------------
% Parametri Mass Transfer
rho1 = P*MW/(R*T)/1000;                                  % Kg/m3

% Legge di Sutherland

mu0 = 1.78e-5;        % Pa*s Parametri per aria in condizioni
ambiente
T0 = 288;                                                    %K
S = 110;                                                     %K
mu = mu0*((T/T0)^1.5)*(T0+S)/(T+S);          %Pa*s = Kg/(s*m)

por = 0.75;
tau = 2;
% Correlazione Fuller, Schettler, and Giddings---------------
M1 = 30;
M2 = 28.97;
M = 1/M1 + 1/M2;
Vair = 20;
Vno = 5.69+5.48;
Dno = 10^-3*T^1.75*M^(1/2)/(P*(Vno^(1/3)+Vair^(1/3))^2)/10000
(T/(200+273))*100000/P;             % coeff. di diffusione NO

Re = rho1*v*d/mu                    % numero di Reynolds
Sc = mu/(rho1*Dno)                   % numero di Schmidt


A = 4*L/(v*d);
% mol/m4*s
%-------------------------------------------------------------

% CIN di NH3 NO  Bulk e parete
CIN =[CNH3In CNOxIn  1e-6 1e-6]';

% risoluz. dei bilanci in fase fluida e all'interfaccia,
lungo z, fino a L
M = [1 0 0 0
     0 1 0 0
     0 0 0 0
     0 0 0 0];     % ADE (ODE le prime 2 eq, AE le altre)

options = odeset('Mass',M);
```

```
% trova le coordinate dei dati sperimentali, raccolti dopo
0,3 0,6 0,9 m
z = [linspace(0,L,100) 0.3 0.6];
z = unique(z);

I = [find(z==0.3); find(z==0.6); length(z)];

tic
[z,Y]= ode15s(@BM,z,CIN,options,v,a,T,A,d,L,Re,Sc,Dno,por,P);
toc

length(z);
Y(end,:)
% GRAFICA
%-------------------------------------------------------------

% disegna i profili di concentrazione di NO, NH3 e
separatemente di Theta
% figure (1)
%
plot(z,(Y(:,1)/Ct),z,(Y(:,2)/Ct),z(I(1)),0.0253/Ct,'g+',z(I(2
)),0.0153/Ct,'g+',z(I(3)),0.0084/Ct,'g+')
% hold on
% plot(z,(Y(:,3)/Ct),'--',z,(Y(:,4)/Ct),'--')
% hold off
% xlabel('z [m]'), ylabel('x
reagente'),legend('NH3','NO')%,'real')
% axis([0 L 0 max(CIN(1)/Ct,CIN(2)/Ct)])
%
% figure (2)
% plot(z,Y(:,3))
% xlabel('z [m]'), ylabel('Theta'),legend('Theta')
% axis('auto')

% Disegna i profili a 3 coordinate sD = [[2.9; 4.2]*1e-
6*(T/473)^1.75*por^2; 0]';celte I di Ci nel poro

%  N = 3;
%  por = 0.75;
%  tau = 2;
%     c = 101325/8.314/(T);
%     D = [[5; 4.2]*1e-5*(T/473)^1.75*por^2; 0]';
%     xi = [1e-3; 1e-3];
%
%     k = [1.3e3;
%          3.9e10;
```

```
%           2.2e8*exp(-55000/8.314/(T));
%           1.1e9*exp(-118000/8.314/(T));];
%
%      nu = [-1  1  0  0
%              0  0 -1  0
%              1 -1 -1 -1 ];
%
%      L1  = 0.25e-3;
%      K =8.2;
%      beta = 0.27;
%      Po2 = 0.14;
%      E = 117000/8.314/(T);
%      gamma = 0.51;
%      omega = 200e-3*2000;
%      nu(end,:) = nu(end,:)*omega;
%
%      pars = {k, nu, c, K, beta, Po2, E, gamma, omega};
% I = [1; round(length(z)/2); length(z)];
% for i = 1:3
%      catalystpore(N,[Y(I(i),1)/c;
Y(I(i),2)/c],D,pars,L1,true);
% end
% Calcolo Conversione e MT coeff
X = 1-(Y(end,2))/(Y(1,2))
KmNO = kmNO(d,L,Re,Sc,Dno)


function ADE = BM(z,y,v,a,T,A,d,L,Re,Sc,Dno,por,P)
% ========================================
% formulazione dei bilanci in fase fluida e all'interfaccia
y = y.*(y>0);
Cnh3 = y(1);
Cno= y(2);
Cnh3w = y(3);
Cnow = y(4);

    N = 3;
    c = 101325/8.314/(T);
   % por = 0.75;
    tau = 2;
    D = [[5; 4.2]*1e-5*(T/473)^1.75*por/tau*100000/P; 0]';
    xi = [1e-3; 1e-3];

    k = [1.3e3;
         3.9e10;
         2.2e8*exp(-55000/8.314/(T));
```

```
          1.1e9*exp(-118000/8.314/(T));];

    nu = [-1  1  0  0
           0  0 -1  0
           1 -1 -1 -1 ];

    L1  = 0.25e-3;
    K =8.2;
    beta = 0.27;
    Po2 = 0.14;
    E = 117000/8.314/(T);
    gamma = 0.51;
    omega = 200e-3*2000;
    nu(end,:) = nu(end,:)*omega;

    pars = {k, nu, c, K, beta, Po2, E, gamma, omega};
%tic
rates = catalystpore(N,[Cnh3w/c; Cnow/c],D,pars,L1,false);
%toc

ADE = [    -A * kmNH3(d,L,Re,Sc,Dno) * (Cnh3-Cnh3w)
           -A * kmNO(d,L,Re,Sc,Dno) * (Cno-Cnow)
           kmNH3(d,L,Re,Sc,Dno)*(Cnh3-Cnh3w)+rates(1)
           kmNO(d,L,Re,Sc,Dno)*(Cno-Cnow)+rates(2)];
%waitbar(z/0.9)

function kmNH3 = kmNH3(d,L,Re,Sc,Dno)

% Correlazione usata nell'articolo
z = (L/d)/(Re*Sc); % coordinata spaziale ridotta
% Sh = 2.976+6.874*(1000*z)^-0.488*exp(-57.2*z); %
Correlazione usata da Tronconi (1992)

Sh = 0.9260*((d/L*Re)*Sc).^1.078;   % Correlazione Santos CO
kmNH3 = Sh*Dno/d;


function kmNO = kmNO(d,L,Re,Sc,Dno)

% Correlazione usata nell'articolo
z = (L/d)/(Re*Sc); % coordinata spaziale ridotta
% Sh = 2.976+6.874*(1000*z)^-0.488*exp(-57.2*z);
% Correlazione usata da Tronconi (1992)

Sh = 1.2824*((d/L*Re)*Sc).^1.079;   % Correlazione Santos
kmNO = Sh*Dno/d;
```

APPENDIX 2: SECOND PART OF THE MODEL MATLAB SCRIPT

```
function rates = catalystpore(N,xi,D,pars,L1,doplot)

if nargin == 0
    clc
    close all

    T = 273+350;
    N = 3;
    c = 101325/8.314/(T);
    D = [ones(2,1)*5e-6; 0]';
    xi = [1e-3; 1e-3];

    k = [1.3e3;
         3.9e10;
         2.2e8*exp(-55000/8.314/(T));
         1.1e9*exp(-118000/8.314/(T));];

    nu = [-1  1  0  0
           0  0 -1  0
           1 -1 -1 -1 ];

    L1  = 0.5e-3;
    K =8.2;
    beta = 0.27;
    Po2 = 0.14;
    E = 117000/8.314/(T);
    gamma = 0.51;
    omega = 200e-3*2000;
    nu(end,:) = nu(end,:)*omega;

    pars = {k, nu, c, K, beta, Po2, E, gamma, omega};
end
c = pars{3};
% Mesh

nx = 200;                                        %mesh size
dx = L1/nx;

x = 0:dx:L1;
xh = (x(1:end-1)+x(2:end))/2;

% Boundary Conditions
m = 0;
```

```
bc1 = [1 0  0
       1 0  0
       0 0  0];

bc2 = [zeros(N-1,1) ones(N-1,1) -xi; 0 0 0];

b1 = [2*bc1(:,1)/dx./(3*bc1(:,1)/2/dx-bc1(:,2)) -
bc1(:,1)/2/dx./(3*bc1(:,1)/2/dx-bc1(:,2))
bc1(:,3)./(3*bc1(:,1)/2/dx-bc1(:,2))];
b2 = [2*bc2(:,1)/dx./(3*bc2(:,1)/2/dx-bc2(:,2)) -
bc2(:,1)/2/dx./(3*bc2(:,1)/2/dx-bc2(:,2))
bc2(:,3)./(3*bc2(:,1)/2/dx-bc2(:,2))];

b1(end,:) = 0;
b2(end,:) = 0;

% IC
x0 = repmat([xi; 0.5],1,nx-1);
U = x0;
Uold = reshape(U,[],1);

% Matrices
[A, B] = makeA(N,nx,dx,xh.^m,x(2:end-1).^m,D,b1,b2);
A = c*A;
B = c*B;

% Time step iteration
err = 1;
%tic
while err>1e-6
%     soli = reshape(Uold,N,[]);
%     plot(x(2:end-1),soli),drawnow,pause(.1)
    [J, S] = makeJ(N,nx,pars,Uold);
    alpha=1;
    Unew = ((A+J)\(-B-S+J*Uold));
    err = norm(Unew-Uold)/(N*(nx-2));
    Unew = Unew*alpha+(1-alpha)*Uold;
    Uold = Unew.*(Unew>0);

%     U1 = b1(:,1).*Unew(1:N)+b1(:,2).*Unew(N+1:2*N)+b1(:,3);
%     U2 = b2(:,1).*Unew(end-N+1:end)+b2(:,2).*Unew(end-
2*N+1:end-N)+b2(:,3);
%     soli = reshape([U1; Uold; U2],N,[]);
%     plot(x,soli(1:2,:)),drawnow,pause(.1)
end
%toc
```

```
U1 = b1(:,1).*Unew(1:N)+b1(:,2).*Unew(N+1:2*N)+b1(:,3);
U2 = b2(:,1).*Unew(end-N+1:end)+b2(:,2).*Unew(end-2*N+1:end-
N)+b2(:,3);

soli = reshape([U1; Uold; U2],N,[]);
if doplot
    figure
    plot(x,soli(1:2,:))
    xlabel('x (m)'),ylabel('mole fractions'),xlim([0 L1])
%     figure
%     plot(x(2:end-1),soli(3,2:end-1))
end

gradE = (3*soli(:,end)-4*soli(:,end-1)+soli(:,end-2))/(2*dx);
fluxD = -c*D'.*gradE;
rates = fluxD;


function [A, B] = makeA(N,nx,dx,xh,x,D,bc1,bc2)

T = zeros(4*N+3*N*(nx-3),3);

% Boundary 1
for i=1:N
    T((i-1)*2+1,:) = [i,i,  D(i)*(bc1(i,1)*xh(1)-
(xh(1)+xh(2)))/dx^2/x(1)];
    T((i-1)*2+2,:) =
[i,i+N,D(i)*(bc1(i,2)*xh(1)+xh(2))/dx^2/x(1)];
end

% Inner nodes
for j=2:nx-2
    for i=1:N
        T(2*N+(j-2)*3*N+(i-1)*3+1,:) = [N+(j-2)*N+i,N+(j-
2)*N+i-N, D(i)*xh(j)/dx^2/x(j)];
        T(2*N+(j-2)*3*N+(i-1)*3+2,:) = [N+(j-2)*N+i,N+(j-
2)*N+i,-(xh(j)+xh(j+1))*D(i)/dx^2/x(j)];
        T(2*N+(j-2)*3*N+(i-1)*3+3,:) = [N+(j-2)*N+i,N+(j-
2)*N+i+N, D(i)*xh(j+1)/dx^2/x(j)];
    end
end

% Boundary 2
for i=1:N
    T(end-2*N+(i-1)*2+1,:) = [N*(nx-1)-N+i,N*(nx-1)-N+i-
N,D(i)*(bc2(i,2)*xh(end)+xh(end-1))/dx^2/x(end)];
```

```
    T(end-2*N+(i-1)*2+2,:) = [N*(nx-1)-N+i,N*(nx-1)-N+i,
D(i)*(bc2(i,1)*xh(end)-(xh(end)+xh(end-1)))/dx^2/x(end)];
end

A = sparse(T(:,1),T(:,2),T(:,3),N*(nx-1),N*(nx-1));
%spy(A)
B = zeros(N*(nx-1),1);

B(1:N)         = bc1(:,3).*D'*xh(1)/dx^2/x(1);
B(end-N+1:end) = bc2(:,3).*D'*xh(end)/dx^2/x(end);


function [J, S] = makeJ(N,nx,pars,U)

S = zeros(N*(nx-1),1);
J = sparse(N*(nx-1),N*(nx-1));

for i=1:nx-1
    [Ji, Ri] = Jacobian(pars,U((i-1)*N+(1:N)));
    S((i-1)*N+(1:N)) = Ri;
    J((i-1)*N+(1:N),(i-1)*N+(1:N)) = Ji;
end
%spy(J),drawnow

function [J, R] = Jacobian(pars,U)


k  = pars{1};
nu = pars{2};
c  = pars{3};
K = pars{4};
beta = pars{5};
Po2 = pars{6};
E = pars{7};
gamma = pars{8};

xNH3 =  U(1);
xNO =   U(2);
theta = U(3);

rates = [k(1)*c*xNH3*(1-theta);
         k(2)*exp(-E*(1-gamma*theta))*theta;
         k(3)*c*xNO*theta/(1+K*theta/(1-
theta))*(Po2/0.02)^beta;
         k(4)*(Po2/0.02)^beta*theta];
```

```
drates = [k(1)*c*(1-theta)  0
-k(1)*c*xNH3
          0                 0
k(2)*exp(-E*(1-gamma*theta))*(1+E*gamma*theta)
          0                 k(3)*c*theta/(1+K*theta/(1-
theta))*(Po2/0.02)^beta
k(3)*c*xNO*(Po2/0.02)^beta*((1+K*theta/(1-theta))-K*theta/(1-
theta)^2)/(1+K*theta/(1-theta))^2
          0                 0
k(4)*(Po2/0.02)^beta];

R = nu*rates;
J = nu*drates;
```